Università degli Studi di Cagliari

# DOTTORATO DI RICERCA

IN INGEGNERIA ELETTRONICA ED INFORMATICA

Ciclo XXIV

# IEEE 1588 SYNCHRONIZATION IN DISTRIBUTED MEASUREMENT SYSTEMS FOR ELECTRIC POWER NETWORKS

Settore scientifico disciplinare di afferenza

ING-INF/07 (Misure Elettriche ed Elettroniche)


| | |
|---|---|
| Presentata da: | Marco Lixia |
| Coordinatore Dottorato: | Prof. Alessandro Giua |
| Tutor/Relatore: | Prof. Carlo Muscas |


Esame finale Anno Accademico 2010 - 2011

*Dedicated to Luisella*

# Contents

# Introduction

Modern electric power systems can be considered as the consequence of the continuous technological evolution, often pushed by economical, political and social requirements. As an example, the main transformations in electric distribution systems arise from the diffusion of ″Distributed Generation‟(DG), i.e. small production plants, often supplied through renewable energy sources, whose presence has significant implications on both energy management (since ″active networks‟are needed to take into account bidirectional energy flows by means of innovative devices) and protection systems (since adaptive protections can be used to automatically reconfigure the network in the case of fault occurrence).

In general, in both transmission and distribution networks, monitoring, control and protection tasks are usually performed by Intelligent Electronic Devices (IEDs), which can be, by their nature, connected to each other by suitable communication links. A famous example of this approach is represented by the series of Standard IEC 61850 (Communication Networks and Systems in Substations). These standards are related to networks and communication systems within the substation, but are used as a reference in all those circumstances in which an electrical system is managed through the use of IEDs communicating with each other (as in the case of active distribution networks). In this way, control and protection schemes practically become algorithms, whose correct behavior is determined firstly by the availability of data measured in strategic points of the network. The critical role of the above mentioned applications, which clearly emerges from their implications on safety, as well as from economical considerations, makes it of fundamental importance the evaluation of correctness and trustworthiness of the information on which such actions are based. Many of these applications implemented for control and protection purposes in electric power networks require the acquisition of information by Wide Area Monitoring System (WAMS) from strategic points of the system and need that the acquired data have an extremely accurate common time reference. Generally, amplitudes and phases of the positive sequence voltages are the quantities to be estimated in the network nodes. Because of the extension of power networks, suitable measurement devices should be used to ensure proper synchronization be-

tween the collected data. Thus, the key components of WAMSs are represented by Phasor Measurement Units (PMUs) designed to measure synchronized phasors (synchrophasors).

Typical synchronization specifications for synchrophasors measurement are in the order of few microseconds. Such a tight synchronization requirements lead to the need of highly accurate clock settings, such as the ones bases on satellite systems. Currently, the Global Positioning System (GPS) is the only system to provide a time reference with sufficient availability and accuracy for most distributed monitoring and control applications in power systems. As an alternative, in situations where many devices are located in a geographically limited sub-area (e.g a substation) of the system and are connected to each other by suitable communication networks (as described by the series of standard IEC 61850), it could be advantageous to distribute the time reference of a high accuracy clock to the devices through suitable network synchronization protocols. Between them, the PTP (Precision Time Protocol) defined in the Standard IEEE 1588 offers the best accuracy performance. It is worth mentioning that the Standard IEC 61850-9-2 practically indicates Ethernet as a preferred communication solution, thus offering an optimal support to implement 1588 synchronization in electric power plants. In this context, it should be recalled that the IEEE 1588 profile for power system applications (project PC37.238) is being developed under IEEE Power System Relaying Committee (PSRC) and Power System Substation Committee (PSSC). The scope covers all power system applications, including Synchrophasors. The group works in close co-ordination with TC57 WG10, which plans to adopt the PTP profile in the next revision of IEC 61850.

In the first part of this thesis, the state of the art regarding power system evolution, IEEE Standard on synchrophasor measurements and synchronization system is presented.

In particular, the problems related to the evolution of the power system along with some possible advantages due to the implementation of Phasor Measurement Units in Wide Area Monitoring Systems are introduced. After a general description of the architecture of a distributed measurement system based on PMUs, the new synchrophasors standard is analysed, highlighting the differences with previous versions, the requirements for the measurement of synchrophasors and the definition of synchrophasor under steady-state and dynamic conditions. Moreover, a summary of the possible synchronization solutions is introduced. For each solution, advantages and disadvantages are highlighted. In particular, satellite system and network based protocol are analysed in detail.

In the second part of the thesis, a synchronization solution able to exploit the world-wide availability of the GPS and the possibility to disseminate the synchronization signal with high accuracy by means of the network synchronization protocol IEEE 1588 is proposed. This solution is used for the synchronization of PMUs. The objective of this work is to analyse the possibility to synchronize PMUs via PTP and to study the impact that such a synchronization solution has on the performance of measurement systems under both steady-state and anomalous operating conditions, as well as its effects on the applications that make use of their data. Two different versions of the PTP are used: the first one uses hardware-assisted time-stamp mechanism whereas the second one uses software-only time-stamp mechanism. Two experimental systems are characterized in detail with an accurate description of all the used hardware and software components, and their synchronization performances under different operative conditions are analysed.

Finally, among all the sources which may contribute to the uncertainty introduced by PMUs, the last part of this thesis analyses the impact of the phasor estimation models on the accuracy of these devices, with particular attention to algorithms proposed in literature for the estimation of dynamic phasors and studies their performances under several different conditions.

# Chapter 1

# Measurement issues in modern power systems

## 1.1 Wide Area Measurement Systems

Significant modernization is occurring in electric power systems, which are currently experiencing dramatic changes, arising from both technical and economic reasons, such as the liberalization of the energy market, the increasing diffusion of Distributed Generation (DG) and also the constant technical innovation on network components. The deregulation, competition and an increasing complexity of modern electric power system interconnections have led to several power system stability issues, which can result in cascading trips and eventually system-wide blackouts. The two recent blackout occurred in Italy and North America during 2003 and the one occurred in north Europe in 2006, are a clear example of the above mentioned stability problems [1–3]. The North American blackout (August 14, 2003), which was one of the largest blackouts in the North American history, was caused by cascade faults and it affected about 50 million people causing financial losses for around 6 billion US dollars [2]. The European blackout occurred on November 4, 2006 affected 10 countries and more than 15 million people for more than half an hour, causing a lost of 14.5 GW of load [3].

From what it has been mentioned, it is clear that the problems encountered by modern power system operators, related to wide-area system disturbances, cannot be solved by means of traditional protection and control system and the implementation of a complex system of monitoring, management and automation of the power systems is required. As a consequence, in modern transmission and distribution networks, management and monitoring issues are usually performed by Intelligent Electronic Devices (IEDs) connected to each other by suitable communication links.

Control and protection schemes become actually algorithms, whose behaviour is based on the estimated state of the system. Such estimated state depends on data measured in strategic points of the network. The critical role of the above mentioned data clearly emerges considering their implications on safety, as well as on economical aspects. As a consequence, the evaluation of correctness and trustworthiness of the information on which control and protection schemes are based is of fundamental importance. It follows, therefore, the need to have continuously updated information on the electrical parameters. Proper synchronization between the remote instruments is required, so that the quantity measured in different points of the grid are directly comparable. As a consequence, the implementation of a Wide Area Measurement System (WAMS) able to acquire information on different nodes of a network and to distribute synchronized data on the state networks is required. The problem of measurements synchronization is not simple given the complexity and dimensions of the systems to which it is applied. The synchronization accuracy requirements can significantly change depending on the constraints of the applications which vary from system to system. For example, there are methods of measurement based on a real-time knowledge of quantities that are characteristic of the status of the system. In this case, synchronization solutions that can ensure the traceability of temporal data (time-stamping) with fairly stringent synchronization accuracy are required. On the other hand, there are also different applications, including environmental monitoring for example, which are based on the availability of averaged quantities and, therefore, the measures do not necessarily require a high degree of synchronization. Synchronization can be obtained through the use of different sources: for the applications with more strict constraints, such as those which require synchronization accuracy in the order of a few hundreds of nanoseconds, the system based on Global Positioning System (GPS) satellite receivers appears to be the most used. In the case of less stringent specifications, using alternatives, such as those based on the synchronization protocols (eg NTP, Network Time Protocol) can be conveniently. These aspects will be studied in more detail in the following Sections.

## 1.2 Phasor Measurement Units

Phasor Measurement Units (PMUs) are the basis for the implementation of WAMSs. They provide synchronized positive sequence voltage and current measurements and offer the most direct access to the state of the power system. These synchronized data can be used to have a clear picture of the state of the network, and in case of faults, to activate control and protection systems to prevent the occurrence of cascade phenomena [4]. Fig. 1.1 shows the general block diagram of a possible

implementation of a PMU.

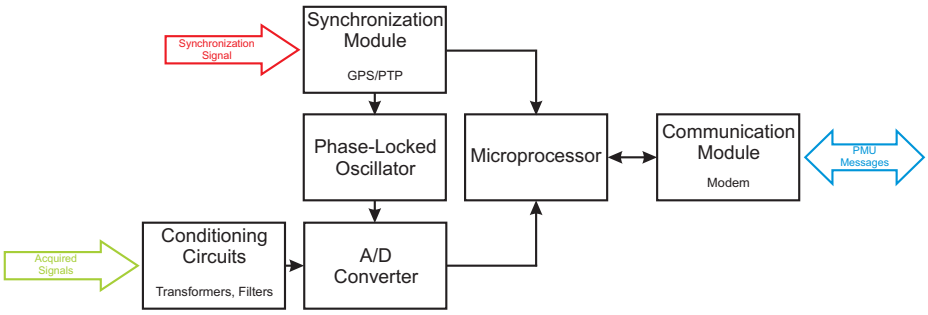


**Figure 1.1:** Block diagram of the main components of a PMU

### Synchronization

Each unit is able to instantly acquire voltage and current signals in a synchronized manner by using a suitable source of synchronization. As will be discussed in Chapter 3, GPS is currently the preferred solution for the synchronization of PMUs. A device may have an integrated GPS receiver, or may receive the synchronization signal from an external receiver. There are also alternative synchronization solutions. As an example, it is possible to equip a PMU with a IEEE 1588 synchronization module which may receive the reference time signal from the grand-master clock of the substation via network communication.

### Conditioning circuits

The analog inputs are currents and voltages signals obtained from the current and voltage transformers. Transducers introduce an uncertainty that is related to their accuracy class. In the usual practice, magnetic core Voltage and Current Transformers (VTs and CTs) are employed. Their accuracy is generally limited to class 0.5, according to the definition of the standards [5] and [6]. This means, at full scale, a maximum ratio error of 0.5 % and a maximum phase error of 6 mrad for VTs (9 mrad for CTs). To minimize the effect of the ratio and phase errors introduced by instrument transformers, compensation routines are usually implemented in commercial PMUs [7]. However, the above compensation requires the transducers to be accurately characterized, which is impractical, especially in existing plants and, even when it is performed, it cannot be considered totally reliable, both because of the unavoidable uncertainty in the metrological characterization of the device and because the behaviour of the transducers can also be affected by actual network and environmental conditions. Therefore, significant uncertainty is expected to affect the

measurement results, so that the transducer can be considered as the major source of uncertainty a PMU can be affected by.

In addition, the input signals can be further attenuated by means of shunts or instrument transformers in order to meet the requirements imposed by the analog-to-digital converter block and they can be filtered by means of an anti-aliasing filter in order to reduce the pass-band. In many cases, these are analog filters whose cut-off frequency depends on several factors including the used sampling frequency.

### Phase-Locked oscillator

In the vast majority of phasor measurement units, the process of data acquisition is directly synchronized by means of the internal Phase-Locked Loop circuit (PLL) to the time reference sources. Currently, most devices on the market use sampling frequencies of the order of tens of ksamples. The sampled values are then converted by a dedicated circuits: the **Analog-to-digital Converter** (ADC).

### Microprocessor

The microprocessor calculates all the magnitudes of interest that can be encapsulated in a Data message (see 2.1.5). It estimates all the current and voltage phasors using one of the many algorithms available in literature (some will be described in the Section 6.1) and generates the time-stamp for the signals derived from the synchronization module (e.g. GPS receiver or PTP module). It also can embed in the PMU messages other locally measured values of interest, such as frequency and rate of change of frequency.

### Communication

The modem is used to transmit or receive the time-stamped data or other types of messages generated by a PMU through the network either to/from Phasor Data Concentrator, a device specially designed to receive input data from different PMUs and to make their time alignment, or to/from Monitor Station. A PMU-based measurement system (see Fig. 1.2) consists of several units installed in different nodes of the grid and connected, usually via WAN, to a hierarchical structure of PDCs.

The measurement values collected by the Local-PDC, with its time references, can be used to take some corrective action at the level of substation or can be transmitted along with other records of other Local-PDC to a Super-PDC that can use them for real-time wide area control and monitoring applications or for storage of data for possible off-line analysis.

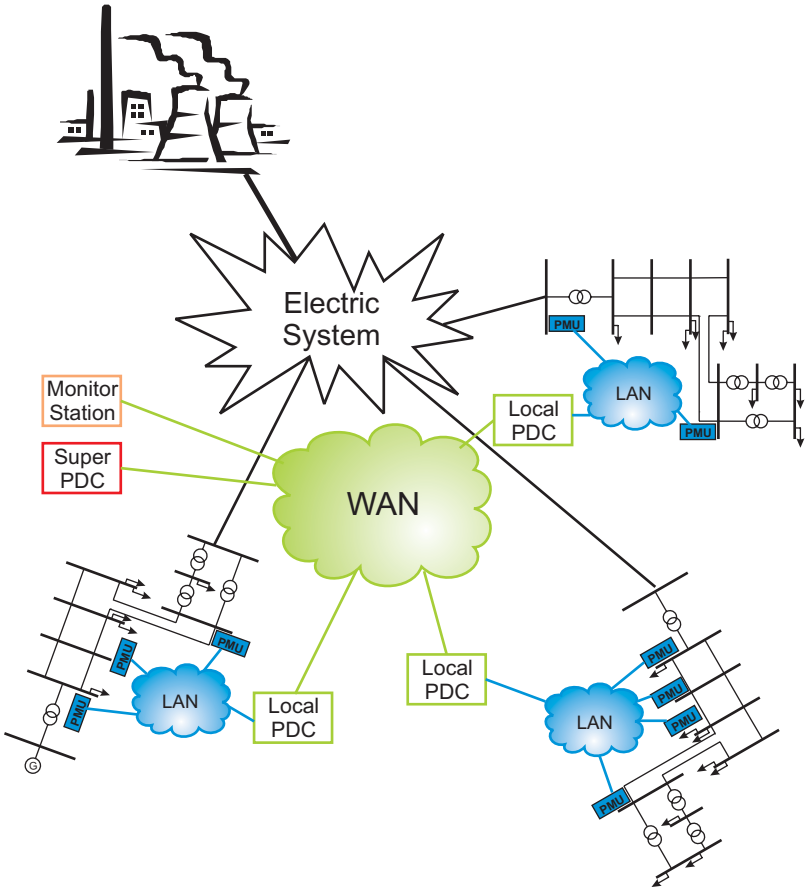


**Figure 1.2:** Example of a PMUs system

## 1.3 PMU applications

Currently, the literature offers a wide range of applications that take advantage from the use of synchronized data from PMUs installed in strategic points of the network [8]. These applications can be organized in two general groups depending on whether they operate in real time or not:

- Real-time Applications
  - State estimation;
  - Power Quality monitoring;
  - Real-time monitoring and control of the power system;
  - Congestion management;

  - Adaptive protection;
  - Identification of sources of disturbing;

- Off-line Applications
  - Post-event analysis;
  - Validation of system models;

Some of these applications are briefly described in the following.

### State Estimation

The objective of State Estimation (SE) in power systems is to determine the best estimate of the state of the system based on the quantities that are measured and their accuracy, and on the available model of the system. The SE is one of the most important applications for system operators, since many of the tasks of network management (including voltage regulation, monitoring of the margin of stability, contingency analysis and dispatching) depend on its data.

Before the advent of the PMU, the SE was based on the active and reactive power flows and voltage amplitudes measured by Remote Terminal Units (RTUs). These data were characterized by poor time synchronization, resulting in low quality SE. Moreover, the traditional SE of a system is obtained as a solution of non-linear problems solved by means of iterative methods which might have long time of convergence. The PMU-based systems have solved these problems, by offering several advantages consisting mainly in a better accuracy and robustness, easier identification of corrupted data and the possibility to obtain faster numerical solutions to linear problems. In fact, in addition to bus voltage phasor measurements, PMUs can also measure the current flows at the lines connected to the bus where they are installed. By measuring the line current phasors and using the $\pi-$line model, the voltage phasor measurements can also be extended to the adjacent buses, where none PMU is installed, through a linear formulation.

In literature, it is possible to find several algorithms for SE [4, 9]: some entirely based on traditional measures, some of which make a combined use of traditional measures and synchrophasors and others entirely based on PMU measurements. In this last case, with a sufficient number of installed PMUs at appropriate locations, the SE problem becomes a linear problem solvable using only data provided by PMUs (voltage phasor and current phasor measurements, and their linear relation based on the $\pi-$line model). Unfortunately, as underlined in [10], the number of PMUs currently deployed in power systems is still too small to allow for a SE process fully based on synchrophasor measurements. At the same time, the use of only voltage

and current measurements generated by PMUs is a reasonable assumption for future scenarios, taking in account the growing presence of these devices [10, 11].

Indeed, looking at future installations, the possibility of having a fully linear state estimation process is an attractive possibility that has led to the development of new state estimation techniques. As an example, the algorithm presented in [4] and used in [12] is based on a Weighted Least Squares (WLS) approach that uses only synchronized voltage and current measurements, rather than active and reactive power measurements. Using only the aforementioned PMU measurement data, the SE problem can be formulated as:

$$[\mathbf{z}] = [\mathbf{A}][\mathbf{E}] + [\boldsymbol{\xi}] \tag{1.1}$$

where:

- $[\mathbf{z}] = \begin{bmatrix} \mathbf{E}_\mathbf{r}^{'} \\ \mathbf{E}_\mathbf{i}^{'} \\ \mathbf{I_r} \\ \mathbf{I_i} \end{bmatrix}$ is the voltage and current phasor measurements vector;
- $[\mathbf{E}] = \begin{bmatrix} \mathbf{E_r} \\ \mathbf{E_i} \end{bmatrix}$ is the state variables vector with all bus voltages;
- $[\mathbf{A}] = \begin{bmatrix} \tilde{\mathbf{I}} \\ \mathbf{Y} \end{bmatrix}$ is the admittance matrix;

The upper part $[\tilde{\mathbf{I}}]$ of the matrix $[\mathbf{A}]$ is a unit matrix in which rows corresponding to missing direct bus voltage phasor measurements are removed, while the lower part $[\mathbf{Y}]$ is composed of conductances and susceptances for the lines where current phasor measurements are available. $[\mathbf{Y}]$ relates the voltages linearly to the currents based on the line model. The vector $[\boldsymbol{\xi}]$ represents the measurement uncertainties that are assumed as random Gaussian variables with covariance matrix $[\mathbf{W}]$. Equation (1.1) is linear, hence the state estimation can be achieved using WLS method yielding the solution:

$$[\mathbf{E}] = [\mathbf{A}^T\mathbf{W}^{-1}\mathbf{A}]^{-1}[\mathbf{A}^T\mathbf{W}^{-1}][\mathbf{z}] \tag{1.2}$$

More details and a comparison with other estimation techniques can be found in [4, 9].

### Power Quality monitoring

In the liberalized energy market, it becomes very important to assess the entities responsible for PQ disturbances. Therefore, suitable parameters, frequently based

on distributed and simultaneous measurements achieved on the network, could be a possible metric to characterize the quality of the services provided by system operators. From this point of view, therefore, the use of PMUs is encouraged, since they provide both the function of communication with a central data collection, and perform measurements with high accuracy time synchronization. As an example, PMU data can be used for PQ monitoring based on harmonic state estimation. The harmonic content of the electrical quantities, in fact, represents an indispensable tool for the practical implementation of some procedures recently proposed for PQ monitoring and, in particular, for the localization of the harmonic sources in power systems [13].

The definition of the harmonic content of the synchronized electrical quantities can be obtained by extending to non-sinusoidal conditions the definition of synchrophasor presented in 2.2, as stated in [14]. In particular, considering the periodic signal $x(t)$ composed by $H$ harmonics, it can be decomposed into $H$ synchronized phasors, each of which has the form:

$$\bar{\mathbf{X}}_{\mathbf{h}} = (X_h)e^{j\phi_h} = (X_h)(\cos(\phi_h) + j\sin(\phi_h)) \tag{1.3}$$

where $X_h$ and $\phi_h$ are the rms and phase values, respectively, of the h-th harmonic component of the signal $x(t)$, with $h = (1, 2, ..., H)$.

### Real-time monitoring and control of the power system

Real-time monitoring and control of the electric system are essential for its proper and efficient management. They allow the system operators to know the system conditions and to take appropriate decisions to increase operational efficiency, in the case of normal operation, or to act immediately when abnormal operating conditions are detected. Since knowledge of the differences between the phase angles of the voltages at system nodes, can provide important information on system stability margins, the use of PMUs, which provide direct measurement of phase angles, involves an obvious advantage in this type of applications.

### Post-event analysis

Given the ability of PMUs to provide data with an high synchronization, and given the hierarchical structure in which the latter can be organized, with PDC, Super PDC and database of data at different levels, post-disturbance analysis is one of the first application for which the PMUs were tested. The synchronized execution of measures allows it to perform the time alignment of the collected data, therefore facilitating the reconstruction of conditions in a given time and permitting easier

identification of the causes that led to the manifestation of certain events or problems.

## 1.4 Evolution of distributed power systems

The current electrical system is the result of a continuous technological and scientific development that began in New York in 1882, when Thomas Alva Edison started the first plant for the production of electricity. Since that date, and already before 1900, several U.S. cities had small plants for the production of electric energy scattered in the metropolitan area and the infrastructures to distribute it. It can be said therefore that the first urban power networks were powered by small plants spread all over the city and not interconnected.

However, the increasing consumption of energy and the growing attention to safety and efficiency of the electrical system led, at first, to the realization of interconnection between different urban systems and, then to the concentration of production of electricity in large power plants located at large distances from the urban area, creating the models of centralized power grid which remained intact, in its configuration, until the second half of the last century. Fig. 1.3 shows an example of centralized architecture of an electrical system characterized by a large factory capable of producing considerable quantities of electricity which were then transported to consumption centres through lines of high, medium and low voltage.

The gradual concentration of power plants in the most economically advantageous points of the city led to the development of increasingly extensive and interconnected energy transmission networks. As a consequence, the focus efforts of the scientific community was addressed to the aspects of electricity transmission over long distances with minimal losses. The power flow was unidirectional and the distribution system (medium and low voltage) was considered as a passive element in the network.

However, as a result of recent climate change, the increase in the pollution level of water and air and the augmentation of global average temperatures, recent years have been characterized by a strong push of research into technologies for the production of the so-called alternative or renewable energy, able to fully respect the environment. In [15], for example, Jacobson and Delucchi report a series of articles dealing with the concrete possibility to replace the use of fossil materials with the use of renewable resources for energy production: Water, Wind, Sun (WWS). In the same article they propose a theoretical study whose results suggest that it is technically feasible to power the world with only renewable energies by 2050. The idea behind this and many other studies is to exploit the presence of sources of clean energy where they are available in abundance and to interconnect renewable energy

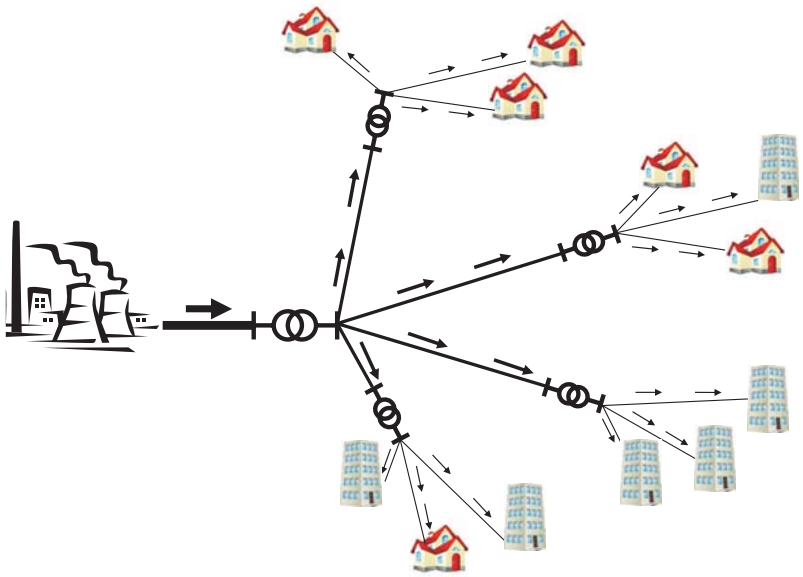

**Figure 1.3:** Traditional Power System

sources based generation plants at various level of the network, thus switching from a centralized to a distributed model (Distributed Generation). Although at the moment it is certainly not possible to say that the world will be powered exclusively by renewable energy sources, surely the fact that in the current scenario the large power plants are accompanied by alternative energy based small plants scattered across the territory for the production of electricity can not be ignored.

The increasing diffusion of DG results in the need for profound changes in the architecture of the electricity grids and in how they are managed. The distribution network no longer plays a purely passive role, but it arises the need to control bi-directional flows of energy (active networks): the loads are no longer seen as a network elements only capable of absorbing power, but they also may be considered as small-scale generators able to inject energy into the power network. In addition, scattered throughout the territory, there are small production facilities that use renewable sources and inject energy at different network layers. Fig. 1.4 shows a representation of a modern power system characterized by the presence of distributed generation plants and active networks where the energy can flow in both the directions.

Considering all these changes, it is reasonable to assume that the traditional management of radial distribution network is no longer sufficient to meet criteria for safety and efficiency and should be abandoned for more flexible architectures such

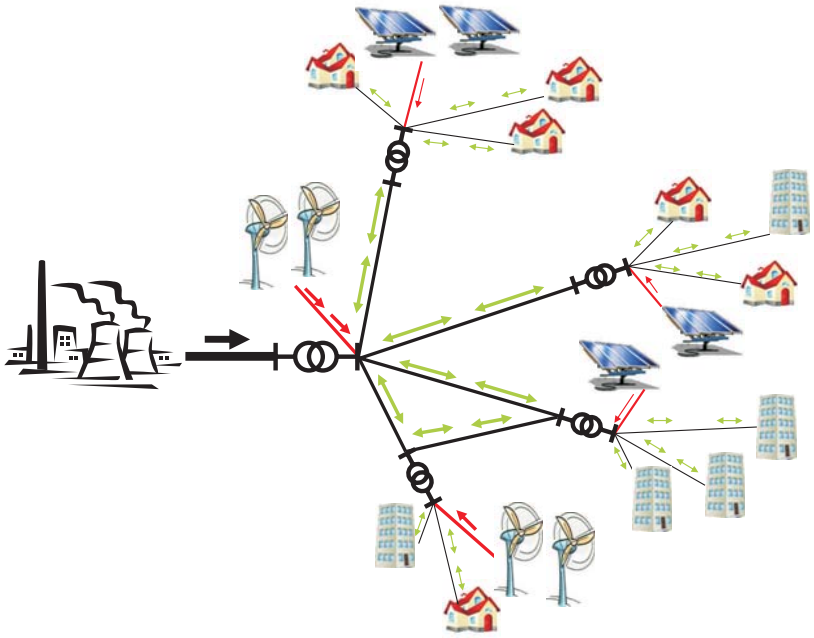

**Figure 1.4:** Modern Power System

as meshed or closed loop. This new scenarios entail big challenges for engineers, which should be able to provide greater flexibility, and exploring new techniques and protocols for network monitoring, management and control. Before the appearance of the DG, the efforts of researchers were mainly focused on lowering costs and increasing efficiency of the apparatus of the transmission lines. The distribution networks were seen as passive elements and therefore did not require great technological innovation. In modern networks, however, the switch from a passive to an active view of the distribution systems requires a higher level of intelligence and automation. It is indispensable to guarantee technical and economic efficiency, security and, given the increasing complexity of modern power grids, it becomes also important to guarantee the ability of the network to automatic regulate and react to unexpected situations. Then the concept of Smart Grids is introduced: an intelligent system, where the final consumer and the supplier of electricity are interconnected by a network characterized by high levels of automation and computerization at all the layers (generation, transmission and distribution) [16].

Such a configuration of the electrical systems seems well suited to meet the needs of the most innovative scenarios where the global demand for electricity is met only through the exploitation of renewable resources and where a grid is divided into cells or micro-grids, each of them able to decide the purchase/sale of energy from/to

the transmission network or from/to other cells according to several factors such as energy prices, the situation of loads and generators, etc.

## 1.5 Advantages and disadvantages of DG

As mentioned in the preceding paragraphs, the DG is now a reality of our times. Among the causes of its rapid diffusion, the need to use energy more functional and attentive to the needs of end users, the forecast growth in energy consumption, the liberalization of the electricity market, the increasingly strong competition of its actors, and the attention to the environmental problem can be listed. The impact of DG on power systems is strongly influenced by specific aspects of the network on which it is installed (type of conductors, length of lines, etc..), by the nature and variability of loads, by the type of sources used for the production of energy. In this Section, some of the advantages and disadvantages due to the diffusion of DG will be listed and briefly described [17–19].

**Environment**

One of the largest and most important advantages of DG is the ability to exploit efficiently, using modern technologies, renewable energy sources (e.g. WWS). These sources, unlike fossil fuels, can be considered practically inexhaustible, and are not subjected to price fluctuations or changes in the market due to unpredictable events, such as natural disasters, or to events whose duration is difficult to estimate, such as wars. In addition, given the increasing global attention to the environment and the increasingly strong pressures to reduce the production and emission of polluting substances, the use of power plants based on clean sources seems the only way to meet the goals that the global community is prefixing to fight pollution and climate changes.

**Economy**

The small size and relatively short construction and payback time of DG plants compared to traditional large power stations allow different actors to invest in the liberalized market of the energy. The characteristics of the DG permit to quickly respond to changes in supply and demand, the development of new technologies and, in general, the evolution of the market. In fact, the DG plants can be very flexible in their operation, size, and expandability. As a consequence, they can be operative during periods of high electricity prices (peak periods) and then they can be switched off during periods of low prices. Moreover, the facility with which they can be installed allows investors to upgrade the capacity of production of a plant

in order to take advantage of the high prices of the energy market or to quickly respond to an increment of the energy demand. In addition, the presence of DG allows an operator to move the plants in the vicinity of the end consumers. This means that the transmission lines and transformers are partially downloaded and there is a reduction of losses due to the transfer of energy through long portions of line [20]. DG provides economic benefits not only to investors and capitalists. The end users have the ability to react to changes in energy prices in a flexible manner by optimizing their consumption as a function of cost and availability of electricity and deciding to sell and transmit energy produced in surplus on the net.

However, difficulties in obtaining permits for the installation of new systems can be considered as a significant obstacle for the diffusion of the DG, especially in some countries. It should also be taken into consideration that there are certain social movements that contest the works of public interest or centres of energy production that could have negative effects on the land where they are built. All these aspects can negatively influence potential investors and cause a real slowdown in the diffusion of the DG.

### Robustness and reliability

The inherent flexibility, which derives from the use of DG and from the changes that it involves in terms of distribution network (transition from radial to meshed architecture), also offers the possibility to dynamically reconfigure the network in case of failure, creating disruptions to a minimum number of clients. In fact, the possibility to disconnect entire portions, of the network for maintenance operations or to prevent cascading failures, having the option not to isolate all the users that are located downstream of the fault and that can be supplied by DG plants is a major advantage and increases robustness and reliability of the all electrical systems.

However, even considering all these advantages related to robustness and reliability, it is also possible to list some disadvantages arising from the use of DG. The use of decentralized energy production plants, in fact, implies the presence of bidirectional flow and, consequently, a greater difficulty in managing networks and setting protection systems. Moreover, the maintenance operations may be more dangerous because the separated part of the network continues to be powered by independent generators which may not be aware of the critical condition.

### Power Quality

The improvement of reliability and robustness of networks is part of a more general topic focused on Power Quality (PQ) [21]. The liaison between DG and PQ is ambiguous. With the liberalization of the market and the multiplication of actors

involved, also the attention to the quality of services for the end users is increased. In fact, there are several service providers that, in order to increase its portfolios of customers, have an interest in offering good quality products which meet their necessity. On the other hand there are the customers, who gain contractual power and, as mentioned, have higher expectations on the quality of services (especially the industries). In addition, the end user can be at the same time producer and consumer, thus complicating the picture. In this scenario it becomes very important to reduce outages and faults such as power interruptions, voltage fluctuations, etc.. Different works in the literature state that the DG offers several advantages in terms of mitigation of PQ problems. In fact, DG helps to limit the voltage drop in the resistive part of the impedances of the line by reducing the active power flow in transit to the loads along the distribution lines. In addition, the use of static power converters for the connection of DG units to the network can help to increase the level of PQ: if managed in a coordinated manner, for example, can contribute to the control of the voltage or of the reactive power.

However, there is a line of research in the literature which states that the diffusion of DG involves also several disadvantages in terms of PQ [19]. The increase of short-circuit power as a consequence of meshed distribution network is an example of that: it brings a greater depth of voltage dips and thus extends the area of influence of faults. In addition, the close dependence of the production of clean energy from renewable sources, the availability of which is by nature more or less aleatory, results in a unpredictable behaviour of the systems and a consequent negative impact on some of the parameters that characterize them. Frequency, for example, is a good indicator of system stability. Ideally, the frequency of a power system should be constant and equal to its nominal value. In the reality, however, frequency of voltage and current signals differs from these ideal conditions. As an example, the European Standard EN 50160 defines and describes the voltage characteristics of electricity supplied by public distribution networks [22]. As for the system frequency, it states that the average value measured in a window of 10 s must be:

- For systems with a synchronous connection to an interconnected system
  1. 50 Hz ± 1 % during the 99.5 % of the year.
  2. 50 Hz +4 % / -6 % during the 100 % of the time.
- For systems without a synchronous connection to an interconnected system
  1. 50 Hz ± 2 % during the 95 % of a week.
  2. 50 Hz ± 15 % during the 100 % of the time.

This means that the system usually operates in a narrow band around the nominal frequency, but also that it is possible to encounter particular occasions where the real frequency of the system is far from the nominal value. Frequency fluctuations indicate a mismatch between generators and loads. The use of DG, whose energy production is based on sources whose availability can not be guaranteed or predicted, could lead to instability of the system frequency. Another example is the impact on the regulation of voltage levels of an electrical system where the presence of DG plants, that contribute to raising the profile of the voltage of the lines on which they are installed, can cause overvoltage or undervoltage problems. In electrical systems where DG plants are present, in fact, the voltage regulation becomes more complex and can not be based solely on traditional techniques [17].

### Protection systems

Most of the traditional protections schemes of the electrical systems are based on the premise that energy flows are unidirectional. Their operation, in fact, is based on the selection of the sections of the network to isolate in functions of the maximum current. However, as already announced in the previous pages, with the diffusion of the DG, it raises the possibility of the presence of bi-directional flows from different sources and it becomes not possible to unequivocally select the section to isolate [23]. The protection system represents therefore one of the critical aspects of meshed networks. This implies the necessity of studying and using new protection algorithms whose operating modes are not based on old models of centralized power systems, but are able to accomplish their functions in the presence of a high incidence of GD, using new technologies of communication and control along with the possibility of intelligent systems based on microprocessors [24].

From what just said, it is clear that a complete and efficient use of the DG to supply the public network cannot be separated from the implementation of a complex system of monitoring, management and automation of the power systems based on WAMSs information.

# Bibliography


[1] S. Corsi and C. Sabelli, "General blackout in Italy Sunday September 28, 2003, h. 03:28:00," in *Power Engineering Society General Meeting, 2004. IEEE*, june 2004, pp. 1691 –1702 Vol.2.

[2] G. Andersson, P. Donalek, R. Farmer, N. Hatziargyriou, I. Kamwa, P. Kundur, N. Martins, J. Paserba, P. Pourbeik, J. Sanchez-Gasca, R. Schulz, A. Stankovic, C. Taylor, and V. Vittal, "Causes of the 2003 major grid blackouts in North America and Europe, and recommended means to improve system dynamic performance," *Power Systems, IEEE Transactions on*, vol. 20, no. 4, pp. 1922 – 1928, nov. 2005.

[3] C. Li, Y. Sun, and X. Chen, "Analysis of the blackout in Europe on November 4, 2006," in *Power Engineering Conference, 2007. IPEC 2007. International*, dec. 2007, pp. 939 –944.

[4] A. G. Phadke and J. S. Thorp, *Synchronized Phasor Measurements and Their Applications*. Springer Science, 2008.

[5] I. E. C. (IEC), *Instrument transformers - Part l:Current transformers*, International Standard IEC 60044-1 Std., 1996.

[6] ——, *Instrument transformers - Part 2:Inductive voltage transformers*, International Standard IEC 60044-2 Std., 1997.

[7] (2007, Feb.) Model 1133A phasor measurement specifications. [Online]. Available: http://www.arbiter.com/files/product-attachments/1133_phasor_measurement_specifications.pdf

[8] D. Novosel, K. Vu, V. Centeno, S. Skok, and M. Begovic, "Benefits of synchronized-measurement technology for power-grid applications," in *System Sciences, 2007. HICSS 2007. 40th Annual Hawaii International Conference on*, jan. 2007, p. 118.

[9] A. Abur and A. Exposito, *Power System State Estimation: Theory and Implementation*. Marcel Dekker, Inc., 2004.

[10] C. Bruno, C. Candia, L. Franchi, G. Giannuzzi, M. Pozzi, R. Zaottini, and M. Zaramella, "Possibility of enhancing classical weighted least squares state estimation with linear pmu measurements," in *PowerTech, 2009 IEEE Bucharest*, 28 2009-july 2 2009, pp. 1 –6.

[11] A. Phadke and R. de Moraes, "The wide world of wide-area measurement," *Power and Energy Magazine, IEEE*, vol. 6, no. 5, pp. 52 –65, september-october 2008.

[12] J. Tang, M. Lixia, J. Liu, C. Muscas, and A. Monti, "Impact of PMU sychronization on wide area state estimation," in *Applied Measurements for Power Systems (AMPS), 2011 IEEE International Workshop on*, sept. 2011, pp. 74 –79.

[13] G. D'Antona, C. Muscas, and S. Sulis, "State estimation for the localization of harmonic sources in electric distribution systems," *Instrumentation and Measurement, IEEE Transactions on*, vol. 58, no. 5, pp. 1462 –1470, may 2009.

[14] A. Carta, N. Locci, and C. Muscas, "GPS-based system for the measurement of synchronized harmonic phasors," *Instrumentation and Measurement, IEEE Transactions on*, vol. 58, no. 3, pp. 586 –593, march 2009.

[15] M. Jacobson and M. Delucchi, "Providing all global energy with wind, water, and solar power, part i: Technologies,energy resources, quantities and areas of infrastructure, and materials." *Energy Policy*, 2010.

[16] T. Garrity, "Getting smart," *Power and Energy Magazine, IEEE*, vol. 6, no. 2, pp. 38 –45, march-april 2008.

[17] P. Barker and R. De Mello, "Determining the impact of distributed generation on power systems. Part I-radial distribution systems," in *Power Engineering Society Summer Meeting, 2000. IEEE*, vol. 3, 2000, pp. 1645 –1656 vol. 3.

[18] "Distributed generation in liberalised electricity markets," *International Energy Agency*, 2002.

[19] G. Pepermans, J. Driesen, D. Haeseldonckx, R. Belmans, and W. Dahaeseleer, "Distributed generation: definition, benefits and issues," *Energy Policy*, vol. 33, no. 6, pp. 787–798, 2005.

[20] P. Dondi, D. Bayoumi, H. C., D. Julian, and M. Suter, "Network integration of distributed power generation," *Journal of Power Sources*, vol. 106, pp. 1–9, 2002.

[21] T. McDermott and R. Dugan, "PQ, reliability and DG," *Industry Applications Magazine, IEEE*, vol. 9, no. 5, pp. 17 – 23, sept.-oct. 2003.

[22] *Voltage characteristics of electricity supplied by public distribution systems*, European standard EN 50160 Std., 1999.

[23] J. C. Gomez and M. M. Morcos, "Coordinating overcurrent protection and voltage sag in distributed generation systems," *Power Engineering Review, IEEE*, vol. 22, no. 2, pp. 16 –19, feb. 2002.

[24] S. Brahma and A. Girgis, "Development of adaptive protection scheme for distribution systems with high penetration of distributed generation," *Power Delivery, IEEE Transactions on*, vol. 19, no. 1, pp. 56 – 63, jan. 2004.

# Chapter 2

# Synchrophasors

## 2.1 The IEEE standard on synchrophasors

The first standard for synchrophasor for power system was introduced in 1995 with the name of IEEE 1344-1995 [1]. The standard has been developed to lead to the IEEE C37.118 version, published in 2005 [2]. IEEE C37.118 concentrates on two aspects: the first one concerns the definition of the synchronized phasor measurements under steady-state conditions used in power system applications, the time synchronization and the application of a time-tags; it also concerns the provision of a method to verify measurement compliance with the standard, tests, and error limits for the test. In the second one, a data communication protocol, including message formats to assure interoperability among Phasor Measurement Units (PMUs) of different manufacturers is addressed.

The standard IEEE C37.118 has been further revised (see [3] for an introduction) to lead to two current standards: C37.118.1 IEEE standard for synchrophasor measurements for power systems and C37.118.2 IEEE standard for synchrophasor data transfer for power systems [4, 5]. The changes applied to [2] are focused, in particular, on PMUs behaviour under dynamic conditions, frequency measurement and the communication compatibility with the standards of the series IEC 61850 "Communication Networks and Systems in Substations" [6]. New limits and requirements are given for specific test cases, like amplitude and phase modulated signals or linear ramp of frequency. Step tests are adopted to describe the response of phasor estimation algorithms to transient conditions.

### 2.1.1 Synchrophasor definition

#### Static phasor model

The definition of phasor has been introduced in 1893 by Charles Proteus Steinmetz with the aim to analyse power system AC signals assuming a constant frequency [7]. However, the already mentioned need for monitoring and control of complex power networks has led to the design of distributed and coordinated measurement systems. Thus, the definition of phasor has evolved, by introducing the correlation between the measurement result (in terms of amplitude and phase) and the precise time of evaluation (time-tag), into the concept of synchrophasor. The standard [2] defines the synchrophasors as *"a phasor calculated from data samples using a standard time signal as the reference for the measurement"*. In other words, the synchrophasor is considered as a complex number representation of the fundamental frequency component of either a voltage or a current waveforms, with a time label defining the time instant for which the phasor measurement has been performed. In particular [2] considers the Universal Time Coordinated (UTC) as reference time.

Given a sinusoidal signal $x(t)$

$$x(t) = X_m \cos(\omega t + \phi) \tag{2.1}$$

where $X_m$ is the signal magnitude, $\omega = 2\pi f$ is the system pulsation and $\phi$ is the initial phase of the signal, which depends on the definition of the time scale, its synchrophasor representation is

$$\bar{\mathbf{X}} = (\frac{X_m}{\sqrt{2}})e^{j\phi} = (\frac{X_m}{\sqrt{2}})(\cos(\phi) + j\sin(\phi)) = X_r + jX_i \tag{2.2}$$

where $X_r$ and $X_i$ are real and imaginary rectangular components of the complex phasor representation, $(X_m/\sqrt{2})$ is the RMS value of the signal and $\phi$ is its instantaneous phase angle relative to a cosine function at nominal system frequency synchronized to UTC. The phase $\phi$ is defined to be 0° when the maximum of $x(t)$ occurs at the UTC time instant, and 90° when the negative zero crossing occurs at the UTC time instant (Fig. 2.1).

#### Dynamic phasor model

The old standard addresses synchrophasor measurements only in stationary conditions (both at nominal and off-nominal frequency). However, it should be considered that the assumption of steady-state conditions in real power systems is only an approximation, since the characteristics of the measured quantities (frequency, amplitude, phase, distortion, etc.) vary more or less rapidly with time. The static

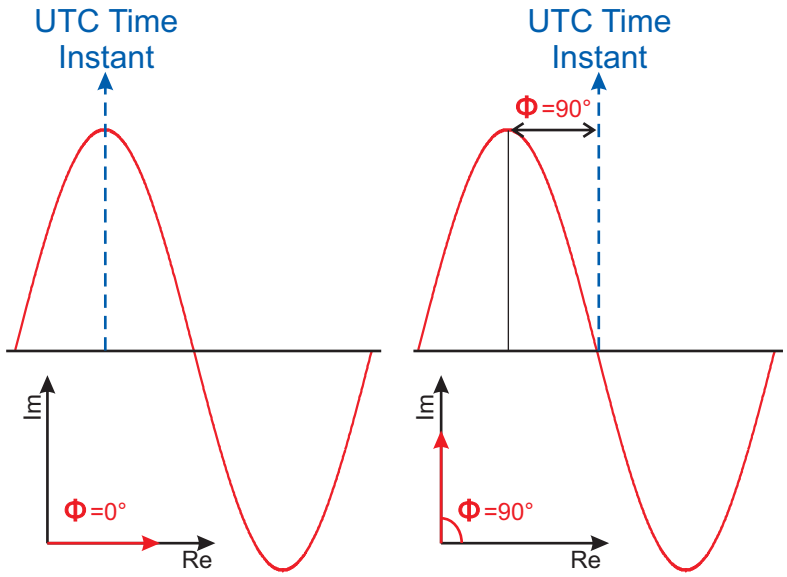


**Figure 2.1:** Synchrophasor representation of a sinusoidal signal.

model of synchropasors previously presented (see 2.2) is not suited to be used under these conditions and, as a consequence, a new model for phasor measurement under dynamic conditions has been addressed in [4]. In particular, a more general representation of a power system quantity can be obtained with a modulated sinusoidal signal $x_m(t)$

$$x_m(t) = X_m g(t) \cos(\omega_0 t + \varphi(t)), \tag{2.3}$$

where $X_m g(t)$ is the modulated signal magnitude, $\omega_0$ is the nominal system angular frequency and $\varphi(t)$ is a real function describing phase modulation. The equivalent phasor can be defined as follows:

$$\bar{\mathbf{X}}(t) = a(t)e^{j\varphi(t)} = \frac{X_m g(t)}{\sqrt{2}} e^{j\varphi(t)} \tag{2.4}$$

The continuous time phasor definition (2.4) can be translated in the following discrete time formulation:

$$\bar{\mathbf{X}}(nT_s) = a(nT_s)e^{j\varphi(nT_s)} \quad n = 0, 1, \ldots \tag{2.5}$$

where $T_s$ is the sampling period. Definition (2.4) is well suited to follow the non-sinusoidal conditions of interest, because it highlights the time changing behavior of phasor amplitude $a(t)$ and phase $\varphi(t)$. The signal (2.3) acts like a passband signal centered at frequency $f_0$ in the frequency domain: all the frequency components

inside the band are considered meaningful, whereas the components outside the band are considered as disturbances (Fig. 2.2). This model gives the dynamic reference for any synchrophasor estimation algorithm, leaving to the estimator the definition of a suitable computational procedure that allows to calculate phasors with given accuracy constraints.

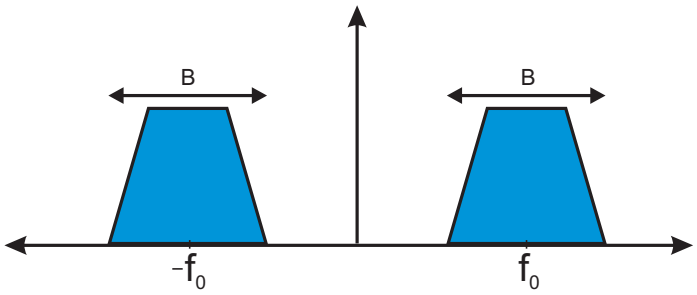


**Figure 2.2:** Qualitative behaviour of the dynamic phasor model in the frequency domain.

### 2.1.2 Synchrophasor estimation

The standards [4, 5] do not provide any detail about algorithms for the evaluation of synchrophasors, leaving free choice to manufacturers. However, it gives precise information about the time-tag, management and data transmission processes, to ensure interoperability among a large amounts of PMUs data from different manufacturers. Moreover, [5] defines the time-tag as the time of the theoretical phasor that the estimated phasor represents and it corresponds to the time of the centre of the estimation window. It has to be expressed as

$$\text{Time-tag} = \text{SOC} + \text{Fraction-of-Second}/\text{T}_{\text{BASE}} \tag{2.6}$$

where SOC is the number of integer second counted starting from midnight 01-Jan-1970, Fraction-of-Second is a 24-bit integer number which represents the actual fraction of second and $\text{T}_{\text{BASE}}$ is an integer which express the resolution of the time-tag.

The standards also define the reporting rate $F_s$ as the number of synchrophasor evaluations per second that each PMU shall support. Values of reporting rates depending on the system nominal frequency are reported in Table 2.1.

By observing the sinusoid at intervals $1/F_s$ which are integer multiples of its period $T = 1/f$ ($1/F_s = nT$, with $n = 0, 1, 2, ...$), the corresponding synchrophasors $(\mathbf{X_0}, \mathbf{X_1}, \mathbf{X_2}, ...)$ are characterized by constant amplitudes and phases. Otherwise, when the observation interval $1/F_s$ is not multiple of the signal period, the estimated

**Table 2.1:** Required PMU reporting rates

| System Frequency | 50 Hz | | | 60 Hz | | | | | |
|---|---|---|---|---|---|---|---|---|---|
| Reporting Rates $F_s$ (frame per second) | 10 | 25 | 50 | 10 | 12 | 15 | 20 | 30 | 60 |

synchrophasors show continuous phase changes with step equal to $2\pi(\frac{F_s - f}{f})$. Fig. 2.3 shows an example of a sinusoidal signal with frequency $f$ observed with intervals multiple of $1/F_s$ with $1/F_s \neq nT$.

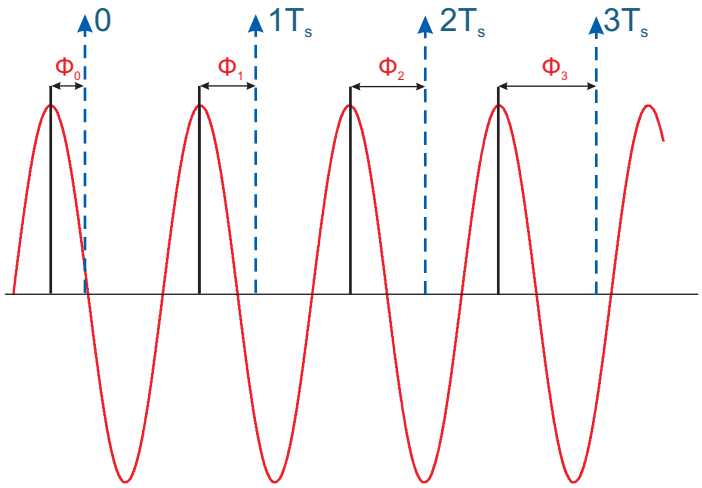


**Figure 2.3:** Synchrophasor estimation with observation frequency $F_s \neq f$.

As for the frequency measurement, [4] states that both the frequency and the Rate Of Change Of Frequency (ROCOF) shall be measured. The estimated frequency of the system $f(t)$ is expressed as

$$f(t) = \frac{1}{2\pi} \frac{d(\Psi(t))}{d(t)} \tag{2.7}$$

where $\Psi(t)$ is the argument of the cosine in 2.3

ROCOF is reported as the derivative $d(f(t))/d(t)$ of the frequency $f(t)$ respect the time $t$.

### 2.1.3 Accuracy limits

As for the accuracy, [4] defines the Total Vector Error (TVE) as a vectorial difference between the measured and theoretical value of the phasor, expressed as a fraction of

the magnitude of the theoretical one. Considering the synchrophasor representation in (2.4), the TVE can be expressed as follow:

$$\begin{aligned} \mathrm{TVE}(n) &= \sqrt{\frac{(\tilde{X}_r(n) - X_r(n))^2 + (\tilde{X}_i(n) - X_i(n))^2}{X_r(n)^2 + X_i(n)^2}} \\ &= \frac{|\tilde{a}(n)e^{j\tilde{\varphi}(n)} - a(n)e^{j\varphi(n)}|}{|a(n)|} \end{aligned} \tag{2.8}$$

where $X_r(n) + jX_i(n)$ is the phasor representation of the reference sinusoidal signal and $\tilde{X}_r(n) + j\tilde{X}_i(n)$ is the measured synchrophasor at the instant $n$.

The standard [4] requires TVE to be maintained below a threshold limit value depending on the type and characteristics of the measured signal, the used reporting rate and other parameters. It also defines the tests to be performed under steady-state and dynamic conditions for different compliance verifications, with reference conditions and influence quantities defined for two compliance levels (Level P and Level M). Class P is characterized by a faster response but narrower operating range and less out-of-band signal filtering, whereas class M guarantees more precise measurements with better filtering and a wider range of performance.

In table 2.2 are reported the steady-state synchrophasor measurement requirements.

Moreover, three different test cases (modulation, ramp and step tests) are identified for PMU performance evaluation under dynamic conditions:

- The modulation tests are used to determine measurement bandwidth by simulating oscillation in the power system. The amplitude and/or the phase of power signal are modulated by means of a sinusoidal signal that is varied in frequency. The positive sequence test signal can be expressed as follow:

$$X_1 = X_m[1 + k_x \cos(2\pi f_m t)] \cos(2\pi f_0 t + k_a \cos(2\pi f_m t - \pi)) \tag{2.9}$$

  where $f_m$ is the modulation frequency, and $k_x$, $k_a$ are respectively the amplitude and phase modulation factors. Table 2.3 show the synchrophasor measurement bandwidth requirements.

- In the frequency ramp test, the reference signal undergoes a linear change of frequency at a constant rate of change. The positive sequence test signal can be expressed as follow:

$$X_1 = X_m \cos(2\pi f_0 t + \pi R_f t^2) \tag{2.10}$$

**Table 2.2:** Steady-state synchrophasor measurement requirements

| Influence quantity | Reference condition | Minimum range of influence quantity over which PMU shall be within given TVE limit | | | |
|---|---|---|---|---|---|
| | | P class | | M class | |
| | | Range | Max TVE (%) | Range | Max TVE (%) |
| Signal frequency range—$f_{dev}$ (test applied nominal + deviation: $f_0 \pm f_{dev}$) | $F_{NOMINAL}$ | ±2.0 Hz | 1 | ± 2.0 Hz for $F_s$<10<br>± $F_s$/5 for 10≤$F_s$<25<br>± 5.0 Hz for $F_s$≥25 | 1 |
| The signal frequency range tests above are to be performed over the given ranges and meet the given requirements at three temperatures: T = nominal (~23 ºC), T = 0 ºC, and T = 50 ºC | | | | | |
| Signal Magnitude Voltage | 100% rated | 80% to 120% rated | 1 | 10% to 120% rated | 1 |
| Signal Magnitude Current | 100% rated | 10% to 200% rated | 1 | 10% to 200% rated | 1 |
| Phase Angle with $\| f_{IN} - f_0 \|$<0.25 Hz | Constant or slowly varying angle | ±π radians | 1 | ±π radians | 1 |
| Harmonic distortion | <0.2% (TDH) | 1%, each harmonic up to 50th | 1 | 10%, each harmonic up to 50th | 1 |
| Out-of-band interfering signal, at frequency $f_i$ where $\|f_i - f_0\| > F_s/2$, $F_s$ = phasor reporting rate, $f_0$ = Fnominal | <0.2% of input signal magnitude | | | 10% of input signal magnitude for Fs≥10. No requirement for Fs < 10. | 1.3 |

where $R_f = d(f)/d(t)$ is the frequency ramp rate in Hz/s. The purpose of this type of tests is to simulate the effects of a sudden system imbalance caused by a separation or a loss of load or generation and to test the tracking capability of the PMU. Table 2.3 reports the synchrophasor performance requirements under frequency ramp tests.

- Step tests, both in magnitude and phase, represent a transition between two steady states are used to simulate various power switching events of the network and to test response time, delay time, and overshoot in the measurement of the PMUs. The test signal can be expressed as follow:

$$X_1 = X_m[1 + k_x f_1(x)] \cos(2\pi f_0 t + k_a f_1(t)) \tag{2.11}$$

where $f_1(t)$ is a unit step function, $k_x$ is the magnitude step size and $k_a$ phase step size. In table 2.5, phasor performance requirements for input step change are reported.

**Table 2.3:** Synchrophasor measurement bandwidth requirements using modulated test signals

| Modulation Level | Reference condition | Minimum range of influence quantity over which PMU shall be within given TVE limit | | | |
|---|---|---|---|---|---|
| | | P class | | M class | |
| | | Range | Max TVE (%) | Range | Max TVE (%) |
| $k_x$ = 0.1, $k_a$ = 0.1 radian | 100% rated signal magnitude, $F_{nominal}$ | Modulation frequency 0.1 to lesser of $F_s$/10 or 2.0 Hz | 3 | Modulation frequency 0.1 to lesser of $F_s$/5 or 5 Hz | 3 |
| $k_x$ = 0, $k_a$ = 0.1 radian | 100% rated signal magnitude, $F_{nominal}$ | | 3 | | 3 |

**Table 2.4:** Synchrophasor performance requirements under frequency ramp tests

| Test signal | Reference condition | Minimum range of influence quantity over which PMU shall be within given TVE limit | | | |
|---|---|---|---|---|---|
| | | Ramp rate (Rf) (positive and negative ramp) | Performance class | Ramp range | Max TVE (%) |
| Linear frequency ramp | 100% rated signal magnitude, and $F_{NOMINAL}$ at start or some point during the testl | ±1.0 Hz/s | P class | ±2 Hz | 1 |
| | | | M class | Lesser of ±($F_s$/5) or ±5 Hz | 1 |

### 2.1.4 Synchronization requirements

The standard [4] says that the synchronizing source shall have sufficient availability, reliability, and accuracy to meet power system requirements. This means that a synchronization source should ensure continuous uninterrupted availability and be accessible to all sites among which the data is to be collected and compared. Several synchronization solutions are available and can be used to synchronize different PMUs. As an example, Global Positioning System (GPS) is, at the moment, the most used technology for the synchronization of PMUs: its widespread availability makes it possible to obtain, at each point of the tested system, a clock signal synchronized with the one generated in other remote places. In Chapter 3, several synchronization solutions will be described.

**Table 2.5:** Phasor performance requirements for input step change

| Step change specification | Reference condition | Minimum range of influence quantity over which PMU shall be within given TVE limit | | | | | |
|---|---|---|---|---|---|---|---|
| | | P class | | | M class | | |
| | | Response time (s) | \|Delay time\| (s) | Max overshoot/ undershoot | Response time (s) | \|Delay time\| (s) | Max overshoot/ undershoot |
| Magnitude = ± 10%, $k_x$ = ± 0.1, $k_a$ = 0 | All test conditions nominal at start or end of step | $1.7/f_0$ | $1/(4F_s)$ | 5% of step magnitude | See Table 11 of IEEE C37.118.1 | $1/(4F_s)$ | 10% of step magnitude |
| Angle ± 10°, $k_x$ = 0, $k_a$ = ± π/18 | All test conditions nominal at start or end of step | $1.7/f_0$ | $1/(4F_s)$ | 5% of step magnitude | See Table 11 of IEEE C37.118.1 | $1/(4F_s)$ | 10% of step magnitude |

### 2.1.5 Data communication protocol

The standard [5] defines a data communication protocol and format of messages in order to ensure the interoperability among PMUs from different producers and among PMUs and other devices like Phasor Data Concentrators (PDC) for real-time data transmission. In [5], it is stated that any communication system or media which guarantees the message frames transmission in their entirety as they are specified may be used. Four types of message format to and from a PMU for use in real-time communication of phasor data have been addressed: data, configuration, header and command messages.

All the messages have some fields in common: they all start with the same five words (SYNC, FRAMESIZE, IDCODE, SOC, FRACSEC) and finish with the same word (CHK). Fig. 2.4 shows an example of a transmission frame.

- SYNC (2 bytes) provides synchronization and frame identification.
- FRAMESIZE (2 bytes) reports the total number of bytes in the frame.
- IDCODE (2 bytes) identifies device sending and receiving messages.
- SOC (4 bytes) is the first part of the time-stamp of the frame. It expresses the integer number of seconds counted starting from midnight 01-Jan-1970.
- FRACSEC (4 bytes) is divided into two components: a 24-bit integer that is the actual Fraction-of-Second count and an 8-bit Time Quality flag.
- CHK (2 bytes) is a cyclic redundancy check which uses the generating polynomial $X^{16} + X^{12} + X^5 + 1$.

The grey fields may change depending on the type of message.

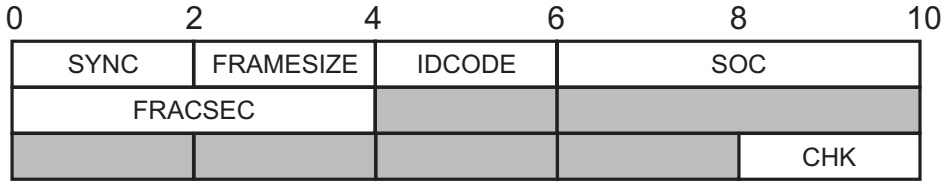


**Figure 2.4:** Example of a transmission frame

### Data frame

Data messages carry the measurements made by a PMU. After the already mentioned six fields that are in common with all the type of messages, the data frame is characterized by the phasor data fields. The number $n_{ph}$ of phasors data depends on the numbers of acquired signals. If a PMU is acquiring three voltage and three current signals, then there will be six phasors in each data frame ($n_{ph} = 6$). It is possible to choose to use 4 or 8 bytes to represent each phasor inside the data frame, depending on the fixed 16-bit or floating-point format used, as indicated by the configuration frame. After the phasor values there are the frequency and the rate of change of frequency (ROC) values, with a length of 2 or 4 bytes, depending again on the indicated format representation. Then, it is possible to find $n_{an}$ analog data, which can have different sizes (2 or 4 bytes each) and $n_{dig}$ digital data values (2 bytes), where $n_{an}$ and $n_{dig}$ are the number of analog and digital data sent in the data frame. The last field is the check word (CHK), which has fixed length (2 bytes). As a consequence, supposing that the data format configuration is the same for each field in the same frame, the dimension of each data frame can be estimated as $22 + (n_{ph} \times 4) + (n_{an} \times 2) + (n_{dig} \times 2)$ bytes, if the PMU is configured to use the fixed 16-bit format, or as $22 + (n_{ph} \times 8) + (n_{an} \times 4) + (n_{dig} \times 2)$ bytes, if the PMU is configured in floating-point format. Fig. 2.5 shows an example of data frame in the case of $n_{ph} = 3$, $n_{an} = 2$ and $n_{dig} = 1$ and fixed 16-bit format configuration. In this case, the size of the message is 40 bytes.

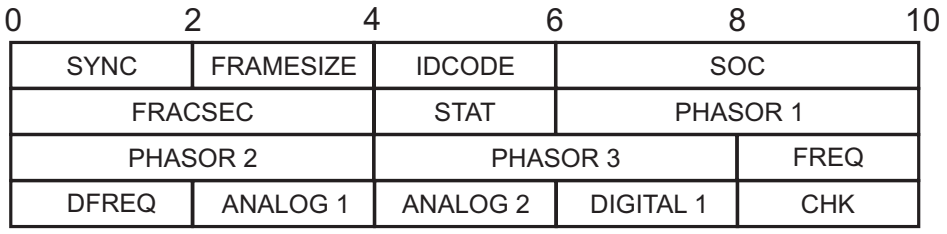


**Figure 2.5:** Example of data frame

### Configuration frame

Configuration Frame is a machine-readable message used to describe the PMU data and to provide calibration factors. Three types of configuration frame exist: CFG-1, which indicates the possible measurements that a PMU may perform, CFG-2, which indicates measurements currently being performed and transmitted in the data frame, and CFG-3, which has the same functions as of CFG-2 but with added information and flexible framing.

### Header frame

Header Frames is a human-readable message used to transfer descriptive information provided by the user. It contains information about the PMU, the data sources, scaling, algorithms, filtering, or other related information.

### Command frame

Command Frame is a machine-readable message sent by the control system and used for control or configuration purposes.

### PC37.118.2: Data exchange and IEC 61850 compatibility

IEC 61850 series refer specifically to communication networks and systems in electric substations and they define services and data exchange method independently from the lower layer protocols, introduce an object model description for equipment and functions and map the services to communication protocols. Since the IEC 61850 series are now taken as a de facto reference in all those circumstances where an electric system is managed with the help of inter-communicant IEDs (e.g. active networks for Distributed Generation management, smart grids, etc.), it seems clear that it is necessary an effort to integrate the synchrophasor measurement requirements and transportation over the IEC 61850 system. The old standard did not specify a communication protocol or medium; it only defined a data format and content specification. Moreover, the content specification provided information about the status of the measurement system, but did not provide remote controls, configuration methods, communication mapping and operation. All these missing requirements are fundamental to assure to merge C37.118 requirements into the IEC 61850 systems and are considered in [5], which represents the first step toward a completely harmonization of the standard IEEE C37.118 with IEC 61850. At the same time, the IEC 61850 working group (WG10) is working to a project for the development of synchrophasor profile in IEC 61850 series. According to [3], this process will be partitioned in five parts (use cases, communication requirements, modelling,

configuration, communication mapping) and will be published as Technical Report IEC 61850-90-5.

## 2.2 Problems related to the TVE definition

TVE blends together two possible sources of error: magnitude and phase. Moreover, the last one includes the contributions arising from both the phase error of the measurement device and the possible lack of synchronization. Ideally, if only one cause is present, the 1 % limit would be reached for either a magnitude error equal to 1 %, a phase shift of 10 mrad or a lack of time synchronization equal to 31.8 µs at 50 Hz (26.5 µs at 60 Hz).

This representation, despite the advantage of being extremely compact, may lead to some misunderstanding in those applications that require strict constraints on a single aspect [8]. In WAMS applications, for instance, the most useful information provided by PMUs is often represented by the phase of the measured synchrophasors. The value of TVE, which aggregates different terms, does not permit to understand directly if constraints on phase and/or synchronization are respected. In fact, a high value of TVE may correspond to a high value of the magnitude error and a low value of the phase differences of the phasors and, consequently, it may erroneously suggest poor synchronization. From another point of view, a high value of magnitude error may use the majority of the TVE budget leaving little margins for synchronization uncertainty, which otherwise might be acceptable.

Fig. 2.6 shows an example of phasors involved in TVE estimation (the phase and amplitude differences in the figure have been enlarged for an easier viewing). In the picture 2.6-a, the two synchrophasors have same module (magnitude difference equal to zero) and a phase difference equal to $\Delta\varphi = 8.7$ mrad. In this case, even if the TVE is below the 1 % limit (TVE= 0.87 %), the phase error is equivalent to a synchronization error of about 28 µs (assuming system frequency of 50 Hz), which can be incompatible with the synchronization requirements of certain application. In the picture (b), the difference between the magnitudes of the two phasors is 0.9 %, whereas the phase difference is equal to zero. In this second case the TVE is close to the 1 % limit (TVE = 0.9 %) but all the error budget is consumed by the magnitude uncertainty leaving a thin phase difference margin.

For clarity, Fig. 2.7 presents the TVE dependence on the magnitude and phase deviations. As an example, if half of the 1 % budget of the TVE was assigned to the magnitude difference, the margin of phase difference would be reduced to 8.72 mrad, which can be too high for some applications whose correct behaviour depends on strictly accurate phase measurements. Nevertheless, the presence of so many terms makes more difficult the interpretation of such a method to analyze

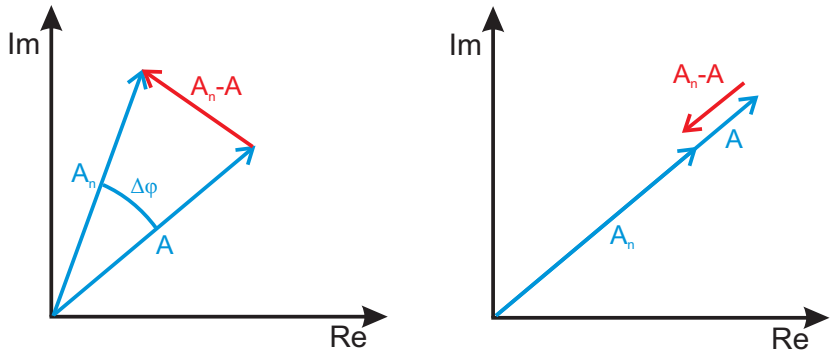


**Figure 2.6:** Examples of problems involved in TVE estimation

measurement accuracy, especially for those applications where some constraints are more significant than others.

When phase errors are not too large, the TVE can be approximated by:

$$\mathrm{TVE} \simeq \sqrt{(\Delta a_{\mathrm{rel}})^2 + \Delta\varphi^2} = \sqrt{|\frac{\tilde{a} - a}{a}|^2 + (\tilde{\varphi} - \varphi)^2} \tag{2.12}$$

where the phase error is expressed in radians. In some cases, then, it could be useful to divide the two components (amplitude and phase) and analyse them as separate indices to emphasize certain results. In particular, the percent amplitude error and the phase error expressed in centiradians can be compared directly with TVE % results.

Alternatively, it can be convenient to use alternative indices more suitable to express measurement performance in particular occasions. For instance, to describe the influence of a step signal onto the phasor estimation the TVE cannot be used because phasor can not be defined at the instant of abrupt change. For this type of conditions, it can be used the TVE settling time, that can be defined as the time difference between the last and the first sample for which the TVE results bigger than a threshold $H_T$ and can be expressed as:

$$\Delta t_R = \sup_t\{\mathrm{TVE}\,\% > H_T\} - \inf_t\{\mathrm{TVE}\,\% > H_T\} \tag{2.13}$$

The TVE settling time represents the duration of the anomalous behaviour of the estimator and gives a synthetic index to describe the algorithm behaviour in a fast changing context. It is obviously possible to define an analogous index for percent amplitude error and phase error, with specific thresholds and for specific analyses [9]. Also the Transient Monitor (TM) can be used as alternative index [10].

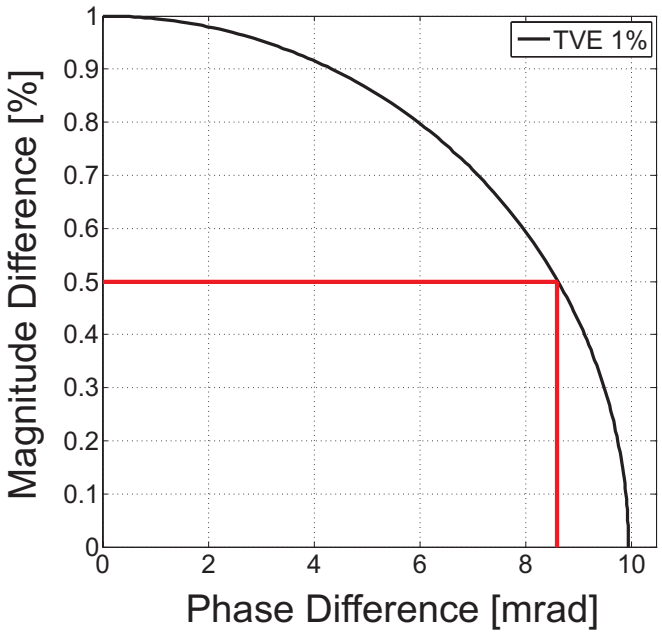


**Figure 2.7:** Example of data frame

It is conceived to provide a measure of the quality of the estimated phasors, in terms of the difference between the actual waveform and the one reconstructed by the synchrophasor. The TM is expressed as follow:

$$\mathrm{TM} = \frac{\sum_{k=0}^{N-1} |x_k - \hat{x}_k|}{N} \tag{2.14}$$

where $x_k$ is the k-th sample of the acquired signal,$\hat{x}_k$ is the k-th sample of the signal reconstructed using the measured synchrophasor, and $N$ is the number of samples used to evaluate the synchrophasor.

# Bibliography


[1] *IEEE Standard for Synchrophasors for Power Systems*, Institute of Electrical and Electronics Engineers IEEE 1344-1995 (R2001), Jan. 1995.

[2] *IEEE Standard for Synchrophasors for Power Systems*, IEEE Std C37.118-2005 (Revision of IEEE Std 1344-1995), 2006.

[3] K. Martin, "Synchrophasor standards development - IEEE C37.118 & IEC 61850," pp. 1–8, Jan. 2011.

[4] "IEEE standard for synchrophasor measurements for power systems," *IEEE Std C37.118.1-2011 (Revision of IEEE Std C37.118-2005)*, pp. 1 –61, 28 2011.

[5] "IEEE standard for synchrophasor data transfer for power systems," *IEEE Std C37.118.2-2011 (Revision of IEEE Std C37.118-2005)*, pp. 1 –53, 28 2011.

[6] *IEC Standard for Communication network and systems in substations*, IEC Standard 61850 Std., 2003.

[7] C. P. Steinmetz, "Complex quantities and their use in electrical engineering," in *Proceedings of the International Electrical Congress.* AIEE, Aug. 1893, pp. 33–74.

[8] M. Lixia, C. Muscas, and S. Sulis, "On the accuracy specifications of phasor measurement units," in *Instrumentation and Measurement Technology Conference (I2MTC), 2010 IEEE*, may 2010, pp. 1435 –1440.

[9] P. Castello, C. Muscas, and P. A. Pegoraro, "Performance comparison of algorithms for synchrophasors measurements under dynamic conditions," in *Applied Measurements For Power Systems (AMPS), 2011 IEEE International Workshop on*, 2011.

[10] A. G. Phadke and J. S. Thorp, *Synchronized Phasor Measurements and Their Applications.* Springer Science, 2008.

# Chapter 3

# Clock Synchronization

The critical role of PMU based applications makes of fundamental importance the evaluation of correctness and trustworthiness of the information on which such actions are based. In particular, synchronization is one of the key issues in applications that make use of distributed measurement system data: the synchronization requirements of those applications lead to the need of highly accurate clock settings.

WAMSs can achieve significant extensions, up to continental dimensions. Each oscillator of each measurement device is affected by an independent frequency drift. the capability to correct that drift and to keep all the clocks synchronized is a fundamental aspect to assure high temporal traceability of collected data. The required level of accuracy of synchronization critically depends on the applications that use the data generated by IEDs and it can vary from system to system: typical synchronization specifications for protection and control systems range from milliseconds, for breaker operations and event reconstruction [1], to microseconds, for synchrophasor measurements (see [2–6]), to a few hundreds of nanoseconds, for fault location applications based on travelling time of the waves [1, 6, 7].

Several synchronization systems exist, differing from each other in terms of functional features, complexity, performance and costs. The terrestrial synchronization systems, for example, are widely used for a multitude of applications. They are characterized by the widespread transmission of signals through the atmosphere (DCF77 based synchronization systems) or through the use of appropriate equipment as controlled optic fibers. The poor accuracy of the first and the limited distribution and high costs of the second, make them not suitable for the synchronization of measuring instruments. On the contrary, the satellite synchronization systems currently appear to be the only used system to provide a time reference with sufficient availability and accuracy for most distributed monitoring and control applications in power systems. However, network synchronization systems are under observation and could be successfully used for the synchronization of distributed measuring

instruments.

In the following, a comparative analysis of the satellite synchronization and the network synchronization technologies is carried out and, for each, the main features and synchronization accuracy are illustrated.

## 3.1 Satellite Synchronization System

Nowadays, satellite systems have a key role in any field of science and technology, and have become an integral part of everyday life. Moreover, satellite systems have two important characteristics that make them suitable to be used for synchronizing clocks scattered across a wide geographical area: the quality and coverage of synchronization. In fact, a satellite-based synchronization system can offer a worldwide availability that makes it possible to obtain, at each point of the earth, a clock signal synchronized with an accuracy that may reach the order of tens of nanoseconds. In recent years there has been a growing presence in the market of devices based on satellite-related technology. These devices allow any user to determine with a good degree of accuracy some important information, such as the geographical position, altitude compared to sea level and the synchronization signal referred to Universal Time (UTC, Coordinated Universal Time). In addition, thanks to technological progress, several applications have been developed, some of them only for the military market, others accessible to the public:

- Synchronization of communications networks and devices;
- Monitoring and control for aviation and marine;
- Remote piloting of vehicles of different types;
- Location of suspected;
- Surveillance through electronic bracelets;
- Geodetic, geophysical and cartographic measurements;
- Medical surveillance applications;
- Applications in anti-theft systems and in services of protection;
- Mobile phone application;

### 3.1.1 Satellite System Functioning

Without loss of generality, it is possible to say that the functioning of a satellite system is based on the measurement of travel time of a signal transmitted from three or more satellites and received by terrestrial receivers. Each satellite is equipped with high accuracy clocks and is continuously monitored by terrestrial control stations. Also each terrestrial receiver is equipped with an internal clock. But in this case, the quality of the performance assured by the clock depends on the type and the class of the receiver. The signal continuously transmitted by the satellites contains, among other information (like orbital information, satellite status etc.), the time the signal has been transmitted. By using its internal clock, a terrestrial receiver is able to generate the time of arrival of the signal to estimate its travel time as a difference between time of arrival and time of transmission and, knowing the speed of propagation of electromagnetic waves, to calculate its distance from the satellite. The set of points equidistant from the position of the satellite has the shape of a sphere, whose intersection with the terrestrial surface, as a first approximation, generates a circumference (see Fig. 3.1).

In the ideal case (perfect estimation of the distances between the receiver and satellites), assuming the altitude of the receiver is known, three satellites are needed to precisely estimate the position of the receiver. In the real case, the three circumferences generated by the intersections of the three spheres with the surface of the earth, do not intersect in a single point. They define a triangle, whose area is proportional to the uncertainties of the estimation of the distances between terrestrial receiver and satellites, and mainly depends on the quality of the receiver clock. To reduce the uncertainty in the distance estimation, usually receivers use four or more satellites to obtain both the location of the receiver and correct time by solving a system of four equations in four variables: latitude, longitude, altitude and time signal. In fact, even if three satellites should be enough to individuate the position since space has three dimensions and a position near the Earth's surface can be assumed, even a very small clock error multiplied by the very large speed of propagation of satellite signals (speed of light) results in a large positional error. It seems clear then, that by using four or more satellites, each receiver is able to continually update its internal clock to the very precise clocks of the satellites and correct the drift, thus ensuring a high synchronization.

### 3.1.2 Global Positioning System

The NAVISTAR-GPS (Navigation System Time And Ranging Global Position System) also known as GPS, is the results of a project conducted by the U.S. Department of Defense, and stared in the second half of the sixties [8]. It is now maintained by

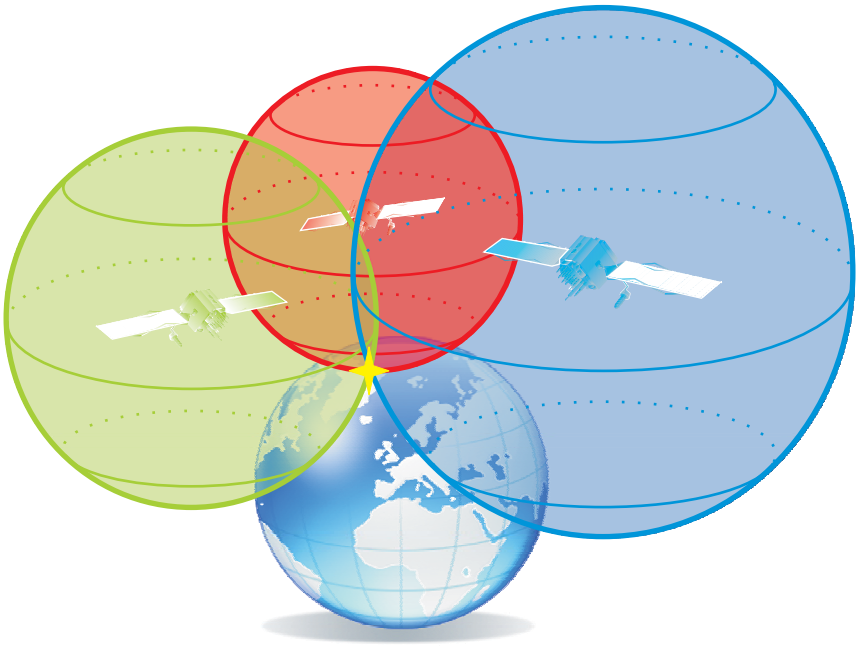

**Figure 3.1:** Example of satellite system functioning

the United States government and freely accessible by anyone with a GPS receiver with some technical and accuracy limitations, which are only removed for military use. The overall configuration of the GPS system can be seen as the set of three subsystems:

- Space segment;
- Control segment;
- User segment;

### Space Segment

The space segment consists of a constellation of 31 satellites, plus 3 satellites that can be reactivated if needed, which orbit 20200 $km$ from Earth's surface. The GPS system has been designed in order to ensure the availability of at least 24 GPS satellites, for the 95 % of the time. Before 2011, only 24 satellite were considered as part of the core constellation which was organized into six equally-spaced orbital planes at an angle of 55° to the equatorial plane, each containing four satellites evenly distributed over the orbital plane of belonging. This arrangement ensured that there are at least four satellites in view from virtually any point of the planet. In 2011,

however, three satellites were added to the core constellation and six satellites were repositioned, so that GPS now effectively operates as a 27-satellites constellation with improved coverage in most parts of the world. The satellites used at the time, are part of the block II, launched in 1989. They are equipped with four oscillators, two rubidium and two caesium, which play the role of atomic clocks and are constantly monitored by the control segment.

### Control Segment

The main functions of the GPS control segment are to track the GPS satellite units, monitor their transmissions, perform analyses, send commands and data to the constellation and supervise the operation of their watches, making the required corrections. It can be seen as a global network of ground facilities organized as follows (the locations of these facilities are shown in Fig. 3.2):

- 1 master control station;
- 1 alternate master control station;
- 12 command and control antennas;
- 16 monitoring sites;

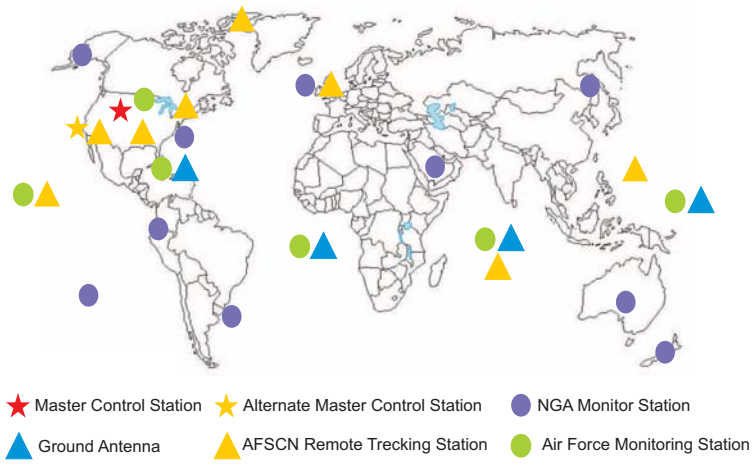


**Figure 3.2:** Control segment representation

The master control station is in Colorado and its tasks are to monitor the system and to provide command and control of the GPS constellation. Monitor stations track the GPS satellites, collect atmospheric data, range/carrier measurements, and

navigation signals and they send everything to the master control station that uses those information to correctly operate. Ground antennas are used to communicate with the GPS satellites for command and control purposes.

### 3.1.3 User Segment

The user segment is composed of ten of millions of end users including both military and civil. To access the information available from GPS, users must be equipped with receiving devices, available on different market segments and with different benefits depending from system to system, which allow them to obtain and display information about position and timing. A GPS receiver can be seen as a special radio receiver tuned to the frequencies used by the satellite system, with decoding and signal processing capabilities and with an internal memory for data storing. They are generally composed by an antenna, used to receive the satellite signals, a decoder for the interpretation of signals, a microprocessor used to elaborate the information contained in the messages, an oscillator (typically quartz) whose quality and accuracy depend on the market segment of the receiver, an internal physical memory and a software to let the user access the data and configure the device.

It is possible to classify the GPS receivers in two main families:

- Sequential receivers: have a single channel for the pursuit of at least four satellites to sequentially determine position. These receivers offer the advantage to be cheap, but they should not be used in cases where processing speed is an important requirement (real-applications time);
- Multi-channel receivers: have more channels for tracking satellites, each of which demodulates the signal and performs a distance measurement. These receivers are more expensive but they are faster and then suitable to be used for applications that require high dynamic and, as a consequence, to be integrated in measurement devices that need high synchronization accuracy and availability (e.g. PMU).

In addition to GPS, other systems are used by other countries or under development. The Russian GLObal NAvigation Satellite System (GLONASS), for example, has an history similar to that of the GPS. It is the result of military researched and, during his first years of life, it has been used by only the Russian military, until it was made fully available to civilians in 2007 [9]. Also the Chinese Compass navigation system, is now operative since December 2011 with coverage of China and partial coverage of adjacent countries. Among the systems under development,

there are the planned European Union Galileo positioning system (see [10]) and the Indian Regional Navigational Satellite System.

## 3.2 Network Synchronization System

As shown in the previuos Section, currently the GPS is commonly used to provide a time reference with sufficient availability and accuracy (in the order of tens of nanoseconds or even less) for most distributed monitoring and control applications in power systems. Its widespread availability makes it possible to obtain, at each point of a WAMS, a clock signal synchronized with the one generated in other remote places. However, this type of systems has also some drawbacks. Equipping each measurement device of a substation with a dedicated GPS receiver can be an optimal solution from a technical perspective, but can be impractical from the economic point of view. In addition, there is a reliability problem related to the GPS receiver of a measurement device: if for some reason it loses the signal, it will be unable to offer backup solutions to ensure synchronization. Therefore the data of the instrument which has lost synchronization could not longer be used.

In the scientific literature, several possible alternative synchronization solutions can be found. In particular, the option considered in this thesis exploits the possibility of distributing an accurate time reference by means of communication networks and specific network synchronization protocols. This solution appears particularly suited for those substations where the series of IEC 61850 standards has been introduced [11]. These standards present significant innovations in the communication among the several electronic devices that co-exist and co-operate for Substation Automation System (SAS) purposes in a modern electric substation or in an active distribution network. In particular, the Standard IEC 61850-9-2 (see [11]) practically indicates Ethernet as a preferred solution, thus offering an optimal support to use network synchronization protocols in electric power plants.

The remainder of this Section describes the main features of the synchronization network protocol over Ethernet currently available: Network Time Protocol (NTP) and Precision Time Protocol (PTP).

### 3.2.1 Network Time Protocol

Standard NTP over Ethernet is used to synchronize clocks over packed switched network with variable propagation delay and provides a time accuracy at the millisecond level, which is enough for processes that are not time critical [12, 13]. It was developed in 1988 at the University of Delaware (United States) and is one of the oldest protocols still in use, arrived recently in its fourth version. This sys-

tem is capable of continuously maintain synchronization among different nodes in a completely automatic way. These characteristics make it suitable for both synchronization of a single computer or an entire Wide Area Network (WAN). The operation of the NTP is based primarily on a hierarchical semi-layered structure of clock sources willing to numbered levels called strata as shown in Fig. 3.3, where blue arrows represent direct connections, whereas red arrows represent network connections. The number of the level indicates the distance from the reference clocks which are always in stratum 0:

- Stratum 0 is the stratum which contains the reference clocks such as atomic (caesium, rubidium) clocks, GPS clocks or other radio clocks. The clocks are not integral part of the network, but are usually connected to computers of stratum 1 and synchronize them by means of Pulse Per Second (PPS) signal.
- Stratum 1 is composed by computers that are directly connected with the reference clocks and with computers of Stratum 2. These computers act as servers for computers of level 2 and communicate with them using NTP messages.
- Stratum 2 is composed by computers that send NTP requests to Stratum 1 servers. Normally, they use more than one server of level 1 as a reference and, by means of an exchange of NTP messages they are able to choose the most accurate among the reference computers. Computers of strata lower then the second employ the same NTP functions of peering and data sampling of Stratum 2 and can themselves act as servers for lower strata. NTP supports up to 256 levels depending on the used version.

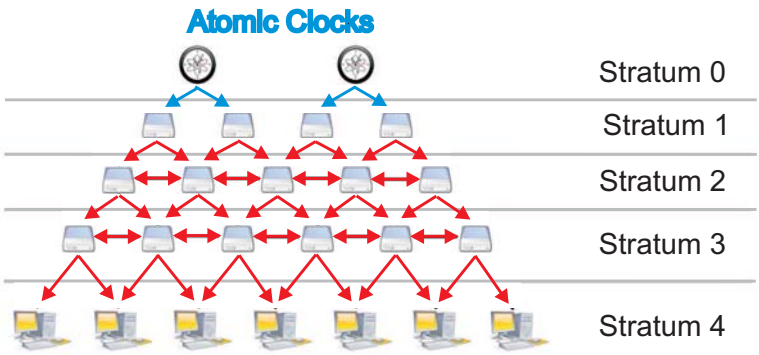


**Figure 3.3:** NTP architecture representation

The synchronization accuracy depends on several factors, like quality of reference clocks, server and client clock, network traffic conditions and dimension of the

network. Anyway, intuitively it is possible to say that the synchronization accuracy of a clock decreases with the separation between its layer and Layer 1. The synchronization performance can vary from 10 msec for WAN up to 200 nsec for LAN during optimal conditions.

### Clock Synchronization Algorithm

The Clock Synchronization Algorithm of NTP is based on the exchange of non-periodic massages between NTP servers and a clients. A client, in fact, is able to estimate the synchronization difference between its clock and the reference one and to correct it, by estimating round-trip delay time $\gamma$ value and the offset $\theta$ value based on 64-bit (32-bit seconds part and a 32-bit fractional second part) time-stamps of the exchanged messages with the server. In Fig 3.4, the operations between a NTP client and server are shown schematically.

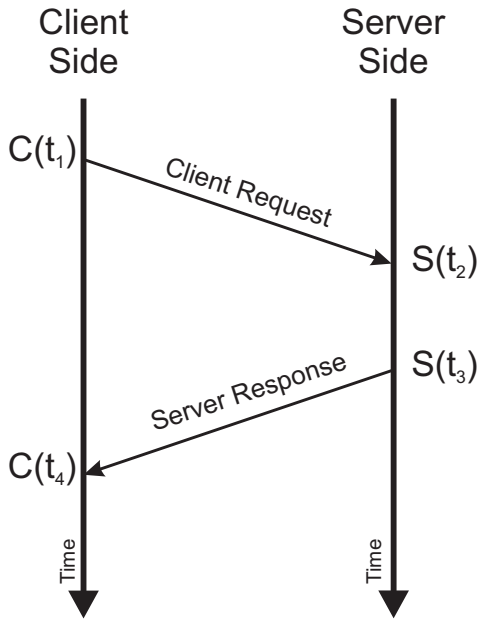


**Figure 3.4:** NTP clock synchronization algorithm

Values of $\gamma$ and $\theta$ are estimated by using the four time-stamps: $C(t_1)$ is the transmission time of the request packet send from the client C to the server S, $S(t_2)$ is the reception time of the request packet received by the server, $S(t_3)$ is the transmission time of the response packet transmitted from the server to the client and $C(t_4)$ is the reception time of the response packet received by C. Each message contains the last three NTP time-stamp, while the fourth one is calculated when the message return to the client.

Value of $\gamma$ and $\theta$ are computed as follow:

$$\gamma = (C(t_4) - C(t_1)) - (S(t_3) - S(t_2)) \tag{3.1}$$

$$\theta = \frac{(S(t_2) - C(t_1)) + (S(t_3) - C(t_4))}{2} \tag{3.2}$$

The NTP synchronization is correct when both the client-server and server-client paths have symmetrical nominal delay. Otherwise, the synchronization has a systematic bias of half the difference between the forward and backward travel times. The characteristics of the NTP make it not suitable for the synchronization of all the measurement device in WAMSs.

### 3.2.2 Precision Time Protocol

The IEEE 1588 standard, also known as *IEEE Standard for a Precision Clock Synchronization Protocol for Networked Measurement and Control Systems* or PTP was first published in 2002 (see [14]) and revised in its current version in 2008 [15]. IEEE 1588 is a distributed protocol that is able to properly work both in networks consisting of PTP devices only and in networks consisting of a combination of PTP and non-PTP devices. It specifies that the real-time clocks, organized into a master-slave synchronization hierarchy, synchronize with each other by means of an exchange of PTP timing messages, with the slaves using the timing information to adjust their clocks. PTP provides synchronization for both software-only and hardware-aided implementations. For the former, timing deviations of tens of microseconds have been demonstrated [16]. For the latter, deviations of tens to hundreds of nanoseconds, depending on the devices used and the traffic conditions [17], have been demonstrated. Event messages and general messages are defined in the protocol.

Event messages need to be accurately timestamped at both transmission and receipt side. They consist of:

- **Sync**: the master element sends Sync messages with period $T_{\text{SYNC}}$ to the directly connected slaves. $T_{\text{SYNC}}$ has a default value of 2 $s$ but it can be changed by the administrator of the network. The message is timestamped both with the transmission time, by the master, and with the reception time, by the slave;
- **Delay_Req**: Delay Request messages are sent from the slave to the master. The slave clock generates a time-stamp based on its local clock when the Delay_Req message is sent. The master clock generates a time-stamp based on its local clock when it receives the message;

- **Pdelay_Req** and **Pdelay_Resp**: Peer delay Request and Peer delay Response messages are used to estimate the link delay between two clocks that are configured to use peer delay mechanism (see [15] for more information);

Unlike the Event messages, General messages do not need any time-stamp:

- **Announce**: Announce messages are used during the best master clock algorithm to establish the master-slave hierarchy;
- **Follow_Up**: the master may sand it immediately after the Sync message to communicate to the slave the Synch transmission time. Alternatively, the Synch time-stamp is embedded in the Synch messages, but it can be less accurate;
- **Delay_Resp**: the Delay Response messages are used by the master to send to the slave the time-stamp of the arrival time of the Delay_Req messages;
- **Pdelay_Resp_Follow_Up**: also this type of message is used when peer delay mechanism is implemented;
- **Management**: Management messages are used to query and update the PTP data sets maintained by clocks. These messages are also used to customize a PTP system and for initialization and fault management;
- **Signaling**: This type of messages are used for the rest of communication among PTP devices.

All messages are composed by a common header (see Fig. 3.5), a body which may vary depending on the type of message, and a suffix which may have zero length.

Five PTP device types are also described in [15], each of them implementing one or more aspect of the protocol:

- **Ordinary clock** is a clock that has a single PTP port. It can be a reference clock (grand-master) providing a source of time or it can be a slave clock.
- **Boundary clock** is a clock that has several PTP ports. Each port independently works like the port of an ordinary clock. It allows the synchronization of IEEE 1588 clocks across subnets, by eliminating the large fluctuations in communication latency typically generated by bridges.
- **Transparent clock** is a device able to estimate the time that a packet needs to cross the device, and able to include this information in the same message. The client, by using this information, can take into account the delay due

| Bits | | | | | | | | Octets | Offset |
|---|---|---|---|---|---|---|---|---|---|
| 7 | 6 | 5 | 4 | 3 | 2 | 1 | 0 | | |
| TransportSpecific | | | | MessageType | | | | 1 | 0 |
| Reserved | | | | VersionPTP | | | | 1 | 1 |
| MessageLength | | | | | | | | 2 | 2 |
| DomainNumber | | | | | | | | 1 | 4 |
| Reserved | | | | | | | | 1 | 5 |
| FlagField | | | | | | | | 2 | 6 |
| CorrectionField | | | | | | | | 8 | 8 |
| Reserved | | | | | | | | 4 | 16 |
| SourcePortIdentity | | | | | | | | 10 | 20 |
| SequenceId | | | | | | | | 2 | 30 |
| ControlField | | | | | | | | 1 | 32 |
| LogMessageInterval | | | | | | | | 1 | 33 |

**Figure 3.5:** PTP common message header

to the forwarding of the message and to more accurately synchronize its own clock to the master. There are two types of transparent clock: **end-to-end transparent clock**, that supports the use of the end-to-end delay measurement mechanism between slave clocks and the master clock, and **peer-to-peer transparent clock** that supports the peer-to-peer delay measurement mechanism and, in addition, is also able to provide corrections for the propagation delay of the link connected to the port receiving the PTP event message.

- **Management node** is the device used for the configure and monitor PTP clocks.

The normal execution of the protocol can be divided in two parts: determining the clock with the best time accuracy (grand-master clock) by means of the Best Master Clock (BMC) algorithm and measuring and correcting time skew caused by clock offsets and network delays. Devices are then organized in a Master-Slave hierarchy. The protocol synchronizes slave clocks to the grandmaster clock, ensuring that the time scale of the entire system will be traceable to the time scale of the grandmaster clock and that events and time-stamps in all devices will use the same time base.

### Best Master Algorithm

In its initial phase, the PTP runs the BMC algorithm to select, among all the PTP devices of the system, a grand-master clock (the reference clock of the network), which provides the reference time to the other clocks (slave clocks), and to define the master-slave hierarchy. During this phase, each clock sends announce messages which contain, among other information, its characteristics and the characteristics of the clock that at the moment it considers the grand-master. Then each port of each PTP device examines the contents of all received announce messages and according to these messages, if there is a better quality clock then the one that is considered the grand-master, the device selects this one as the grand-master clock.

At the end of the BMC algorithm, moreover, each port of each PTP clock assumes a state between master, slave and passive:

- MASTER: the port is the source of time on the path served by the port.
- SLAVE: the port synchronizes to the device on the path whose port is in the MASTER state.
- PASSIVE: the port is not the master on the path nor does it synchronize to a master. It is a port in a sort of IDLE state to avoid closed loop in the network. It can be activated in case of reconfiguration of the network.

In Fig. 3.6, an example of tree structured master-slave hierarchy has been reported. Clock 1 is the better clock in the LAN and it has been chosen as grand-master. The state of all the port has been chosen to guarantee the proper synchronization of each clock avoiding closed loops. Port in the master, slave and passive state have been indicated whit M, S, and P, respectively.

### Clocks Synchronization

Once the tree-structured master-slave hierarchy has been completed, the PTP is reduced to the synchronization of pairs PTP ports, one master and one slave. This phase of the protocol is based on the exchange of messages between the master and the slave. This last one, thus, uses the timing information obtained during the communication to adjust its clock. Fig. 3.7 illustrates a basic synchronization message exchange among a master and a slave.

The master sends to the slave the Sync message at instant $t_1$ and immediately after it sends a Follow_Up message containing the value of $t_1$. When the slave receives the Sync message, it timestamps it with the reception time $t_2$ and sends a Delay_Req message to the master at the instant $t_3$. The master, then, generates a time-stamp $t_4$ when the Delay_Req message is received and sends this value to the

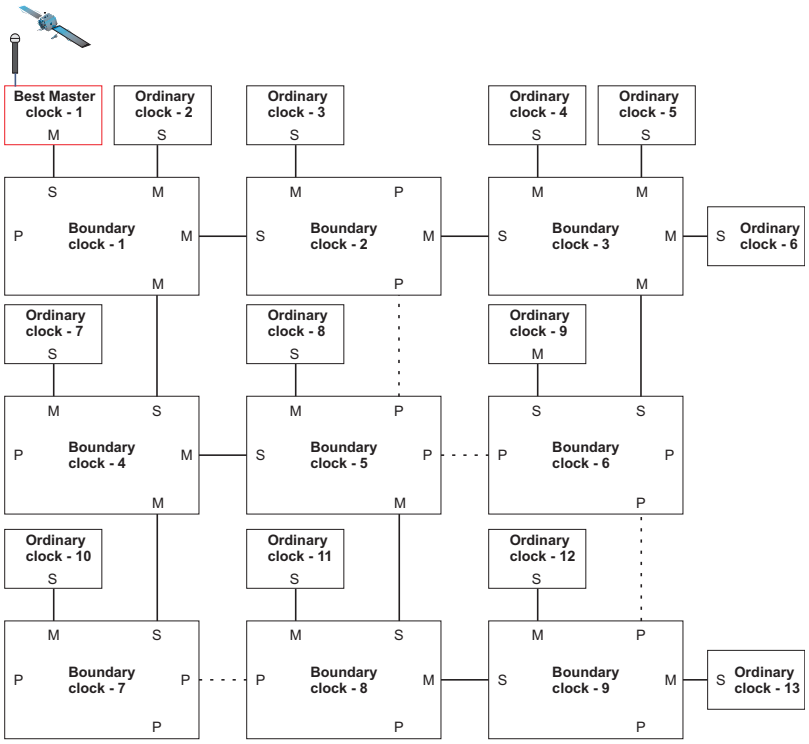


**Figure 3.6:** Best master clock algorithm example

slave with a Delay_Res message. These messages are sent periodically to allow the slave to continuously synchronize its clock.

With these four time values $t_1, t_2, t_3, t_4$, the slave is able to estimate both the offset $O$ from the master and the one-way delay $D$ and synchronize itself to the master. In fact it is possible to obtain the two following expressions:

$$t_2 = t_1 + O + D_{M \to S} \tag{3.3}$$

$$t_4 = t_3 + O + D_{S \to M} \tag{3.4}$$

where $D_{M \to S}$ and $D_{S \to M}$ are the master to slave and slave to master delays, respectively. In the case it is possible to assume symmetrical delay $D_{M \to S} = D_{S \to M} = D$ then:

$$D = \frac{(t_2 - t_1) + (t_4 - t_3)}{2} \tag{3.5}$$

$$O = (t_2 - t_1) - D \tag{3.6}$$

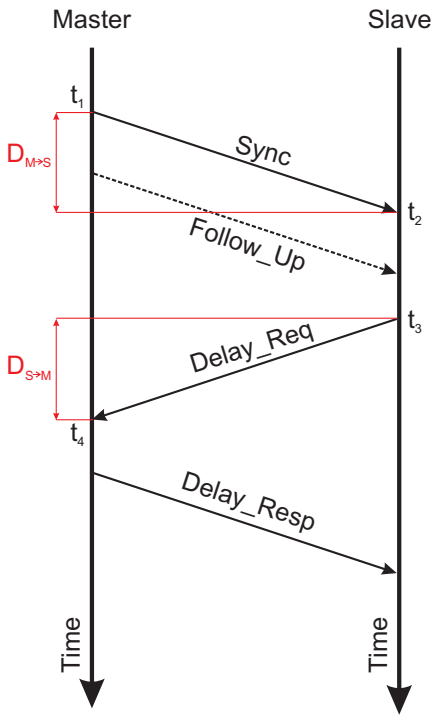


**Figure 3.7:** Basic synchronization message exchange

### PTP Synchronization Uncertainty Sources

The uncertainty of a synchronization mechanism based on message exchange on a network strictly depends on several sources [18]. One of these sources is due to the time reference of the master and is strictly related to the quality of the used clock.

A clock can be generally summarized as consisting of an oscillator and a counter. The counter, by counting the repeatable time intervals generated by the oscillator, establishes a time scale. The time scale value $c(t)$ at a given absolute reference time $t'$ can be expressed as:

$$c(t') = \lfloor c_0 + \int_0^{t'} f(t)\, dt \rfloor \tag{3.7}$$

where $c_0$ is the origin of the time scale, f(t) is the evolution of the frequency over the time and $\lfloor \cdot \rfloor$ calculates the floor of a number.

Ideally, the frequency of an oscillator $f(t)$ is constant but, in a real case, it is a complex function of the time because it is affected by different factors, like changes of temperature and pressure and also the age of the oscillator. However, in practice, $f(t)$ can be approximated by using a linear model and can be expressed as:

$$f(t) = f + \Delta f t \tag{3.8}$$

where $f$ is the initial frequency of the oscillator and $\Delta f$ represents the constant speed drift. By replacing 3.8 in 3.7, a new expression of time scale is obtained:

$$c(t') = \left[ c_0 + ft' + \frac{\Delta f}{2} t'^2 \right] \tag{3.9}$$

Comprehensive understanding of the oscillators can be found in [19] and [20].

Among the various uncertainty sources there are also the traffic conditions, the number of network devices on the path between a master and a slave, the presence of no-PTP compliant devices, the network load and the presence of an asymmetrical delay ($D_{M\to S} \neq D_{S\to M}$). All these components can decrease significantly the performance of the protocol because contribute to increase the unpredictability of the network. In the literature several reports (e.g. [17, 21, 22]) show different cases of synchronization performance with IEEE 1588, expressed in terms of deviations of the PPS provided by clocks linked via either repeaters, switches, etc.. Evaluating how these deviations affect the accuracy of synchrophasor measurement is straightforward, since there is a linear relationship between time deviations and phase shifts. For instance, according to [21] the time deviations in presence of either a repeater or a switch are in the order of tens to few hundreds of nanoseconds. As a consequence, phase deviations in the order of $10^{-5}$ to $10^{-4}$ rad would be introduced in the synchrophasor measurement for a fundamental frequency of 50 Hz. This would lead to a TVE far below the 1 % limit allowed by [2], even adding the deviation introduced by the GPS receiver (e.g. a maximum of $100\,ns$). In Table 3.1, expected contribution of time deviation to synchrophasor accuracy have been reported.

**Table 3.1:** Expected contribution of time deviation to synchrophasor accuracy

| **Network Devices** | **Phase Deviation** | | **TVE** | |
|---|---|---|---|---|
| | Mean Value ($rad$) | Standard Deviation ($rad$) | Mean Value (%) | Standard Deviation (%) |
| Repeater | $6.9E-06$ | $3.1E-05$ | $6.9E-04$ | $3.1E-03$ |
| Switch | $1.5E-05$ | $7.3E-05$ | $1.5E-03$ | $7.3E-03$ |

Nevertheless, the use of ordinary switches or router should be avoided in critical timing applications where sub-microseconds or better accuracy is needed. In these cases, the two presented kinds of IEEE 1588 compliant components (boundary clocks and transparent clocks) should be utilized. Some recent works investigated about advantages and disadvantages arising from the use of these devices. Particularly [23–25]

analysed performance of boundary clocks and transparent clocks for a line topology configuration where different bridges are organized in a cascade configuration. In such a system the only employment of boundary clocks, which compensate the frequency drift by means of a control loop (e.g. PI-Loop), may not be efficient in the case of many levels of cascade. This is because in a chain of boundary clocks, a sequence of control loops is established and may cause unacceptable instabilities and deviations of the clocks. The utilization of transparent clocks, instead, allows to avoid the problems resulting from cascade of control loops and permits to consider bridges as network elements with known delay. In this way, the delay of the Sync message between the PTP master and a PTP slave can be estimated as follows:

$$D_{Sync} = \sum_{i=1}^{n} LD_i + \sum_{i=1}^{n-1} BD_i \tag{3.10}$$

where $n$ is the number of links between the master and the slave, $BD$ is the bridge delay for handling time frames and $LD$ is the line delay to the previous node (see [23]). Moreover, authors of [23] show that in a line topology, after three boundary clocks in cascade, the absolute error may exceed $4\,\mu s$ (1.2 mrad for a sinusoidal signal at 50 Hz). After ten levels the absolute error may reach $150\,\mu s$ (47.1 mrad). On the contrary, a chain of transparent clocks leads to a delay between master and slaves almost independent of the number of bridges in cascade and below $1\,\mu s$ even after ten bridges. Authors of [24, 25] explore, in an analytic way, the effects of jitter and frequency drift on the performance of a cascade of transparent clocks. They obtain, for the first 66 levels of cascade, a synchronization error below $1\,\mu s$ in presence of jitter, while the error was over $2\,\mu s$ in presence of frequency drift. In [26], it is reported that for two clocks separated by 50 equal transparent clocks (characterized by an accuracy of $40\,ns$ the expected degradation would be between $(\sqrt{50} \cdot 40)\,ns$ and $(50 \cdot 40)\,ns$, depending on the error distribution. This means that, from a synchrophasor measurement point of view, the error for a sinusoidal signal at 50 Hz would be between 88 $\mu$rad and 0.62 mrad.

Finally, the time-stamp fluctuations can concretely affect the performance of the protocol [27]. The correctness of the time information used for the synchronization depend on the implementation of time-stamp mechanism in a PTP device. The most general implementation of PTP protocol generates the timestamps at the application level of the protocol stack by using software-only routines. However, Protocol stack delay fluctuation causes errors in the range from hundreds microseconds up to milliseconds. To reduce these fluctuations, the best thing to do is to try to generate the time-stamp for an incoming or outgoing packet as close as possible to the physical layer of the protocol stack. In the Annex A of [15], for example, it has been reported

that a time-stamp at the interrupt level is affected by delay fluctuations in the order of tens of microsecond. Such a time-stamp mechanism is still based on software only routines. However, by implementing an hardware-aided time-stamping technique, it is possible to generate the time-stamp at the physical level, thus reducing fluctuations to the order of nanoseconds.

In the following, tests on PTP systems based on both the software-only and the hardware-assisted time-stamp mechanisms, used for the synchronization of phasor measurement systems, will be presented.

# Bibliography


[1] B. Dickerson, *Time in the Power Industry: How and Why We Use It.* Arbiter Systems.

[2] "IEEE standard for synchrophasor measurements for power systems," *IEEE Std C37.118.1-2011 (Revision of IEEE Std C37.118-2005)*, pp. 1 –61, 28 2011.

[3] "IEEE standard for synchrophasor data transfer for power systems," *IEEE Std C37.118.2-2011 (Revision of IEEE Std C37.118-2005)*, pp. 1 –53, 28 2011.

[4] A. Carta, N. Locci, C. Muscas, and S. Sulis, "A flexible GPS-based system for synchronized phasor measurement in electric distribution networks," *Instrumentation and Measurement, IEEE Transactions on*, vol. 57, no. 11, pp. 2450 –2456, nov. 2008.

[5] A. Carta, N. Locci, and C. Muscas, "GPS-based system for the measurement of synchronized harmonic phasors," *Instrumentation and Measurement, IEEE Transactions on*, vol. 58, no. 3, pp. 586 –593, march 2009.

[6] L. Peretto, R. Sasdelli, E. Scala, and R. Tinarelli, "Performance characterization of a method for locating faults in power distribution networks," in *Instrumentation and Measurement Technology Conference Proceedings, 2007. IMTC 2007. IEEE*, may 2007, pp. 1 –6.

[7] A. O. Ibe and B. J. Cory, "A traveling wave-based fault locator for two-and three-terminal networks," *Power Engineering Review, IEEE*, vol. PER-6, no. 4, p. 55, april 1986.

[8] [Online]. Available: http://www.gps.gov

[9] [Online]. Available: http://www.glonass-ianc.rsa.ru

[10] [Online]. Available: http://ec.europa.eu/enterprise/policies/satnav/galileo/

[11] *IEC Standard for Communication network and systems in substations*, IEC Standard 61850 Std., 2003.

[12] D. L. Mills, "Internet time synchronization: the network time protocol," *IEEE Transactions on Communications*, vol. 39, pp. 1482–1493, 1991.

[13] D. Mills, "Precision synchronization of computer network clocks," *ACM SIGCOMM Computer Communication Review*, vol. 24, no. 3, pp. 28–43, April 1994.

[14] "IEEE standard for a precision clock synchronization protocol for networked measurement and control systems," *IEEE Std 1588-2002*, pp. i –144, 2002.

[15] "IEEE standard for a precision clock synchronization protocol for networked measurement and control systems," *IEEE Std 1588-2008 (Revision of IEEE Std 1588-2002)*, pp. c1 –269, 24 2008.

[16] K. Correll and N. Barendt, "Design considerations for software only implementations of the IEEE 1588 precision time protocol," in *In Conference on IEEE 1588 Standard for a Precision Clock Synchronization Protocol for Networked Measurement and Control Systems*, 2006.

[17] P. Ferrari, A. Flammini, D. Marioli, S. Rinaldi, and A. Taroni, "Synchronization of the probes of a distributed instrument for real-time ethernet networks," in *Precision Clock Synchronization for Measurement, Control and Communication, 2007. ISPCS 2007. IEEE International Symposium on*, oct. 2007, pp. 33 –40.

[18] P. Ferrari, A. Flammini, S. Rinaldi, A. Bondavalli, and F. Brancati, "Evaluation of timestamping uncertainty in a software-based IEEE1588 implementation," in *Instrumentation and Measurement Technology Conference (I2MTC), 2011 IEEE*, may 2011, pp. 1 –6.

[19] *IEEE standard definition of physical quantities for fundamental frequency and time metrology-random instabilities.*, IEEE Std 1139-1999, 1999.

[20] "International Telecommunication Unit. Definition and terminology for synchronization networks. ITU-T G.810," 1996.

[21] J. Eidson and J. Tengdin, "IEEE 1588 standard for a precision clock synchronization protocol for networked measurement and control systems and applications to the power industry." in *Distributech*, feb. 2003.

[22] J.-C. Tournier and X. Yin, "Improving reliability of IEEE 1588 in electric substation automation," in *Precision Clock Synchronization for Measurement, Control and Communication, 2008. ISPCS 2008. IEEE International Symposium on*, sept. 2008, pp. 65 –70.

[23] J. Jasperneite, K. Shehab, and K. Weber, "Enhancements to the time synchronization standard IEEE-1588 for a system of cascaded bridges," in *Factory Communication Systems, 2004. Proceedings. 2004 IEEE International Workshop on*, sept. 2004, pp. 239 – 244.

[24] R. Scheiterer, C. Na, D. Obradovic, and G. Steindl, "Synchronization performance of the precision time protocol in industrial automation networks," *Instrumentation and Measurement, IEEE Transactions on*, vol. 58, no. 6, pp. 1849 –1857, june 2009.

[25] C. Na, D. Obradovic, R. Scheiterer, G. Steindl, and F.-J. Goetz, "Synchronization performance of the precision time protocol," in *Precision Clock Synchronization for Measurement, Control and Communication, 2007. ISPCS 2007. IEEE International Symposium on*, oct. 2007, pp. 25 –32.

[26] J. C. Eidson, *Measurement, Control, and Communication Using IEEE 1588 (Advances in Industrial Control)*. Secaucus, NJ, USA: Springer-Verlag New York, Inc., 2006.

[27] P. Ferrari, A. Flammini, S. Rinaldi, A. Bondavalli, and F. Brancati, "Evaluation of timestamping uncertainty in a software-based IEEE 1588 implementation," in *Instrumentation and Measurement Technology Conference (I2MTC), 2011 IEEE*, may 2011, pp. 1 –6.

# Chapter 4

# Test system architectures

In order to test the possibility to synchronize a PMU-based measurement system by means of IEEE 1588 protocol, two different experimental setups have been realized, both described in this Chapter. Both the systems are based on a PTP synchronization solution, but the first one is characterized by an hardware-assisted time-stamp mechanism of the PTP messages, whereas the second one uses a software-only time-stamp mechanism. To realise both the architectures, general-purpose hardware technologies have been adopted: their use permits the different parts of the system to be easily reconfigured, depending on the specific applications.

## 4.1 Test system based on hardware-aided PTP synchronization

Fig. 4.1 illustrates a schematic representation of the considered measurement system, whose synchronization is based on PTP with hardware-assisted time-stamp mechanism. The management of the experimental setup is achieved by the use of virtual instrumentation. In particular, data acquisition, phasor estimation and synchronization functions have been implemented on the computer by means of Virtual Instruments (VIs) implemented in the LabVIEW environment.

### 4.1.1 Master

The master unit is implemented in a National Instrument (NI) PXI 1042Q hardware platform. The two main hardware components of this PMU are a NI PXI-6682 Timing and Synchronization module (that can also be used as IEEE 1588 master) and a NI PXI-6133 data acquisition module.

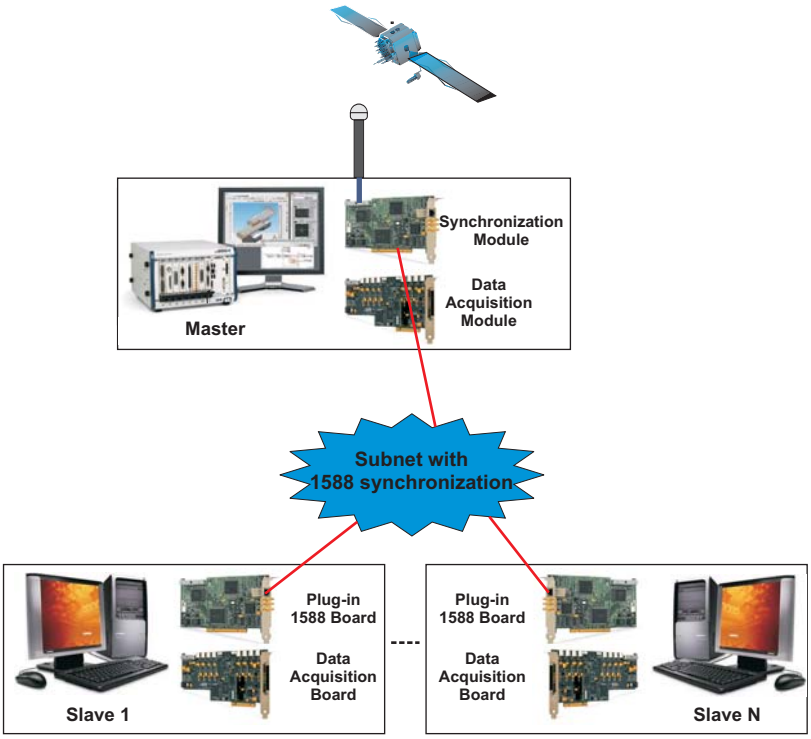


**Figure 4.1:** Hardware-assisted GPS-PTP System

### Hardware platform

The NI PXI is a modular system designed specifically to integrate, within its chassis, up to eight components with different functionalities (Fig. 4.2). Generally, it consists of a dedicated processor, a built-in reference clock, a PXI trigger bus, a start trigger, and a local bus. Its structure makes it suitable to operate in industrial environment. In particular, the used model NI PXI 1042Q (see [1]) is equipped with:

- an embedded processor dual-core 2.16 GHz with 512 MB of RAM;
- a built-in 10 MHz reference clock with an accuracy of 25 parts per million (ppm), less than 5 ps jitter, and a slot-to-slot skew of 250 ps;

### Timing and synchronization module

The NI PXI-6682 board achieves synchronization by using GPS, with a maximum tolerance of $\pm 100$ ns to UTC. It is also equipped with a standard RJ-45 connection for Ethernet communication (up to 100 Mbps), with Programmable Function

**Figure 4.2:** National Instrument PXI chassis

Interface (PFI) terminals, and with a 10 MHz Temperature Compensated Crystal Oscillators (TCXO) which is characterized by a initial accuracy of ±1 ppm (part per million), a temperature stability (0° to 55° C) of ±1 ppm and an aging per year of ±1 ppm [2]. The Synchronization module is connected via a 30 m coaxial cable to a GPS antenna characterized by a gain at 1575.42 MHz of 35 dB ±3 dB and by a PPS accuracy within 15 ns to GPS/UTC. This module can work as a PTP master and synchronizes other devices by means of an Ethernet connection through the RJ-45 port. It can also work as a simple GPS receiver by disseminating the IRIG-B signal or the PPS signal through the PFI connectors.

**Figure 4.3:** National Instrument PXI-6682 synchronization module

### Data Acquisition module

The NI PXI-6133 Data Acquisition (DAQ) board (Fig. 4.4) has a maximum sampling rate of 2.5 MSample/s on each of its 8 analog input channels (simultaneous sampling), and it is equipped with a 14 bits analog-to-digital converter [3].

**Figure 4.4:** National Instrument PXI-6133 data acquisition module

### 4.1.2 Slaves

The slave units are PC-based systems with a 2.20 GHz dual-core processor with 2GB RAM memory, each with a multifunction data acquisition board and a 1588 plug-in board.

#### Synchronization board

Two possible solutions have been chosen to synchronize each slave: GPS receiver or PTP board.

- The used GPS receiver is Symmetricom XL-750 characterised by a time accuracy of ±100 ns with respect to the UTC [4].
- The NI PCI-1588 is used as PTP board. This is equipped with a standard RJ-45 connection for Ethernet communication (up to 100 Mbps), with PFI terminals and with a 10 MHz TCXO characterized by an initial accuracy of ±1.5 ppm, a temperature stability (0° to 55° C) of ±2 ppm and an aging per year of ±1 ppm [5].

#### Data Acquisition board

The DAQ is a NI PCI-6132 data (4 analog inputs, resolution of 14 bits and maximum sample rate of 2.5 MSample/s, simultaneous sampling) [6].

### 4.1.3 Labview virtual instrument

The methodologies for the measurement of synchronized phasors implemented on hardware platforms (PXI and PCs) have been managed with the help of LabVIEW

software package. In particular, a virtual PMU has been developed. Fig. 4.5 illustrates the front panel of the realised VI. In the front panel, it is possible to configure several parameters of the PMU, like duration of the acquisition, sampling frequency, input channels, dimension of the buffer, reporting rate, and duration of the observation window. Moreover, it is also possible to monitor some results, like trend of the observed signal, instantaneous estimated module and phase values, and estimated frequency.

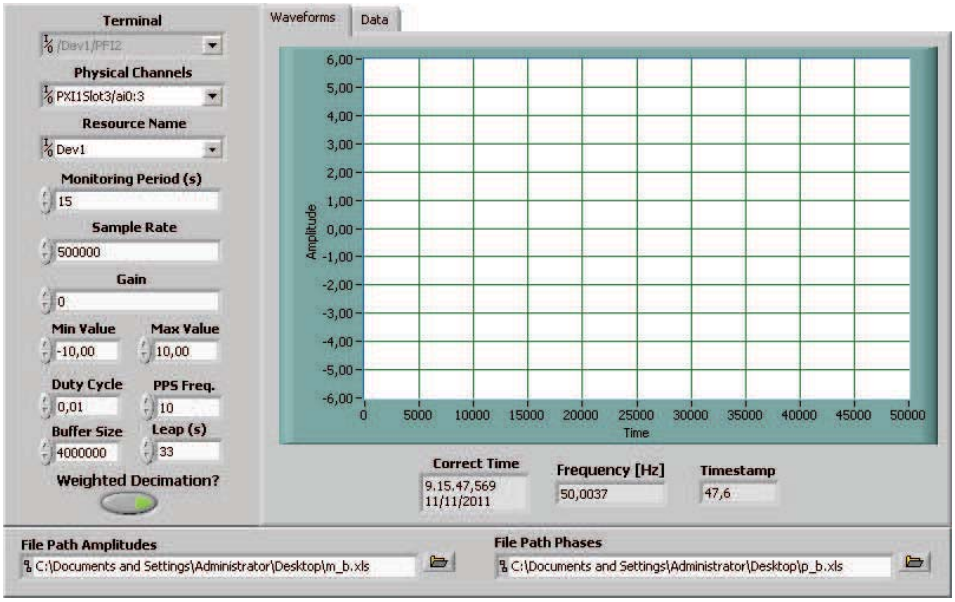


**Figure 4.5:** Front Panel of the virtual PMU

The virtual device essentially works like a real PMU, enabling the synchrophasors calculation. The VI can be considered as composed by six sub-parts, each of which has several functions that are performed in sequence:

- acquisition of the voltage signal and the 10 PPS signal;
- reallocation of samples;
- frequency estimation;
- decimation of samples;
- computation of synchrophasors;
- compensation of synchrophasors.

Fig. 4.6 illustrates the blocks diagram of the virtual PMU. Each part of the schema will be briefly described in the following.

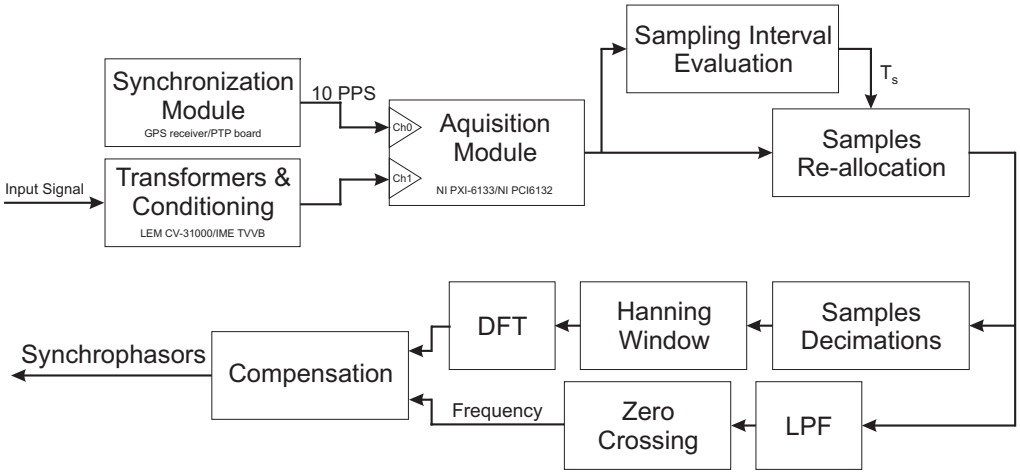


**Figure 4.6:** Schematic of the realized virtual PMU

### Data acquisition

This part of the VI manages the acquisition board by means of NI drivers and takes as input on channel zero (Ch0) the 10 PPS signal from the NI PXI 6682 module in the case of the master unit, and either from PCI-1588 board or from Symmetricom XL-750 in the case of the slave units. Moreover, it takes as input on channel one (Ch1) the electrical signal. Each channel acquires with a sampling rate of 500 ksample/s.

### Samples re-allocation

The use of general-purpose technology makes it necessary to implement some tricks to obtain performance comparable to that of the commercial PMUs with dedicated hardware. In fact, these lasts are equipped with PLL circuits that allow the sampling clock to be locked to the synchronization source. On the other hand, in general-purpose data acquisition systems the accuracy of the internal clock, whose value is generally rated on the order of $10^{-4}$, can affect significantly the overall timing positioning of acquired samples. Their sampling clock may be decoupled from the synchronization source and it is necessary to use compensation routines. The implemented PMU uses a sample re-allocation function that consists in using a high sampling rate (500 ksample/s for all the tests) to acquire input signals and to accurately individuate the raising edges of the 10 PPS signal, and in calculating the

actual number of samples $N_s$ between two rising edges of the 10 PPS signal. Knowing the exact value of $N_s$ makes it possible to estimate the actual frequency of sampling $f_s = 1/T_s$ and calculate synchrophasors based on this value rather than using the nominal value $f_0$.

### Frequency estimation

The frequency, in addition to being an important additional parameter to be observed to asses the stability of a power system, is essential for the correct behaviour of a DFT-based algorithm used to estimate phasors under off-nominal condition. It can be used either to adapt the observation windows to contain an integer number of cycles of the acquired signal or to provide some sort of post-compensation for the phasors evaluated using a fixed observation window. The frequency calculation is implemented by assessing the number of samples between two positive or negative zero-crossings of the signal. To avoid problems of false zero-crossing related to the possible presence of acquisition noise, the signal has been previously filtered with a Butterworth low-pass filter of the fourth order.

### Decimation of samples

While sampling at very high speeds permits to use routines to compensate for the lack of a sampling clock coupled to the synchronization source, on the other side the implementation of a synchrophasor estimation algorithm on a window containing a large number of samples creates several problems related to the computational load, computational time, and memory saturation. As an example, it is worth remembering that the number of complex operations necessary to perform a simple DFT computation of a vector of $N$ samples is equal to $N^2$. This means that for a sampling rate of 500 ksample/s and an observation period of 0.1 s, $2.5 \cdot 10^9$ complex operations are needed to execute the DFT, which can be considered a critical problem when general-purpose hardware is used. To avoid these problems, a down-sampling procedure is applied to the array of samples before the synchrophasor estimation. The procedure consists of choosing a sample every $R$ and averaging it with both the previous one and the next one in order to reduce the effects of sampling noise. As a consequence, the number of complex operation after the down-sampling procedure is reduced to the value $(\frac{N}{R})^2$. In the used PMUs, a value of $R = 5$ has been chosen.

### Estimation of synchrophasors

Since one of the goals of this thesis work is to evaluate the impact of the proposed synchronization solution on the synchrophasor measurement, the traditional DFT-based algorithm presented, among others, in last chapter of the thesis has been used

for the computations of the phasors. Although the other presented algorithms, in fact, assure better performances in presence of no-ideal conditions (see [7, 8]), they are likely to mask or mitigate any effect due to the synchronization system, thus hiding any problems or advantages of the proposed solution.

An observation window of fixed duration of five cycles (0.1 s) of the signal at the nominal frequency of 50 Hz has been chosen. Before the execution of the DFT algorithm, a Hanning smoothing window is applied to the array of decimated samples to reduce the effects due to off-nominal conditions. In an ideal case, in fact, the power system should work in a sinusoidal steady state, characterized by a nominal frequency of either 50 Hz or 60 Hz. In the reality, however, voltage and current signals differ from these ideal conditions, in terms of both variable fundamental frequency and distorted waveform [9]. Just when these critical events occur, the used algorithm shows some problems. In fact, during off-nominal condition, the fixed observation window contains a number of samples which is not representative of an integer number of periods of the observed signal. As a consequence, DFT provides incorrect results due to spectral leakage whose effects are reduced both by applying an Hanning weighting window to the array of decimated samples and by means of post-processing compensation routines.

### Compensation of synchrophasors

The accuracy of the phase and amplitude evaluations can be significantly improved by means of suitable compensation algorithms, such as those proposed in [10] and reported in the following. The implemented phasor compensation algorithm uses the value of the actual frequency of the observed signal to compute corrective factors (both for the fundamental and the others harmonics), which are used to compensate the errors due to off-nominal conditions.

Considering a periodic signal composed by $H$ harmonics, the phase $\varphi_h$ of the harmonic $h$ can be evaluated as a function of the phases of both the $i_h$-th bin obtained by the DFT ($\phi_{ih}$) and the adjacent bins ($\phi_{ih-1}$ or $\phi_{ih+1}$) depending on the sign of the term $f_h - i_h f_w$ as follows:

- if $f_h - i_h f_w > 0$ and $\phi_{ih} > \phi_{ih+1}$

$$\varphi_h = \frac{(2-\delta_h)\phi_{ih} + (1+\delta_h)\phi_{ih+1} + (1-2\delta_h)a}{3} \tag{4.1}$$

- if $f_h - i_h f_w > 0$ and $\phi_{ih} < \phi_{ih+1}$

$$\varphi_h = \frac{(2+\delta_h)\phi_{ih} + (1-\delta_h)\phi_{ih-1} - (1+2\delta_h)a}{3} \tag{4.2}$$

- if $f_h - i_h f_w < 0$ and $\phi_{ih} > \phi_{ih-1}$

$$\varphi_h = \frac{(2-\delta_h)\phi_{ih} + (1+\delta_h)\phi_{ih+1} + (1-2\delta_h)a}{3} \tag{4.3}$$

- if $f_h - i_h f_w < 0$ and $\phi_{ih} < \phi_{ih-1}$

$$\varphi_h = \frac{(2+\delta_h)\phi_{ih} + (1-\delta_h)\phi_{ih-1} - (1+2\delta_h)a}{3} \tag{4.4}$$

where $f_h$ is the frequency of each harmonic and can be expressed as $f_h = i_h f_w + \delta_h f_w$ with $f_w = \frac{1}{T_w}$, $T_w$ is the observation time, $i_h$ is an integer value representing the DFT bin closest to the actual harmonic component of order $h$ and $\delta_h$ can assume a value in the range $[-0.5, 0.5]$ and is a displacement term caused by non-coherent sampling, $a = \pi(N-1)/N$ and $N$ is the number of samples.

Moreover, the amplitude $\hat{A}_h$ of the harmonic $h$ can be expressed as a function of the amplitudes of both the $i_h$-th bin obtained by the DFT ($A_{ih}$) and the adjacent bins ($A_{ih-1}$ or $A_{ih+1}$) as follows:

$$\hat{A}_h = \frac{\pi\delta_h(1-\delta_h^2)(4-\delta_h^2)\lfloor |A_{ih-1}| + 2|A_{ih}| + |A_{ih-1}| \rfloor}{3\sin(\pi\delta_h)} \tag{4.5}$$

## 4.2 Test system based on software-only PTP synchronization

Fig. 4.7 shows a schematic representation of the second considered system whose synchronization is based on a software-only version of the PTP. This system has been entirely realised in the laboratories of the Eon Energy Research group of the RWTH Aachen University, Germany. It is composed by PMUs implemented in general-purpose hardware, synchronized by means of a software implementation of the PTP and it acquires electrical signals of simulated power systems.

### 4.2.1 Real Time Digital Simulator

For the simulation of complex power systems, a Real Time Digital Simulator, also known as RTDS, has been used [11]. The RTDS is a platform which utilizes a

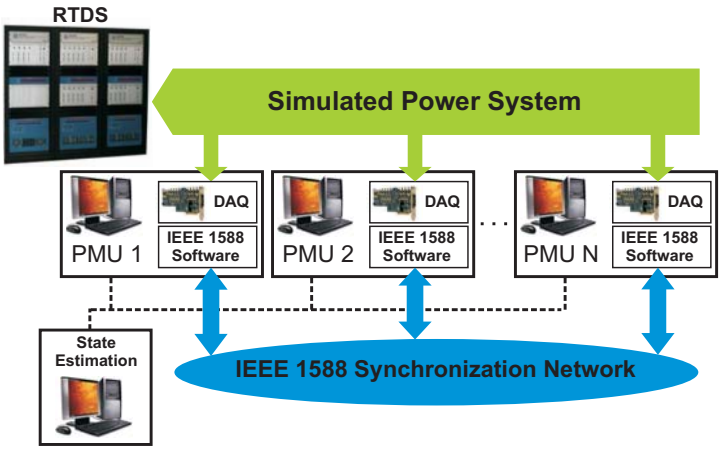


**Figure 4.7:** Software-only based measurement system example

combination of custom software and hardware to perform real-time simulations of power systems, with a time resolution up to 50 µs. The possibility to perform the exchange of analog signal with external devices by means of the Gigabit Transceiver Analog Output card (GTAO) enables the acquisition (in real-time) of voltage and current signals in every part of the simulated power system. The GTAO card features twelve 16-bit analogue output channels and can provide output signals in the range of ±10 V. Moreover, the RTDS custom user interface software gives the possibility to plot and save simulated signals directly on the PC, and to import the saved data into Matlab for the computation of synchrophasors and post-processing functions.

### 4.2.2 Implemented Phasor Measurement Units

The PMUs used in this work have been entirely developed using C language. A general-purpose PC with a Real-Time Application Interface (RTAI) for Linux was chosen as processing unit [12]. The PCs used in the experiment are equipped with an Intel Core2 Quad CPU (Q8400, 2.66 GHz) and 4 Gb of RAM. The measurement signals generated by RTDS are acquired using a general purpose NI PCI-6220 DAQ, with 16 analog inputs, a resolution of 16 bits and maximum sampling rate of 250 kSample/s. The DAQ is managed by means of the open-source drivers named Comedi [13].

### 4.2.3 Precision Time Protocol daemon

A widespread open source software implementation for Linux environment of the PTP, named Precision Time Protocol Daemon (PTPd), has been used to synchro-

nize the PMUs [14, 15]. The main idea behind this choice is that a PTP synchronization in the order of few microseconds in a substation is not achievable without a dedicated hardware but, at the same time, if the communication infrastructure of the substation is hardware-assisted and the measurement devices operate only as end-points, the PMUs can be synchronized by using a software implementation of the IEEE 1588 standard.

The PTPd has been developed for test and measurement systems. It presents pros and cons in comparison to the hardware-assisted solution. In fact, on one hand, PTPd is suited to run in embedded computer platforms with minimal computing resources (its CPU utilization is below 1 % on a 66 MHz m68k processor) and in typical multi-task computing environments. On the other hand, it uses a software clock and it provides time-stamps in the software layers of the network stack rather than in the physical layer, and this introduces a large jitter and may cause a degradation of the performance of the synchronization system.

In Fig. 4.8, a schematic representation of the software time-stamp mechanism used by the PTPd has been reported [16]. It is worth noting that time-stamp process implies a set of operations at kernel level. In fact, when an event occurs, such as receiving or transmitting a packet, the socket passes the time-stamp generated at the kernel level to the net layer through an *ioctl*() command. The operative system uses the function *getstimeofday*() to read the time value from software clock of the kernel *SysClock* which is updated using as time source the High Precision Event Timer (HPET) or the Power Management Timer (ACPI) at hardware level. The clock tick-rate is adjusted by means of the *ClockServo* with the frequency adjustment command, *adjtimex*().

### Clock servo

In Fig. 4.9, a schematic representation of the Clock Servo mechanism used by the PTPd has been reported. The PTPd engine periodically samples the master-to-slave delay and slave-to-master delay values. These two values are thus used to estimate the one-way delay value. The Clock Servo filters the one-way delay value with a first-order Infinite Impulse Response low-pass (LP IIR) filter with variable cutoff and phase, to mitigate the detrimental effect of input jitter on clock coordination. The behaviour of the filter can be described by the following equation:

$$s \cdot y[n] - (s-1) \cdot y[n-1] = x[n]/2 + x[n-1]/2 \tag{4.6}$$

where $s$ is a parameter called *stiffness* which controls the cutoff and phase of the filter. By increasing the value of the parameter $s$, it increases the time needed to achieve a stable synchronization, but it also decreases the cutoff properties of the filter and then the accuracy of the synchronization.

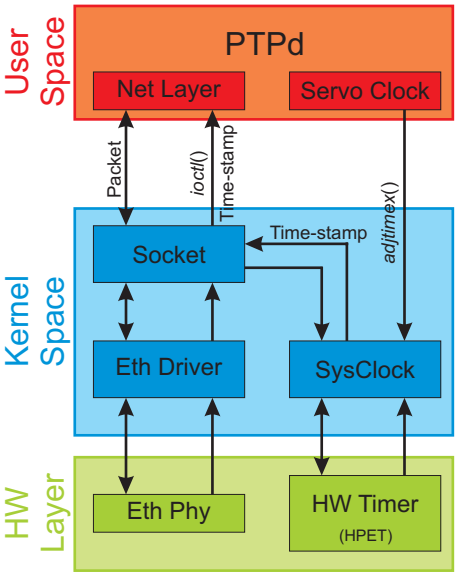


**Figure 4.8:** Schematic representation of the PTPd time-stamp mechanism

Master-to-salve delay and one-way delay are then used to estimate the offset from the master, which is filtered by a Finite Impulse Response low-pass (LP FIR) filter with a high cutoff and minimal delay:

$$y[n] = x[n]/2 + x[n-1]/2 \tag{4.7}$$

The Clock Servo then sends the offset from master value to the Proportional-Integral (PI) controller to correct both the time and the rate of the local clock, and to coordinate it with master clock.

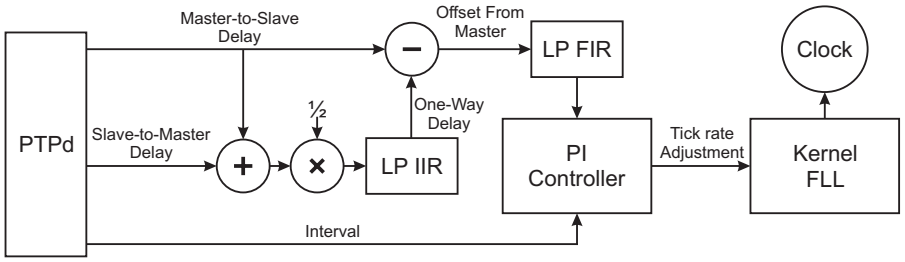


**Figure 4.9:** Schematic representation of the servo clock

### 4.2.4 Realised PMU routines

The entire routines for the synchrophasors estimation has been realised using C language. It is possible to highlight some differences compared to the routines presented in Section 4.1. Fig. 4.10 shows the blocks diagram of an implemented PMU.

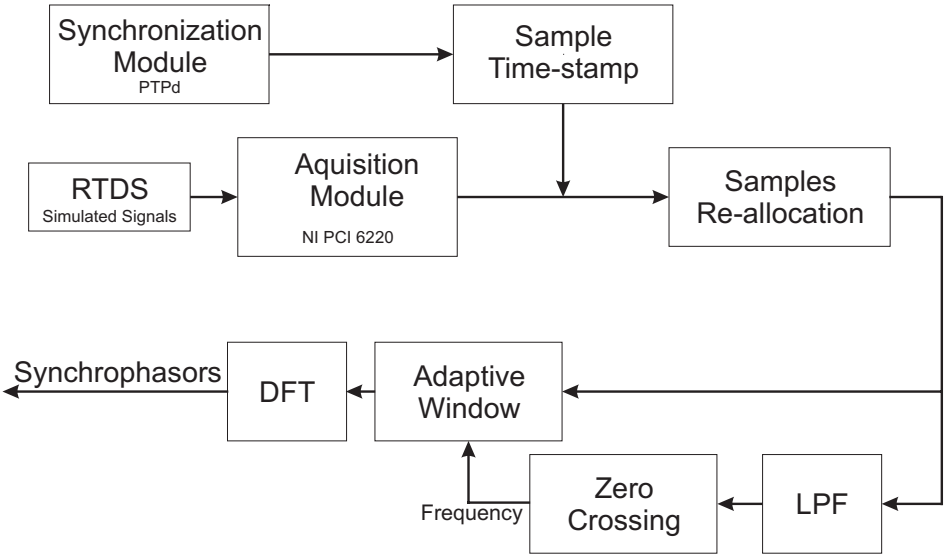


**Figure 4.10:** Blocks diagram of the implemented PMU

#### Data acquisition

The observed signals are acquired with a sampling rate of 10 ksample/s. The used DAQ is capable of much higher sampling rate but, since each sample must be timestamped in order to implement the re-allocation process and the frequency estimation algorithm, a low sampling frequency has been chosen to avoid additional jitter on both the synchronization and the time-stamp mechanism due to an excessive load of the CPU.

#### Samples re-allocation

Once again, the use of general-purpose hardware managed with open-source drivers implies that some ad-hoc procedures must be implemented to improve the overall system accuracy. To deal with this problem, a routine similar to the one presented in Section 4.1 has been implemented and applied to the input signal to re-allocate the samples in their correct time position. In other words, by evaluating the number of samples acquired in a fixed period of time (using their time-stamps), it is possible

to estimate the actual sampling frequency and give a correct position on the time axis to each sample.

### Synchrophasor estimation

Since the PMU module runs in parallel with the PTPd one, in order to maximize the performance of both the modules and to avoid overloading the CPU, a DFT estimation algorithm based on a adaptive observation windows of one cycle at the current frequency of the system has been chosen. This technique uses the real frequency of the system, estimated using the zero-crossing algorithm already presented in Section 4.1, and adapt the length of the observation windows to contain an integer cycle of the signal. This choice has allowed not only to mitigate the computational load due to the complex operations of the DFT, but also to avoid to weigh the samples and to calculate the compensation factors needed to mitigate the effects of leakage in case of fixed-length window.

# Bibliography


[1] [Online]. Available: http://www.ni.com/pxi

[2] [Online]. Available: http://sine.ni.com/nips/cds/view/p/lang/en/nid/203944

[3] [Online]. Available: http://sine.ni.com/nips/cds/view/p/lang/en/nid/14110

[4] [Online]. Available: http://www.symmetricom.com/

[5] [Online]. Available: http://sine.ni.com/nips/cds/view/p/lang/en/nid/202345

[6] [Online]. Available: http://sine.ni.com/nips/cds/view/p/lang/en/nid/201936

[7] P. Castello, M. Lixia, and C. Muscas, "Measurement of synchrophasors under dynamic conditions," in *Applied Measurements For Power Systems (AMPS), 2010 IEEE International Workshop on*, 2010, pp. 1–6.

[8] P. Castello, C. Muscas, and P. A. Pegoraro, "Performance comparison of algorithms for synchrophasors measurements under dynamic conditions," in *Applied Measurements For Power Systems (AMPS), 2011 IEEE International Workshop on*, 2011.

[9] *Voltage characteristics of electricity supplied by public distribution systems*, European standard EN 50160 Std., 1999.

[10] D. Agrez, "Improving phase estimation with leakage minimization," *Instrumentation and Measurement, IEEE Transactions on*, vol. 54, no. 4, pp. 1347 – 1353, aug. 2005.

[11] [Online]. Available: http://www.rtds.com/index/index.html

[12] [Online]. Available: https://www.rtai.org/

[13] [Online]. Available: http://www.comedi.org/

[14] K. Correll and N. Barendt, "Design considerations for software only implementations of the IEEE 1588 precision time protocol," in *In Conference on IEEE 1588 Standard for a Precision Clock Synchronization Protocol for Networked Measurement and Control Systems*, 2006.

[15] [Online]. Available: http://ptpd.sourceforge.net/

[16] P. Ferrari, A. Flammini, S. Rinaldi, A. Bondavalli, and F. Brancati, "Evaluation of timestamping uncertainty in a software-based IEEE 1588 implementation," in *Instrumentation and Measurement Technology Conference (I2MTC), 2011 IEEE*, may 2011, pp. 1 –6.

# Chapter 5

# Test Results

## 5.1 Tests on the hardware-assisted synchronized system

In order to experimentally evaluate the metrological performance of the proposed synchronization system, several kinds of experimental tests have been performed considering different master-slave network configurations and different synchronization conditions. All the results have been compared whit those obtained with the same measurement system in which each PMU is directly synchronized by means of a GPS receiver. Fig. 5.1 illustrates the GPS based measurement system used as comparison for the proposed GPS-PTP based measurement system (see Fig. 4.1 in Section 4.1). In the following, a selection of all the performed tests is presented [1, 2].

### 5.1.1 Tests under normal operative conditions

The duration of each test is thirty minutes, with ten evaluations per second, thus leading to the calculation of eighteen thousand amplitude and phase values.

#### Test A

Two measurement units connected to two different GPS receivers are considered. They measure the same voltage, acquired through a LEM CV 3-1000 transducer (maximum peak voltage $U_P = 1\,\text{kV}$; bandwidth 500 kHz at $-1\,\text{dB}$; accuracy 0.2 % of $U_P$) from the low voltage system that supplies the Measurement laboratory at the Department of Electrical and Electronic Engineering, University of Cagliari. A unit (PMU 0 in Fig. 5.1) is constituted by the PXI-based module. The second one

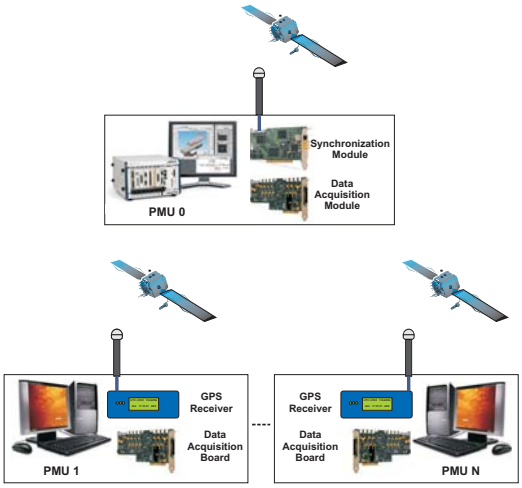


**Figure 5.1:** GPS-based measurement system

(PMU 1) is not actually a 1588 slave unit in this configuration , but is an independent measurement unit connected to a Symmetricom XL-750 GPS receiver (see Fig. 5.2).

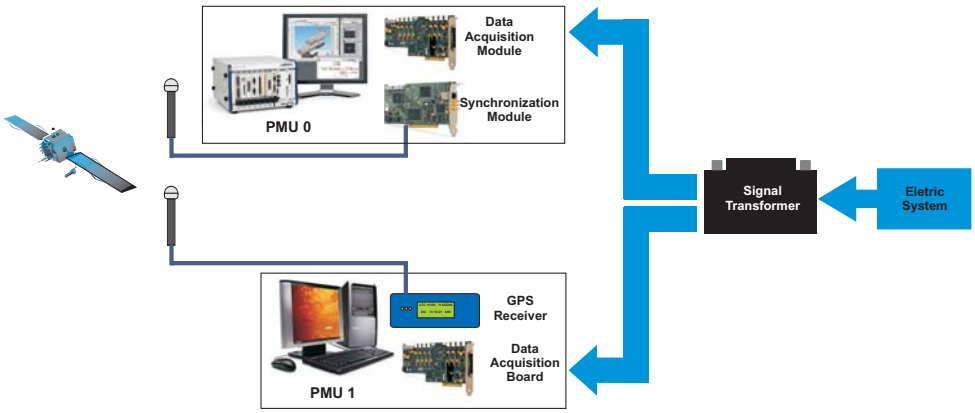


**Figure 5.2:** Setup of the Test A

The differences between the quantities measured by the two units have been evaluated and statistically analysed. Since a reference PMU was not available, the TVE has been calculated as vector difference between the outputs of the two PMUs in all the tests. Fig. 5.3 shows the TVE trend of the Test A. It is possible to notice that the TVE always remains under the 1 % limit imposed by [3]. Figs 5.4-a and 5.4-b show the amplitude difference and phase difference trends. Figs 5.5-a and 5.5-b show respectively the distributions of the difference of amplitude and phase measured by the two units. As expected, the performances of the GPS-based synchronization

system completely satisfy the requirement of the synchrophasor measurement standard. The mean value and standard deviation of the amplitude difference among the two PMUs are, respectively, 1.1E−2 % and 9E−4 %,whereas the mean value and standard deviation of the phase difference are 0.24 mrad and 0.26 mrad, respectively.

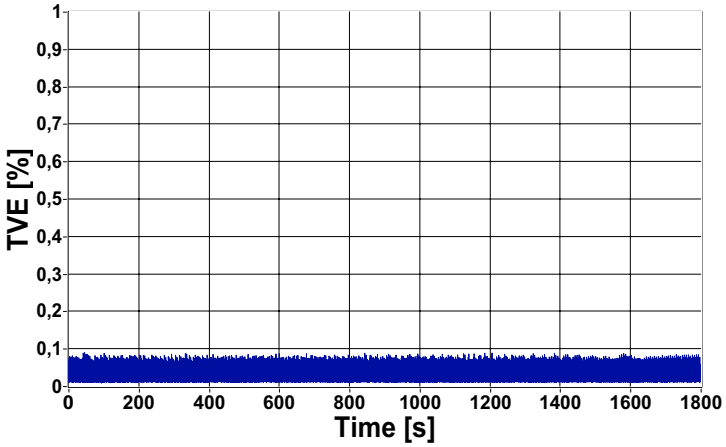


**Figure 5.3:** TVE trend for test A

### Test B

The master unit and the slave unit are considered in a GPS-PTP system to test the performance of such architecture with respect to the GPS one. The units are connected via crossover cable with the only presence of PTP traffic over the link and they measure the same voltage, i.e. the output voltage of a single transducer as in the configuration ot the previous test. (see Fig.5.6).

Fig. 5.7 shows the TVE trend for Test B. Also in this case the TVE is well below 1 %. Figs. 5.8-a and 5.8-b show the amplitude difference and phase difference trends.

Fig. 5.9 shows the distributions of amplitude difference (a) and the phase difference (b) for the Test B. It is possible to observe that the performances obtained with the GPS system (Figs. 5.5) and the ones obtained with the GPS-PTP system (5.9) are very similar: in this second case, the mean value and the standard deviation for the amplitude difference are 1.1E−2 % and 1.1E−3 %, respectively. As for the phase difference, instead, the mean value and the standard deviation value are 0.21 mrad and 0.26 mrad.

Table 5.1 summarizes the main statistical data of Test A and Test B, emphasizing the excellent performance obtained whit the GPS-PTP solution.

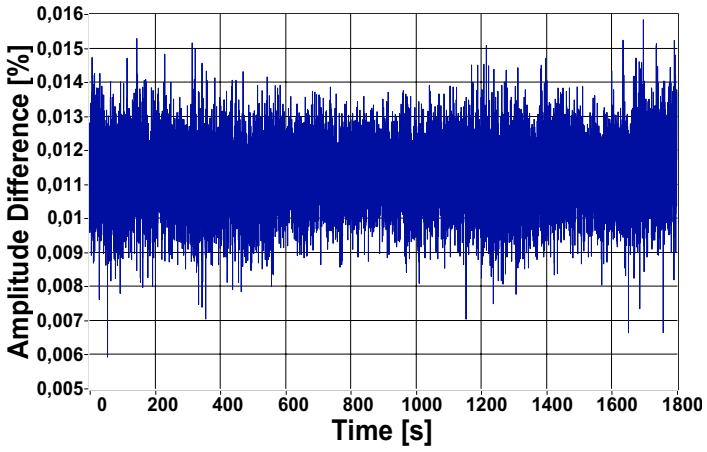


(a)

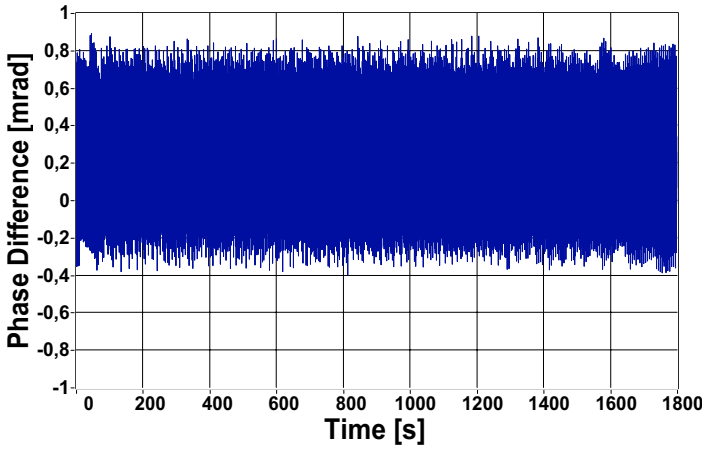


(b)

**Figure 5.4:** Trends of amplitude difference (a) and phase difference (b) in Test A

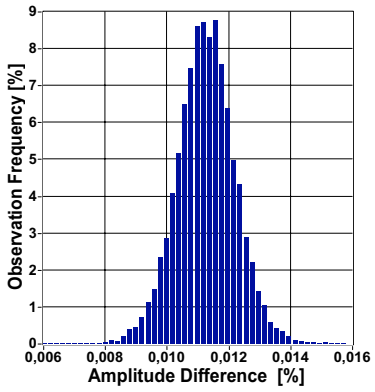


(a)

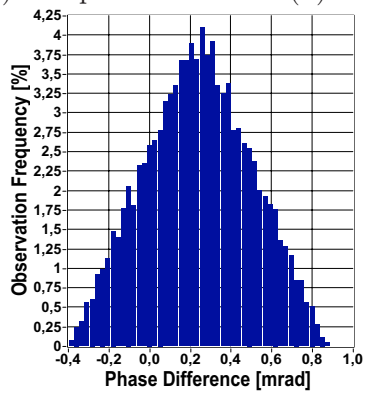


(b)

**Figure 5.5:** Distributions of amplitude difference (a) and phase difference (b) in Test A

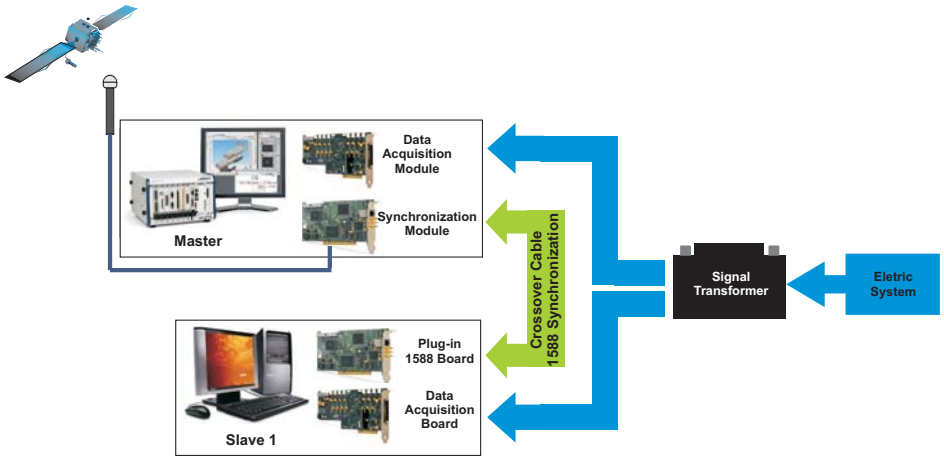


**Figure 5.6:** Setup of the Test B

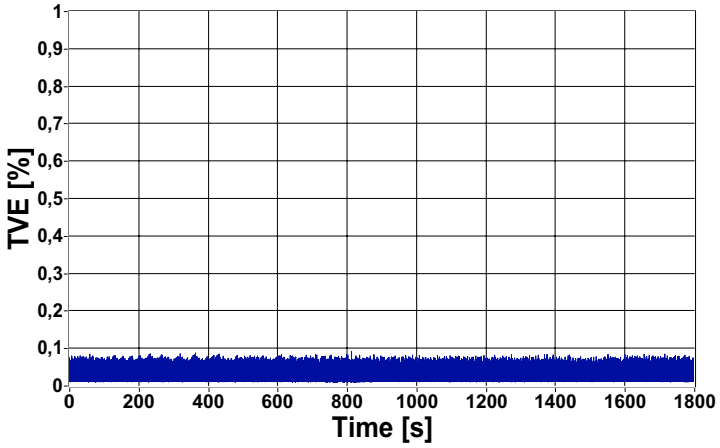


**Figure 5.7:** TVE trend for test B

**Table 5.1:** Synchrophasor amplitude and phase difference for Test A and Test B

| Test | Amplitude Difference | | Phase Difference | |
|---|---|---|---|---|
| | Mean Value (%) | Standard Deviation (%) | Mean Value (mrad) | Standard Deviation (mrad) |
| A | 1.1E−2 | 9E−4 | 0.24 | 0.26 |
| B | 1.1E−2 | 1.1E−3 | 0.21 | 0.26 |

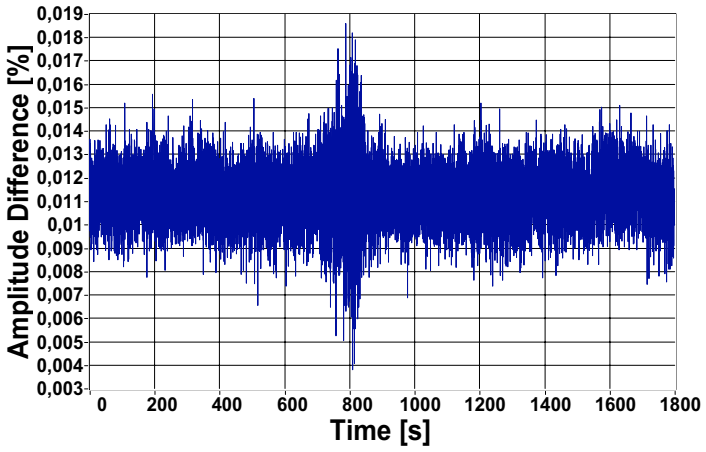


(a)

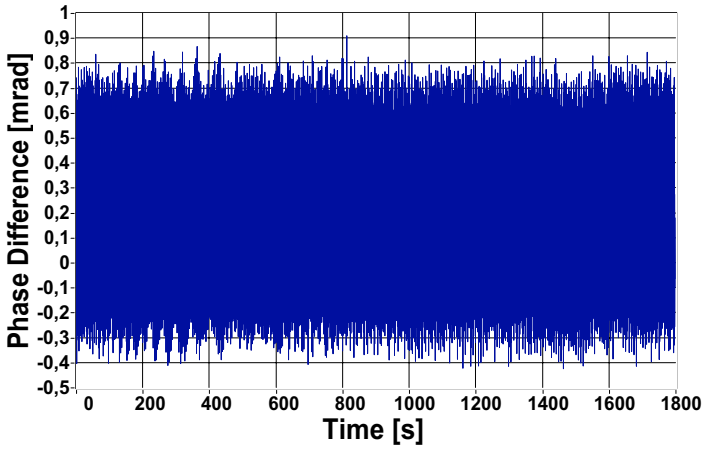


(b)

**Figure 5.8:** Trends of amplitude difference (a) and phase difference (b) in Test B

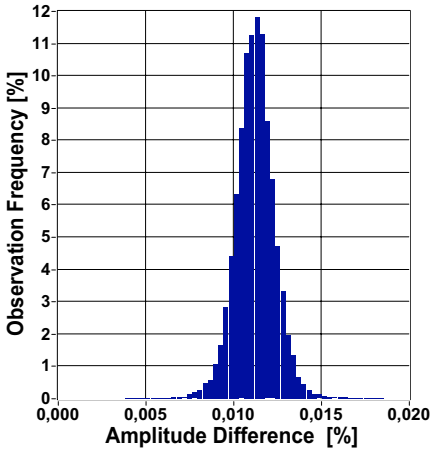


(a)

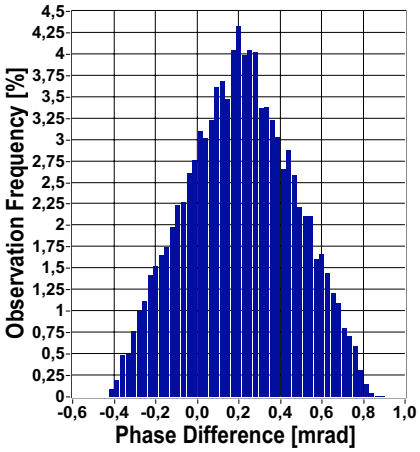


(b)

**Figure 5.9:** Distributions of amplitude difference (a) and phase difference (b) in Test B

### Test C

In power systems, the voltages to be measured are preliminarily reduced to values compatible to the PMUs inputs by suitable transducers, such as magnetic core Voltage Transformers (VTs)

The PMUs of different substations may be connected to different transducers. Thus, it can be useful to analyse the contribution to the TVE of the amplitude and phase deviations introduced by the transducers, with respect to the contribution of the synchronization system. By considering this, further tests were performed to evaluate the performances of the measurement system in the presence of such devices.

In Test C, same conditions of Test B have been reproduced with the difference that the two PMUs measure the same voltage through two LEM CV-3100 transducers. As a consequence in this case, the value of the TVE increases because of an additional term due to the amplitude and phase deviations between the two transducers.

Fig. 5.10 shows the TVE trend for Test C whereas Figs. 5.11-a and 5.11-b show the amplitude difference and phase difference trends. Finally, Fig. 5.12 shows the amplitude difference distribution (a) and the phase difference distribution (b).

### Test D

To deepen the study of the transducers contributions in the synchronization problem, it has been consider the situation in which different types of transducers are used. The same conditions of Test C are considered, but now a PMU acquires the signal through a LEM CV 3-1000 transducer whereas the other PMU acquires the signal through a magnetic core voltage transformer (VT). A IME TVVB model, with a nominal ratio of 400 V/100 V and class 0.5 (voltage error $\pm 0.5$ % and phase displacement $\pm 0.6$ crad) has been utilized.

Fig. 5.13 shows the TVE trend for Test D whereas Figs. 5.14-a and 5.14-b show the amplitude difference and phase difference trends. Finally, Fig. 5.15 shows the amplitude difference distribution (a) and the phase difference distribution (b).

For the sake of clearness, results of Tests C and D are reported in Table 5.2. Even with the contribution of the uncertainty due to the use of different transducers, the values of the TVE are always under the 1 % limit. However, by comparing the results with those obtained in Test B, it is possible to notice a marked deterioration in the performances of the measurement system. In particular, in the case of Test C, the use of two LEM CV-31000 transducers results in a deterioration of the TVE, which passes from values always below the 0.1 % (in Test B) to values around 0.3 %. In the case of Test D, the TVE reaches values around 0.7 %. From the simple observation

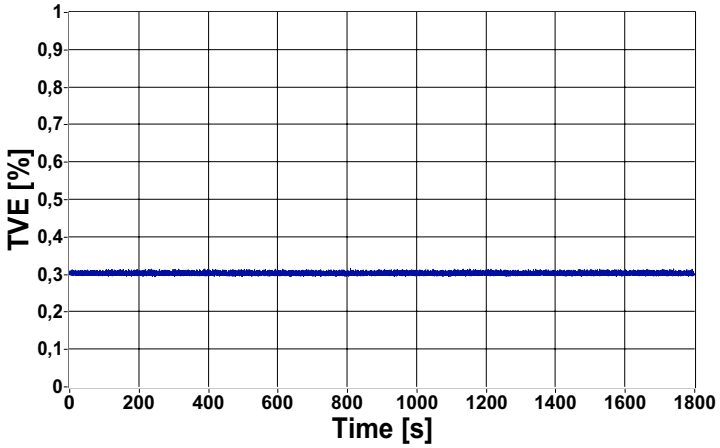


**Figure 5.10:** TVE trend for Test C

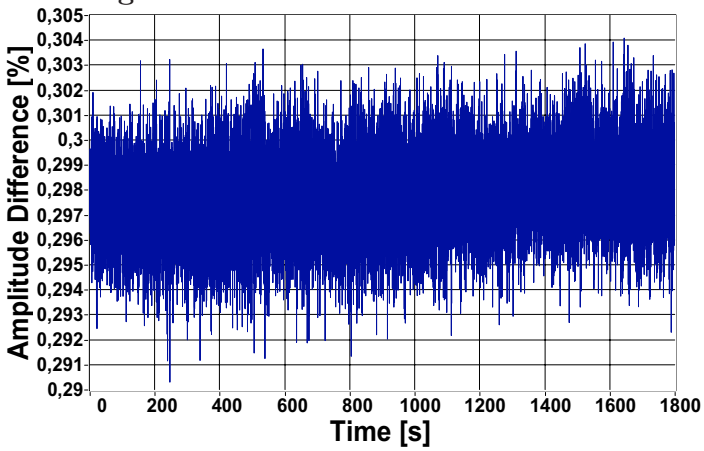


(a)

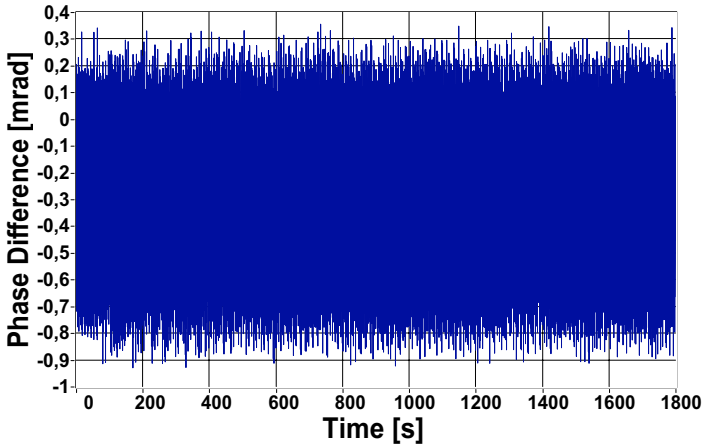


(b)

**Figure 5.11:** Trends of amplitude difference (a) and phase difference (b) in Test C

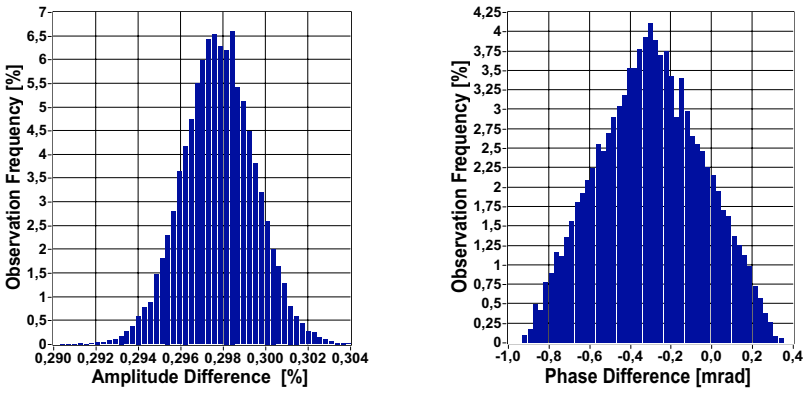


(a) (b)

**Figure 5.12:** Distributions of amplitude difference (a) and phase difference (b) in Test C

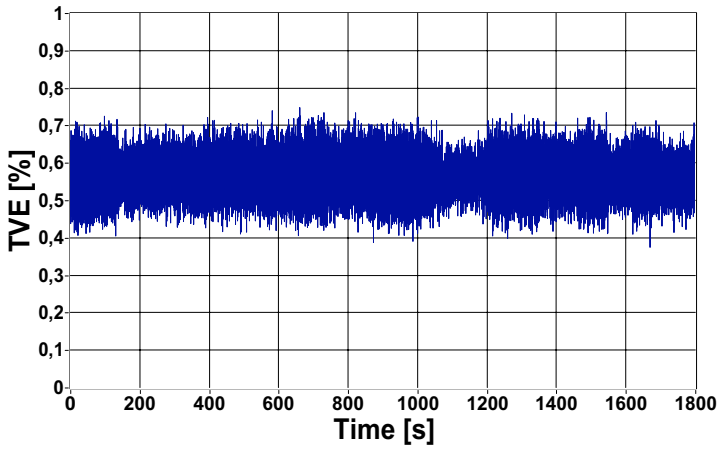


**Figure 5.13:** TVE trend for test D

of the TVE trends (Fig. 5.10 and Fig. 5.13) it is possible to see that the use of two transducers of different type (Test D) implies a bigger deterioration of the measurement performances. The TVE of Test D easily reaches values bigger than half of the 1 % limit even in condition of perfect synchronization. Contrariwise, it is not possible to understand to what extent the module and phase components, due to the transducer use, contribute to the deterioration of the performances. However, from the observation of Figs. 5.11 and 5.12 it can be inferred that in case of Test C, the deterioration of the performances is mainly due to the amplitude contribution, whereas in the case of Test D, from the observation of Figs. 5.14 and 5.15 it is possible to understand that the deterioration is mainly due to the phase contribution of the uncertainty introduced by the transducers.

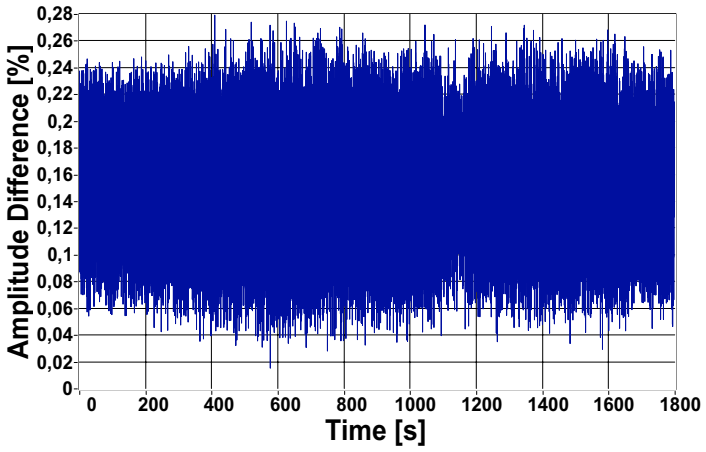


(a)

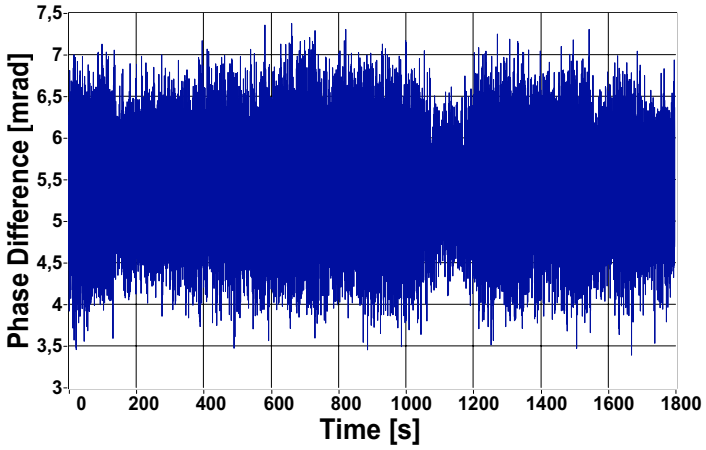


(b)

**Figure 5.14:** Trend of amplitude differences (a) and phase differences (b) in Test D

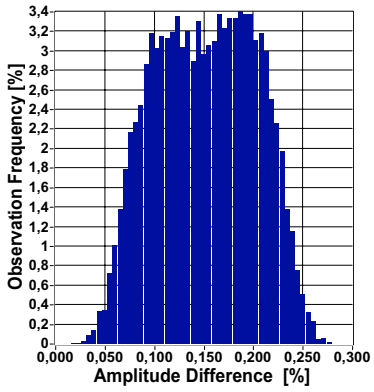


(a)

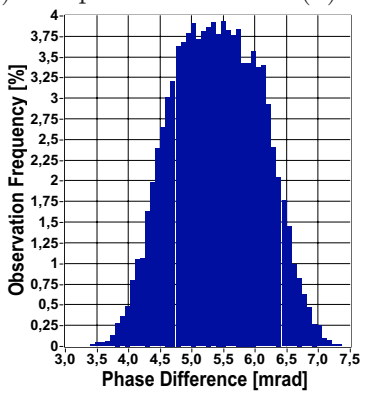


(b)

**Figure 5.15:** Distribution of amplitude differences (a) and phase differences (b) in Test D

**Table 5.2:** Synchrophasor amplitude and phase difference for Test C and Test D

| Test | Amplitude Difference | | Phase Difference | |
|---|---|---|---|---|
| | Mean Value (%) | Standard Deviation (%) | Mean Value (mrad) | Standard Deviation (mrad) |
| C | 0.29 | 1.6E−3 | 0.3 | 0.26 |
| D | 0.15 | 5E−2 | 5.33 | 0.68 |

### 5.1.2 Test under anomalous operative conditions

One of the goals of this work is to investigate the robustness of the proposed synchronization system in the presence of anomalous operative conditions (e.g. caused by faults). The measurement system must be capable of receiving time from a highly reliable source, which can provide sufficient time accuracy to keep the TVE within the required limits. Indication of loss of synchronization must be provided. A loss of time synchronization shall be asserted when loss of synchronization could cause the TVE to exceed the limit or within one minute of actual loss of synchronization, whichever is less [4]. Thus, the system behaviour has been tested in different possible loss of synchronization conditions. The duration of each test is forty minutes, with ten evaluations per second, thus leading to the calculation of twenty-four thousand amplitude and phase values. In the considered cases, the fault event begins about five minutes after the start of the acquisition and holds until the end of the test.

#### Test E

To test the effects of the loss of the GPS signal, the same system configuration of Test A has been considered. The loss of one of the two GPS signals was simulated by either artificially obscuring the GPS antenna of the PXI-based instrument or disconnecting the coaxial cable from the synchronization module. In both situations similar system performance was observed. As an example, Fig. 5.16 shows the trends of the amplitude difference (a) and of the phase difference (b) in the case of coaxial cable disconnection, whereas Fig. 5.17 shows the trend of the TVE (%) for the same test.

The test results permit to underline the robustness of the system from the point of view of faults tolerance. In this test the system is able to meet the specification on TVE without GPS signal for more than twenty-eight minutes. However, the current synchronization systems based on GPS technology do not provide a back-up solutions in presence of a fault like the one tested. This means that, in case of loss of

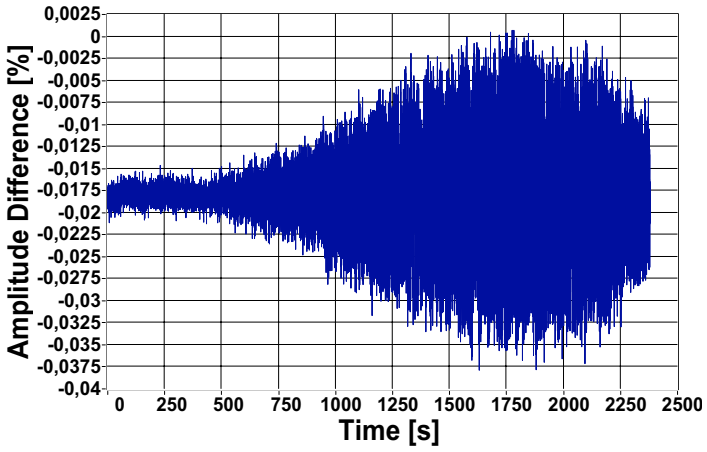


(a)

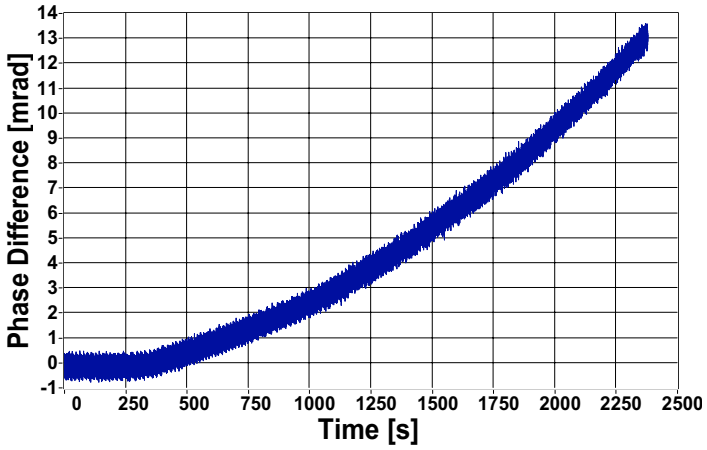


(b)

**Figure 5.16:** Trends of amplitude difference (a) and phase difference (b) in Test E

synchronization due, for example, to the loss of the GPS antenna, the data produced by the instrument will be not usable until the synchronization functions are restored by the intervention of the system operator.

### Test F

To investigate the effects of the loss of PTP synchronization, several tests were performed by artificially causing a loss of the Ethernet communication between the slave unit and the master unit in the proposed system. The loss of the PTP synchronization was simulated by disconnecting the crossover cable on the slave side whereas in the master unit the NI PXI-6682 Timing and Synchronization module

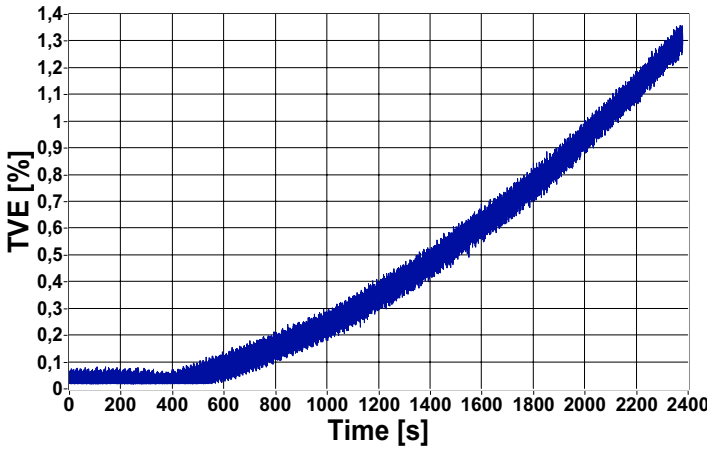


**Figure 5.17:** TVE trend for Test E

is able to receive the GPS signal for the entire duration of the performed test. Fig. 5.18-a and Fig. 5.18-b show the trends of the amplitude and of the phase differences measured by the two units, respectively. Fig. 5.19 presents the TVE trend for Test F. It can be noticed that the GPS-PTP system presents similar performances to those obtained in Test E: it is, in fact, able to meet the specification on TVE for more than thirty minutes after a fault event. Moreover, contrarily to the GPS system, the PTP system provide back-up solutions in case of the loss of the reference clock. Using the best master clock algorithm, in fact, the system is able to select the most accurate clock as reference among the ones still synchronized in the network.

During the period following the loss of synchronization signal, the phase difference values for both Test E (Fig. 5.16-b) and Test F (Fig. 5.18-b) are very high. In Test E, for example, during the five minutes preceding the moment when the TVE reaches the 1 % limit, the phase difference keeps a value greater than 6.5 mrad, which can be considered equivalent to a synchronization error of 20.6 µs at 50 Hz, if the phase deviation is entirely caused by the synchronization error. Such a long period of lack of synchronization could be unacceptable in some applications based on synchrophasors measurement even if the TVE limit is respected. Contrary, the 1 minute limit of actual loss of synchronization (coinciding with the 360-th second, on the time axis) is reached in correspondence of a TVE value largely lower then the 1 % limit and of a phase difference value lower than 1 mrad (equivalent to 3.1 µs at 50 Hz). The same situation can be found in the Test D. This helps to emphasize the inadequacy of TVE to express the accuracy of measures in certain situations, as already pointed in the Section 2.2.

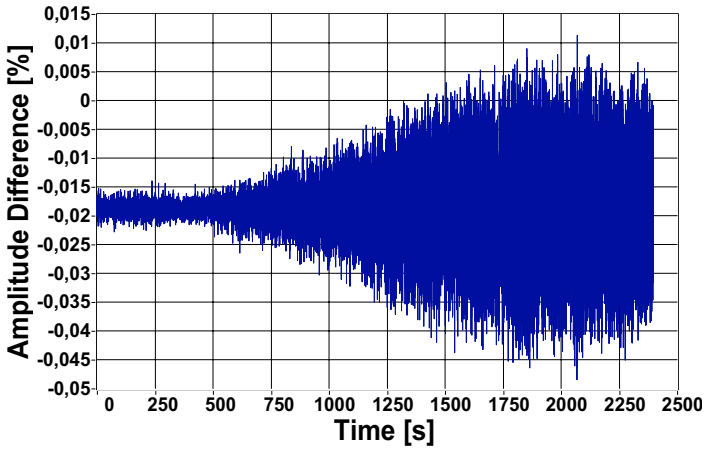


(a)

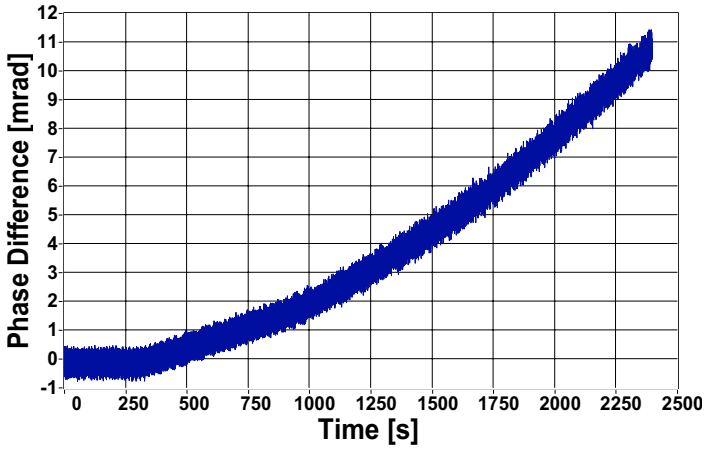


(b)

**Figure 5.18:** Trends of amplitude difference (a) and phase difference (b) in Test F

### Test G

For the Test G, same conditions of Test F have been reproduced, but this time the PMUs acquire the signal through two LEM CV-31000 transducers. Figs. 5.20-a, 5.20-b and 5.21 show the amplitude difference, phase difference and TVE trends, respectively, for Test G.

Once again, as it has been observed for Test C, the TVE increases because of an additional term due to the amplitude and phase deviations between the two transducers. In fact the 1 % TVE limit value is reached after about twenty-five minutes of the loss of the synchronization signal, about five minutes less than the value obtained in Test F.

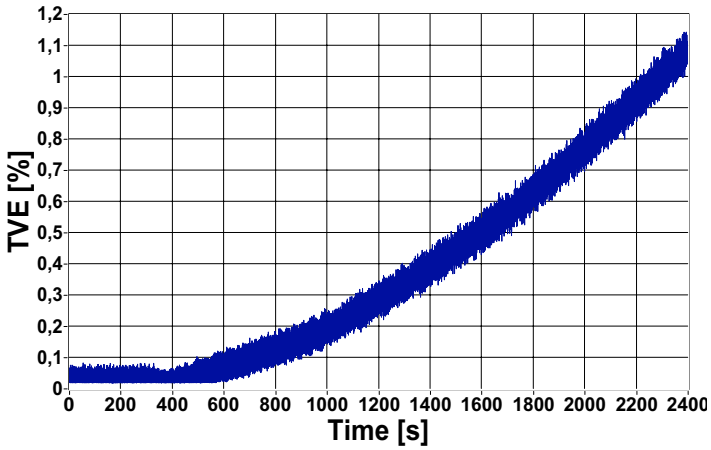


**Figure 5.19:** TVE trend for Test F

### Test H

For the Test H, same conditions of Test G have been reproduced, but this time the one PMUs acquire the signal through a LEM CV-31000 transducer whereas the other one through a magnetic core voltage transformer. Figs. 5.22-a, 5.22-b and 5.23 show the amplitude difference, phase difference and TVE trends, respectively, for Test H.

Already in stationary conditions the phase difference measured between the two transducers were around 6 mrad−7 mrad. Hence, the TVE starts from a value around 0.6 %−0.7 % and only about eleven minutes after the loss of synchronizations are required to reach to limit of 1 % (fifteen minutes earlier than Test G and twenty minutes earlier then Test F). This means that the main causes of uncertainty in the evaluation of synchronized phasors may arise from the input transducers rather than the synchronized acquisition system [5, 6]. In order to deal with this problem, most commercially available PMUs allow the user to define correction factors for both amplitude and phase of the VTs. This requires a preliminary characterization of the used devices. In any case, owing the possible changes of the parameters that define the model of the device for varying operative and environmental conditions, a non-negligible uncertainty is expected to affect the measurement results, even after the compensation has been implemented.

It should be taken into account that the situations presented in all this tests, where two stations are directly linked through a crossover cable, represents the best case for the PTP synchronization performance. In practical cases, the presence of different network components must be considered. These components (switches, routers,

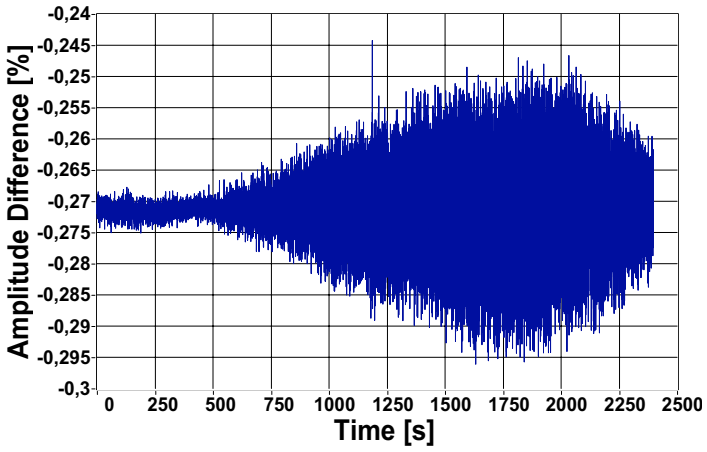


(a)

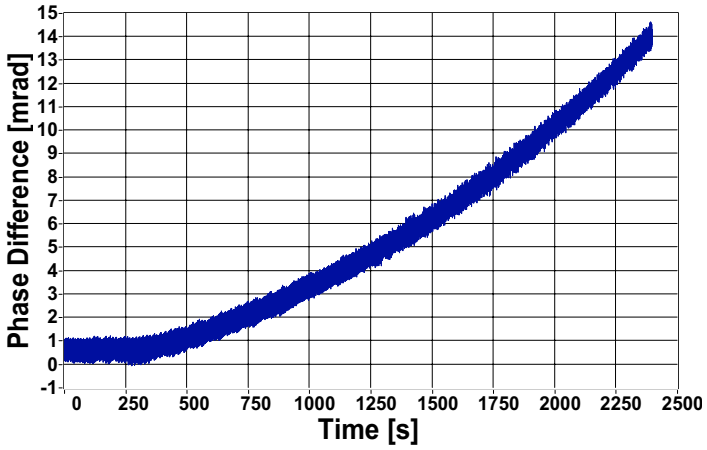


(b)

**Figure 5.20:** Trends of amplitude differences (a) and phase differences (b) in Test G

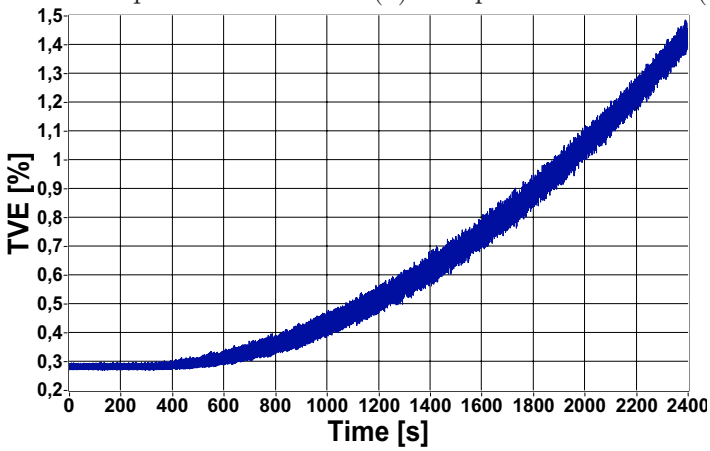


**Figure 5.21:** TVE trend for Test G

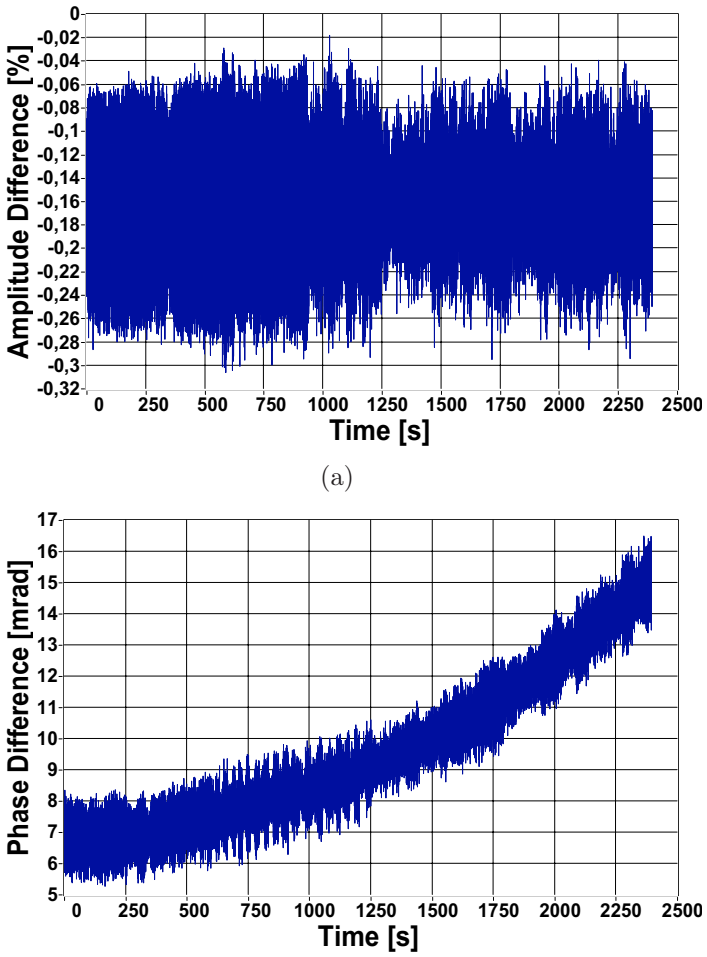


**Figure 5.22:** Trends of amplitude difference (a) and phase difference (b) in Test H

BCs or TCs) can introduce fluctuations in transmission latency that can degrade synchronization accuracy. However, as it has been shown in Section 3.2.2, the uncertainty introduced by PTP-compliant components can be neglected in comparison to the contribution of the transducers.

## 5.2 Tests on the software-only synchronized system

In order to experimentally evaluate the synchronization performances of the PTPd and the impact of its accuracy on applications implemented for wide area system monitoring, several tests with different network architectures, characterized by an

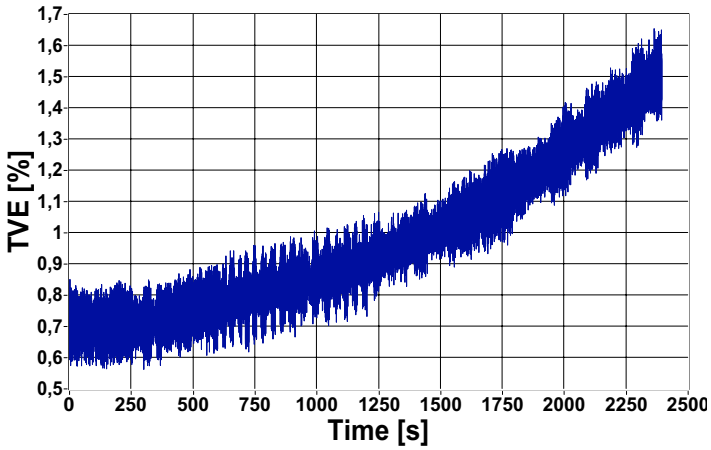


**Figure 5.23:** TVE trend for Test H

increasing complexity, have been executed [7, 8].

### Test I

To analyse the performance of the software-only synchronization system, a preliminary experiment has been conducted. In the test, the PTPd and the PMU software run on two PCs connected via 100 Mbps crossover connection (see Fig. 5.24).

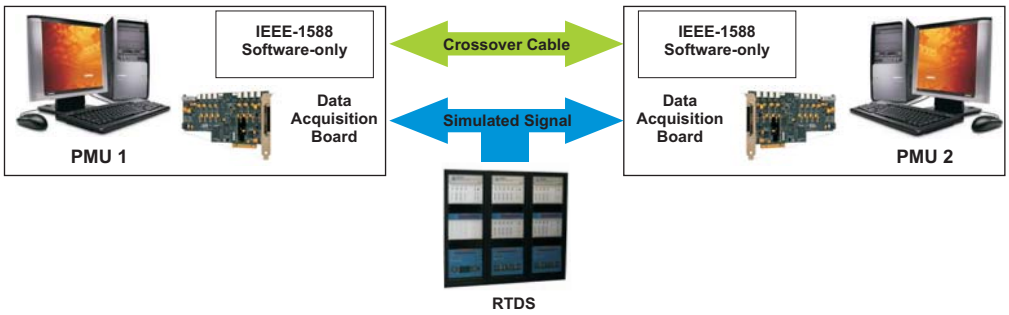


**Figure 5.24:** Setup of the Test I

Only PTPd traffic is present over the link. The test lasts about 70 minutes, with a sync message sending rate of one message per second and one-way delay filter stiffness of $2^6$ as suggested in [9]. Fig. 5.25-a shows the synchronization offset trend between the two clocks of the two PMUs. It is possible to notice that after ten minutes, the two PMUs reach a stable condition of synchronization. By observing Fig. 5.25-b, which shows the offset trend of a portion of the same signal, it is possible

to see that, after the ten minutes necessary to achieve a stable synchronization, the offset remains below 5 µs until the end of the test.

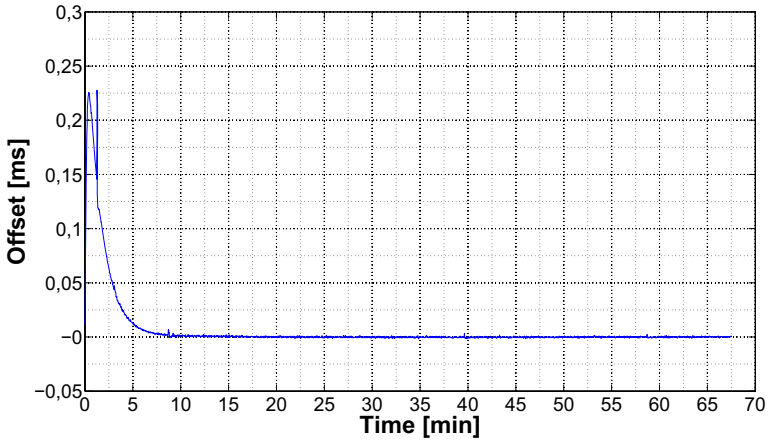


(a)

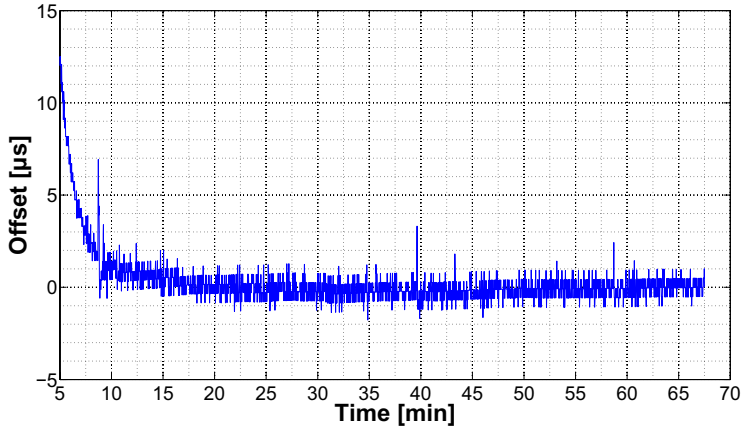


(b)

**Figure 5.25:** PTPd Synchronization offset trend

The accuracy of synchronization seems to be compatible with the requirements of [3]. In Fig 5.26, the frequency distribution of the synchronization error for the period of time between 10 and 70 minutes is reported and in Table 5.3 mean value and variance of the synchronization offset with reference to the same observation time frame are reported.

As already pointed for the hardware-assisted time-stamp based measurement system, it should be considered that the scenario presented in this Section, with two

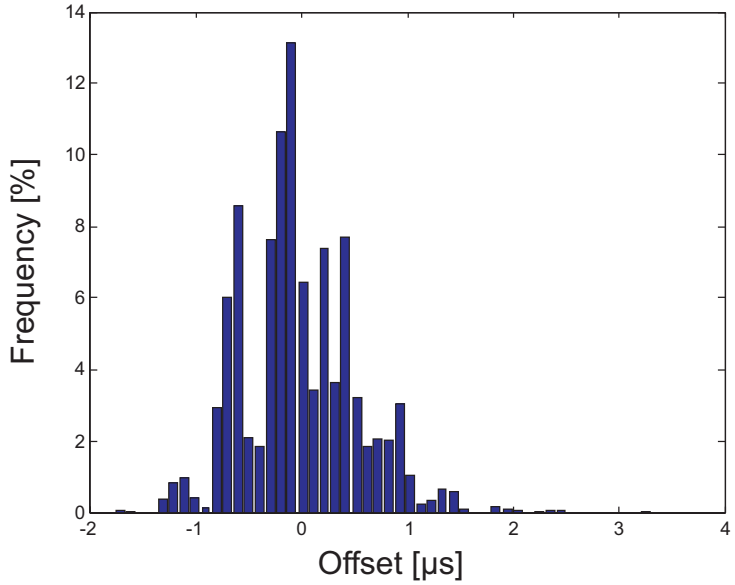


**Figure 5.26:** Distribution of the PTPd synchronization offset

**Table 5.3:** Mean value and standard deviation of the synchronization offset for the period between 10 and 70 minutes

| Synchronization Offset | |
|---|---|
| Mean Value (µs) | Standard deviation (µs) |
| −0.028 | 0.558 |

stations directly linked through a crossover cable, represents an ideal case for the synchronization performance. At the same time, coherently with what has been explained in Section 4.2, the idea of this solution is that every PMU with software-only synchronization is an end-point directly connected with a PTP hardware-assisted device (boundary clocks, transparent clocks). Since these devices have synchronization accuracy below 100 ns, for this analysis the hardware-assisted infrastructure can be considered as "perfectly synchronized".

### Test L

One important consideration arising from the implementation of a completely software-only synchronized PMU is that the latency of the operative system, even if real-time, contributes to the overall jitter in the time-stamping of the single sample, causing an uncertainty on the time-stamp larger than the uncertainty due to the only synchro-

nization offset. As a consequence, several kinds of experimental tests were conducted to analyse the performance of the sample time-stamp process. As an example in the following test, two PMUs synchronized by means of PTPd with a crossover cable, acquire the same voltage signal through the GTAO card of the RTDS platform for a period of 70 minutes, as represented in Fig. 5.24. Each PMU executes the time-stamp of every sample.

In Fig. 5.27, the distribution of the overall jitter that affects the time-stamping process of every sample is reported and, in Table 5.4, values of mean and standard deviation are shown. It is important to notice that, differently from the synchronization offset, that is characterized by a mean value almost equal to zero, the mean value of the complete time jitter is in the order of few microseconds. However, as far as the requirement imposed by [3] are concerned, this offset never reaches values that by themselves would bring the TVE close to the 1 % limit.

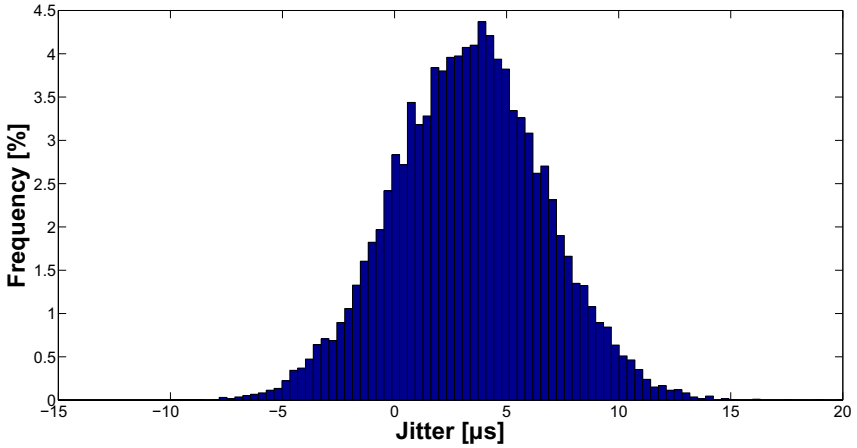


**Figure 5.27:** Distribution of the jitter introduced by the overall time-stamp process

**Table 5.4:** Mean value and standard deviation of the jitter introduced by the overall time-stamp process

| **Time-stamp jitter** | |
|---|---|
| Mean Value (µs) | Standard deviation (µs) |
| 3.33 | 3.35 |

### Test M

Several kinds of experimental tests were executed to study the performance of the designed PMUs. As an example, in the following test, two PMUs in the same configuration of the previous test have been considered. The devices acquire the same signal for a period of 1 s, with twenty-five evaluations per second.

In Figs 5.28 and 5.29, respectively, the phase difference and the TVE trends have been reported. In Fig. 5.30 and Fig. 5.31 the distributions of the phase error and the TVE are respectively reported.

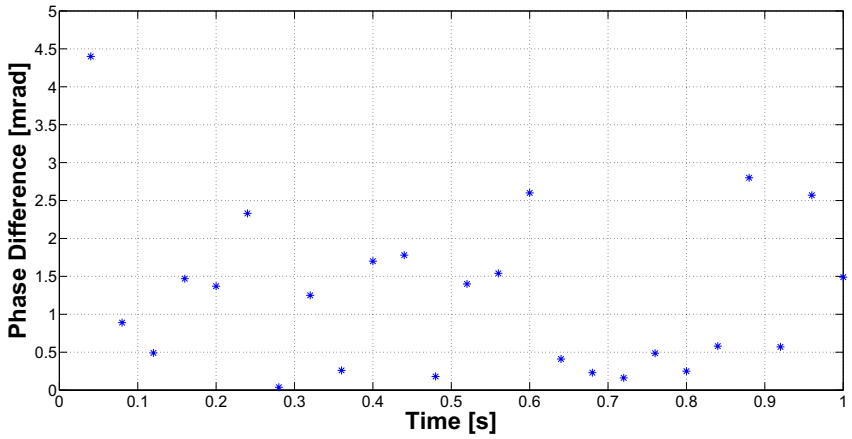


**Figure 5.28:** Phase difference trend for test M

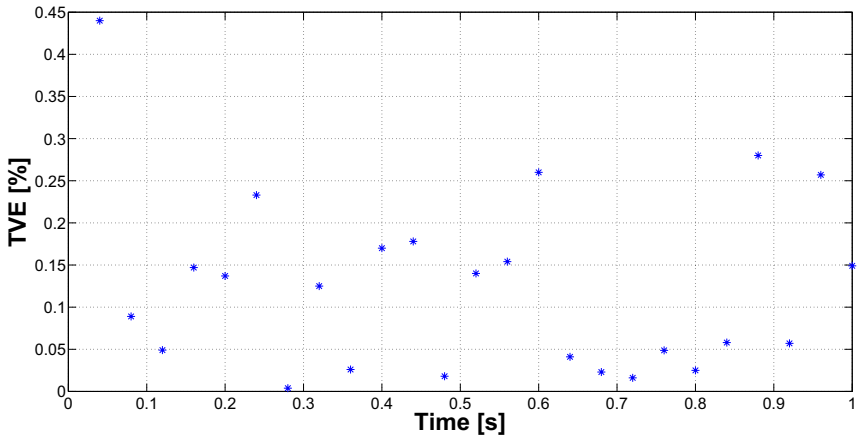


**Figure 5.29:** TVE trend for test M

According to the synchronization performance presented in Fig. 5.25, if the only synchronization error due to the PTPd offset was present, the expected phase difference value, in a 50 Hz system, would be between ±1.5 mrad. The larger values of phase difference shown in Fig. 5.28 can be mainly attributed to the jitter introduced by the time-stamping process of the general purpose acquisition system (board and computer). Anyway, the acquisition system seems to work properly and its TVE is well below the 1 % limit.

For the sake of clarity, Figs. 5.30 and 5.31 show the distributions of the phase difference and the TVE obtained after a Monte-Carlo analysis with 10000 simulations. Table 5.5 summarizes the main statistical data.

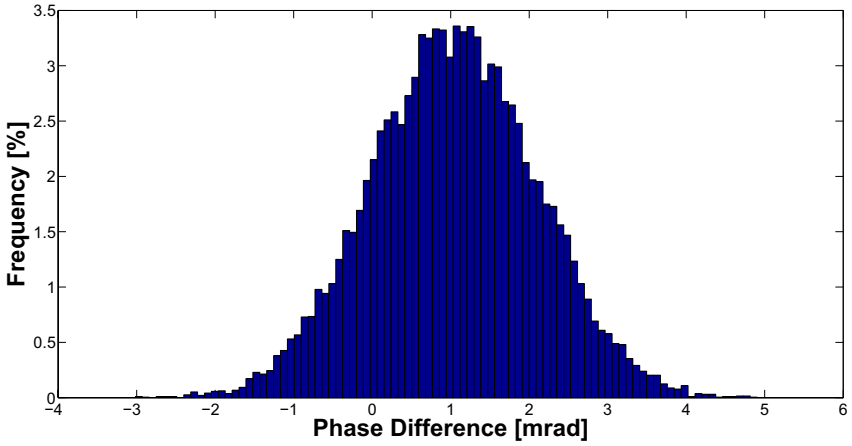


**Figure 5.30:** Phase difference distribution for test M

**Table 5.5:** Mean value and standard deviation of the phase difference and TVE distributions, respectively, in Test M.

| **Phase Difference** | | **TVE** | |
|---|---|---|---|
| Mean Value (mrad) | Standard Deviation (mrad) | Mean Value (%) | Standard Deviation (%) |
| 1.3 | 1.1 | 0.12 | 0.084 |

### 5.2.1 Tests on the State Estimation

One of the objectives of this thesis is the study of the impact of the uncertainty of the proposed synchronization solution on the applications used in WAMSs. Among

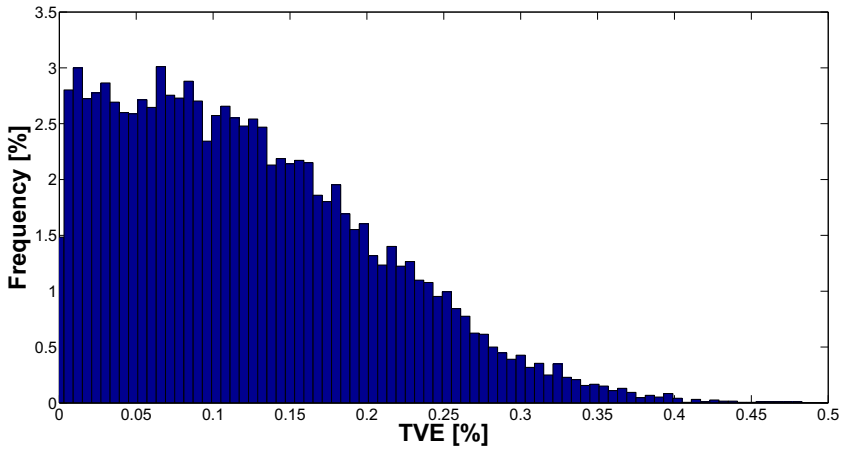


**Figure 5.31:** TVE distribution for test M

the applications presented in Section 1.2, the SE has been chosen as a case of study. The output data of the PMUs have been used to estimate the state of different simulated power networks. In the following, the results of the SE of a 8-bus and a 57-bus networks are presented.

### 8-bus network Test

The 8-bus power system is a portion of the 110 kV network of Aachen (NRW, Germany) operated by STAWAG, the municipal utility of Aachen. The power system is composed of eight buses and six substations (named after their location, as shown in Fig. 5.32). The power system model has been implemented in RTDS and all the measurements acquired by the PMUs are exported in real time on analog output channels.

To perform a valuable SE of the considered power system by using only synchrophasor data, the PMUs have to be properly located. The problem of PMUs placement has been widely addressed in literature and different methods have been proposed to place the minimum number of PMUs to achieve complete or incomplete observability both in case of normal operation and in case of contingency [10–12]. However, since the objective of these tests is to evaluate how synchronization of different PMUs based on software-only IEEE1588 impacts on the power system SE accuracy, only configurations which permit to obtain the complete observability of the network are considered. In this test, the complete observability is obtained by placing two PMUs (a master and a slave) in the Seffent substation (see Fig. 5.32) and a third one, perfectly synchronized to the master of Seffent substation, in the Verlautenheide substation.

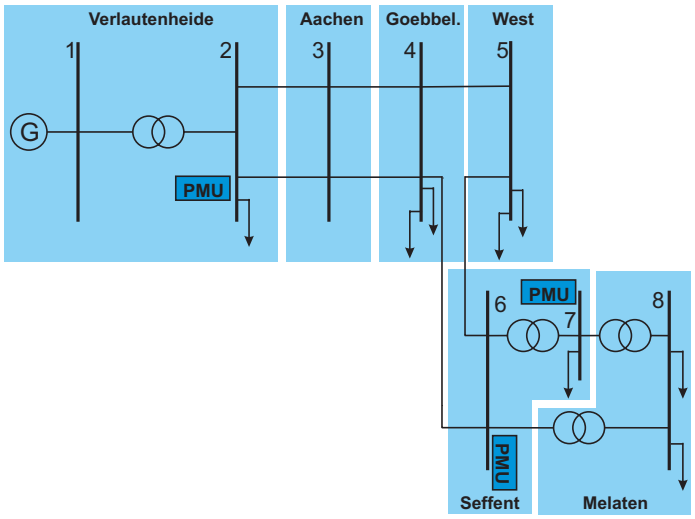


**Figure 5.32:** Power system model

The SE is performed off-line on Matlab, using the method presented in Section 1.3. The three PMUs acquire all the signals (voltages and currents) of the bus in which they are installed. The data of the three PMUs are then used to perform the SE using WLS. To assess the results, a reference case has been created in which all the PMUs were supposed to be perfectly synchronized: the digital time domain values of the generated signals for bus 2, 6 and 7 are exported from RTDS and are used to calculate the phasors. In this reference case all synchronization and acquisition errors have been assumed equal to zero. The procedure of SE has been performed under two different configurations of the experimental setup: one with the master unit in node 6 and the other with the master unit in node 7. To gain a qualitative understanding of the behaviour of the SE process, Fig. 5.33 shows the phases of the voltages over the eight nodes for a generic instant $t$ when the master PMU is assumed to be in node 6 (green stars) and 7 (red stars), respectively. The blue circles represent the reference values.

To have a more quantitative evaluation of how the system uncertainty due to a software-only implementation of the 1588 affects a process of SE a stochastic analysis has been performed. A reporting rate of 25 phasors per second has been chosen and the SE process has been performed 25 times per second for 800 s. As an example in Fig. 5.34-a and Fig. 5.34-b, the distributions of the phase error for the voltage of node 4 when the master is the PMU in the bus 6 and in the bus 7 are respectively reported. It is interesting to notice that these results present a behaviour similar to the one of Fig. 5.30, but the values of error are reduced by the process of SE. This is due to the fact that the SE process based on WLS weights the different measures

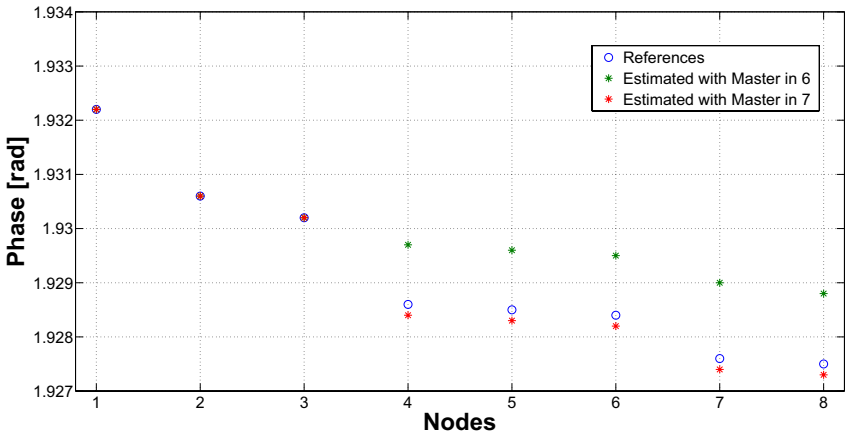


**Figure 5.33:** Voltage phases in the eight nodes when the master is in node 6 (green stars) and in node 7 (red stars)

according to their accuracy (reported in the matrix **W**). In this way the effect of the synchronization error is mitigated.

### 57-bus network Test

In this test, a more complex power system has been simulated by means of the RTDS: the IEEE 57-bus system [13]. A so extended network requires a considerable number of PMUs to guarantee the complete observability of the system and the execution of a SE algorithm entirely based on PMUs data. As a consequence, the PMUs used for these series of tests are not the actual devices described in Section 4.2, but they have been simulated in the Matlab environment according to the characteristic of the realized PMU presented in tests I, L, M. The input data from RTDS and from the synchronization system are imported in Matlab and used to calculate the phasors, which are then used for the execution of the SE algorithm described in Section 1.3. In particular, the arrays of samples obtained from the RTDS software interface are imported in Matlab. Then, the sub-arrays used for the synchrophasors estimation are chosen according to the value of the offset from the master, previously estimated in the simulation of the IEEE 1588 network. Fig. 5.35 shows a representation of the setup used for this test.

Different optimal locations of the PMUs, taken from the literature, have been used. All the chosen configurations guarantee the complete observability of the system without considering zero injection effects. The first configuration, presented in [14], guarantees the complete observability of the system using 17 PMUs. Their optimal placement is selected by means of a numerical optimization method based on

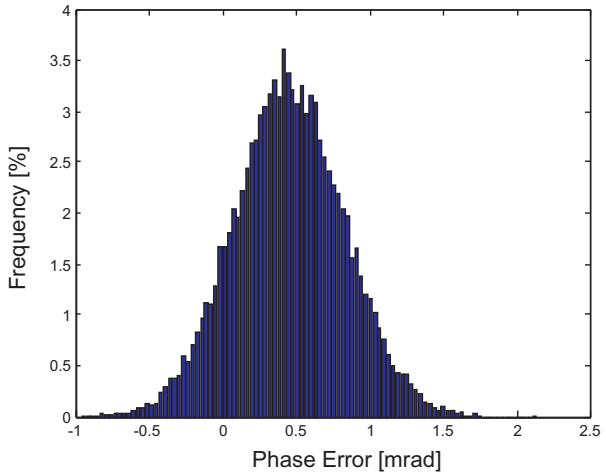


(a)

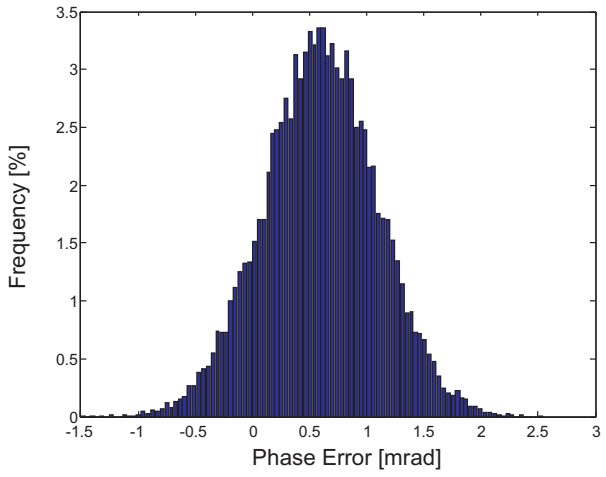


(b)

**Figure 5.34:** Distribution of the phase error when the master is in node 6 (a) and in node 7 (b)

integer programming. The objective of the optimization is to minimize the number of PMUs for a fully observable system. The PMUs placement is shown in Fig 5.36 using red circles.

The second configuration (blue squares in Figure 5.36), presented in paper [15], is also the result of an optimization problem. But in this case the optimal placement of the 17 PMUs is obtained by means of a quadratic programming approach, whose purpose is both to minimize the total number of PMUs required for complete

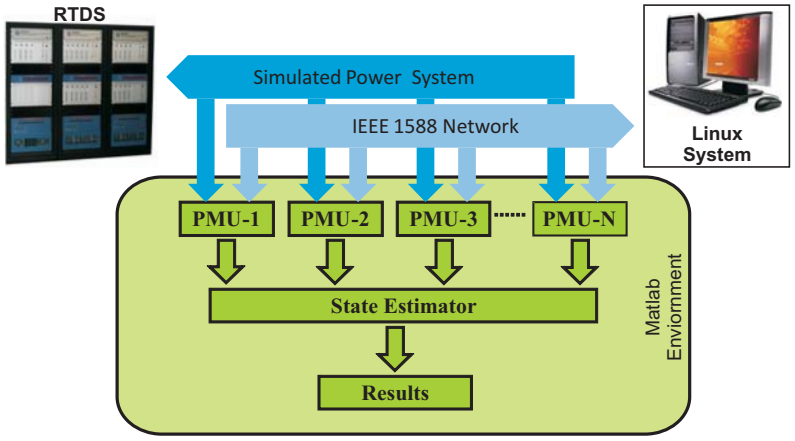


**Figure 5.35:** System experimental setup used for the tests on the IEEE 57-bus network

observability and to maximize the measurement redundancy.

In [16], a probabilistic multi-stage PMU placement technique, which takes into account the stochastic nature of components and their outage probabilities, has been used. It was proven that it is possible to guarantee the complete observability of the tested system by means of 24 PMUs. The placement for the third configuration is shown in Figure 5.36 using green diamonds to indicate the PMUs. For the sake of clarity, Table 5.6 shows the placement of PMUs for the three different configurations.

**Table 5.6:** Optimal Locations of PMUs.

| Configuration | Number of PMUs | Locations of PMUs |
|---|---|---|
| 1 | 17 | 1, 4, 7, 9, 15, 20, 24, 25, 27, 32, 36, 38, 39, 41, 46, 50, 53 |
| 2 | 17 | 1, 4, 6, 9, 15, 20, 24, 25, 28, 32, 36, 38, 41, 47, 50, 53, 57 |
| 3 | 24 | 1, 3, 6, 8, 11, 12, 14, 18, 20, 22, 24, 28, 30, 32, 35, 38, 39, 40, 41, 45, 47, 51, 52, 54 |

A Monte-Carlo analysis with 10000 simulations has been done fore this test. The maximum and mean values of the phase angle deviations of each bus for one of these simulations are shown in Fig. 5.37 and Fig. 5.38, respectively. It is shown that maximum and mean values have a similar trend in Configuration 1 and Configuration 2 in which the peak points are in correspondence of the bus 12. On the other hand, in Configuration 3 the phase angles are estimated more accurately at many buses

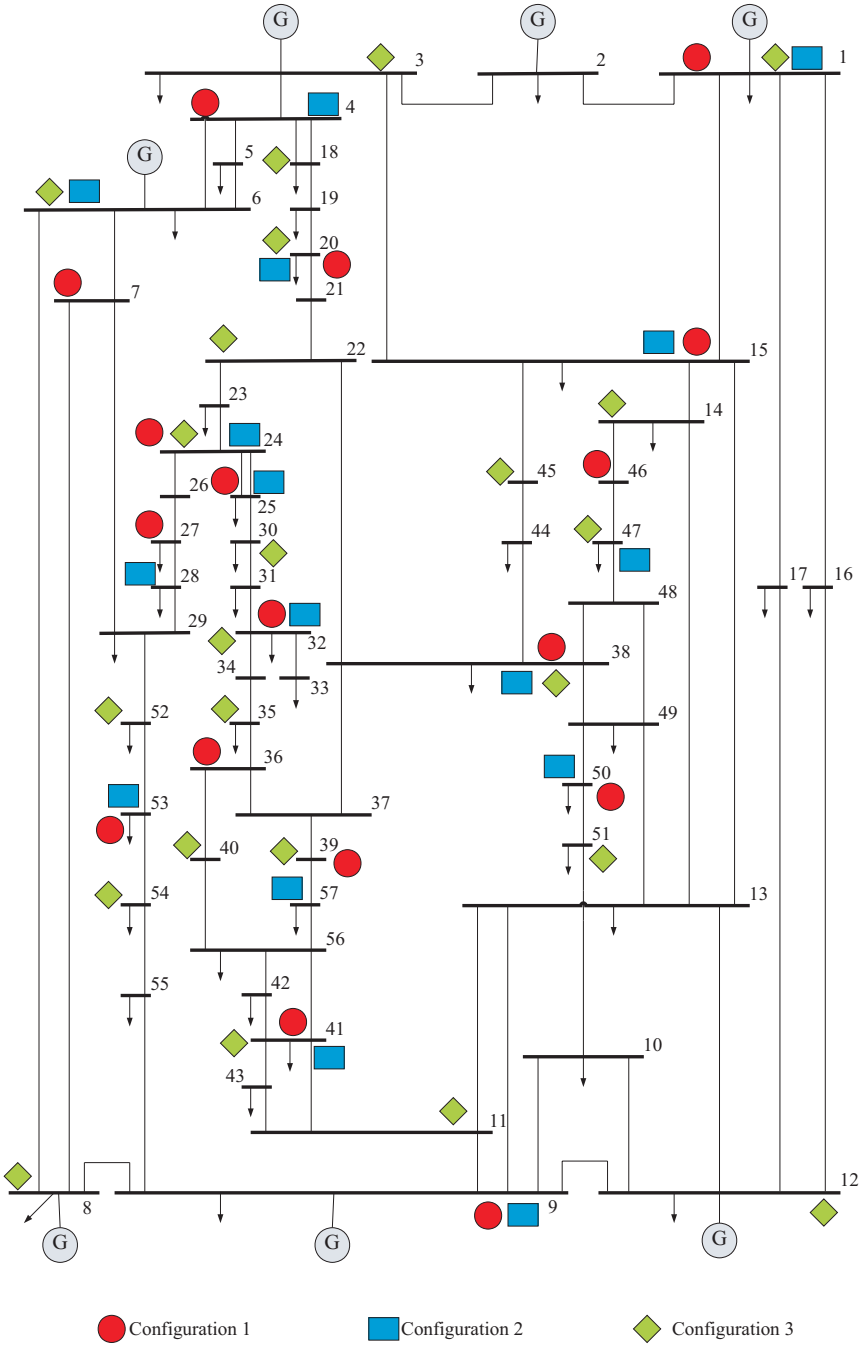


**Figure 5.36:** Schematic of PMU placement for the IEEE 57-bus system

and the critical situation at the bus 12 disappears. This is obviously due to the installation of more PMUs and, in particular, to the installation of a PMU in nodes 12.

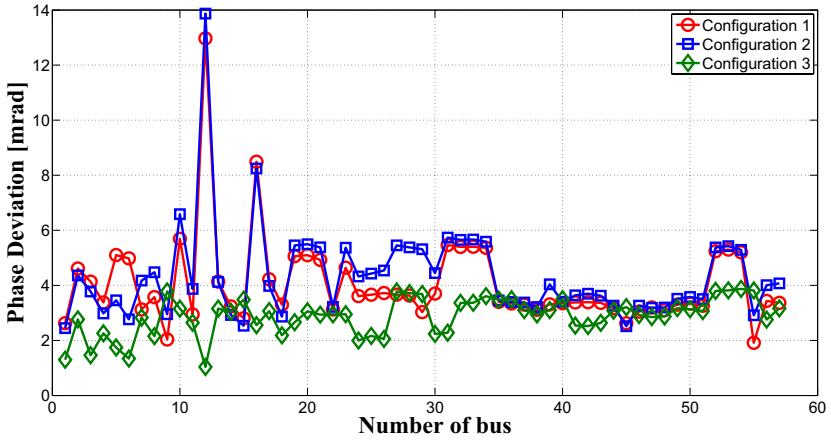


**Figure 5.37:** Maximum deviation of phase angle estimation at each bus

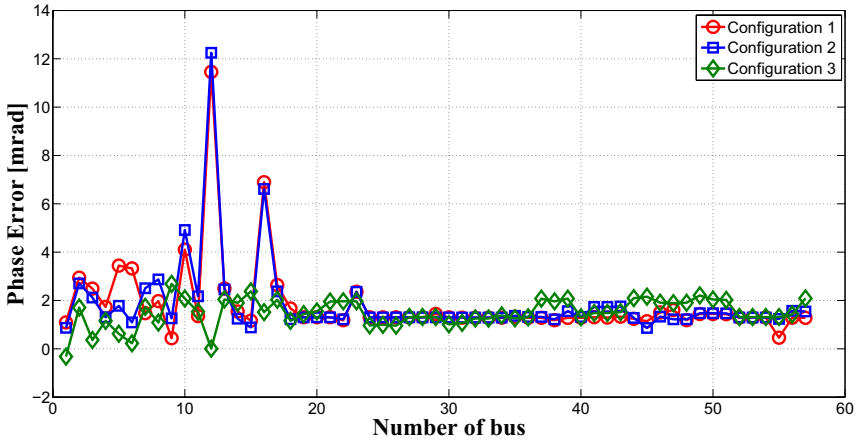


**Figure 5.38:** Mean deviation of phase angle estimation at each bus

To evaluate the impact of the measurement uncertainty caused by PTPd synchronization on the SE application more quantitatively, a detailed statistical analysis is applied to the individual buses. As an example, a closer look is given at the performances of bus 12, which represents the most critical situations in both Configurations 1 and 2. The statistical distributions of the phase deviation for bus 12 in the three cases are depicted in Figs. 5.39, 5.40 and 5.41, respectively.

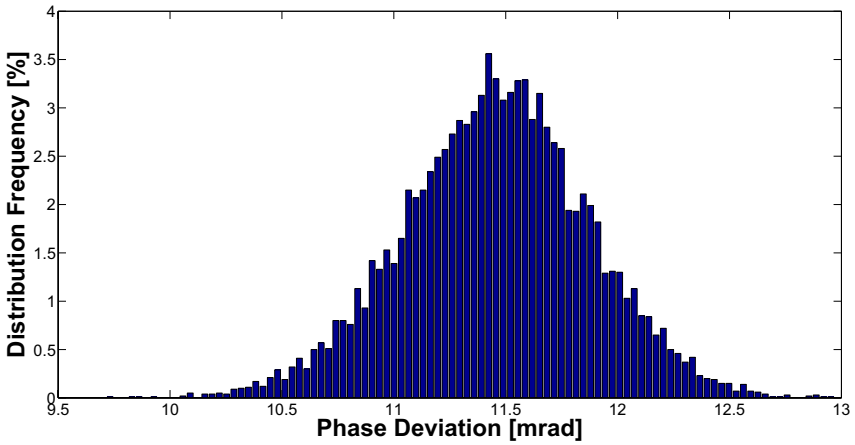


**Figure 5.39:** Distribution of bus-12 phase angle deviation in Configuration 1

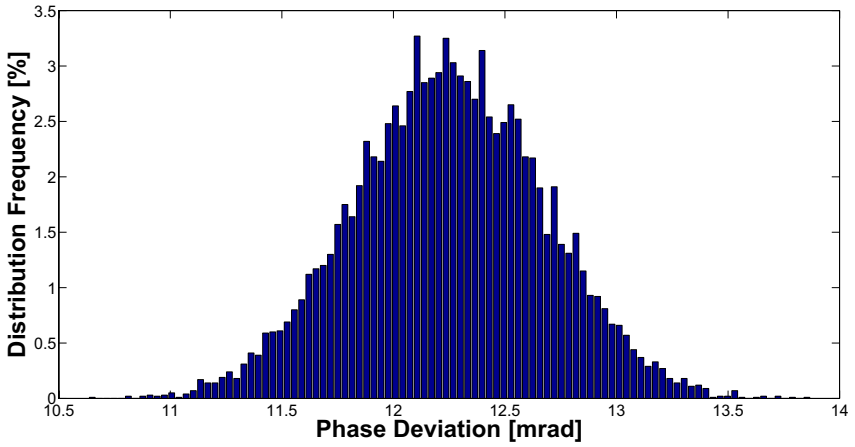


**Figure 5.40:** Distribution of bus-12 phase angle deviation in Configuration 2

It can be observed that in Configurations 1 and 2 the deviations in the evaluation of the phase angles are much higher than the uncertainty arising from a direct PMU measurement, which, according to [3], is in the order of 1 mrad. On the contrary, in Configuration 3 the deviations are, obviously, much smaller, owing to the PMU placement at this bus.

However, the presented results on both the 8-bus and the 57-bus systems show that, even if dedicated hardware is not used in the implementation of the PTP, the single PMU measurement complies with the accuracy required by the IEEE standard on synchrophasors and the impact of the synchronization uncertainty on the

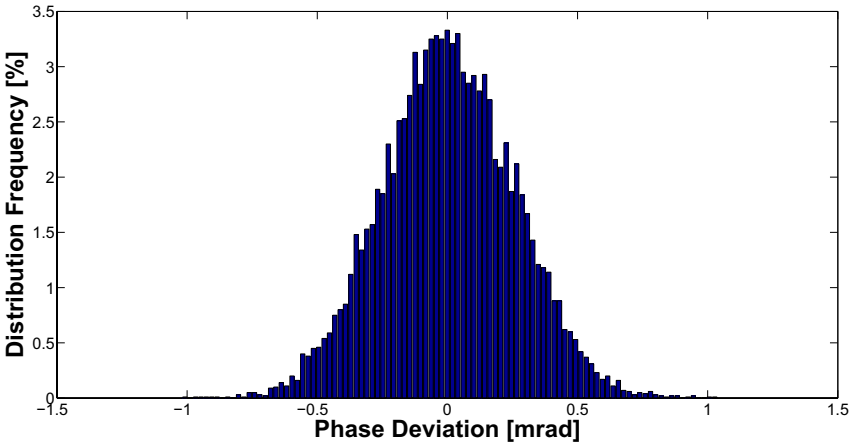


**Figure 5.41:** Distribution of bus-12 phase angle deviation in Configuration 3

estimated quantities can be low.

# Bibliography


[1] M. Lixia, N. Locci, C. Muscas, and S. Sulis, "Synchrophasors measurement in a GPS-IEEE 1588 hybrid system," *European Transactions on Electrical Power*, no. 21, pp. 1509–1520, 2011.

[2] M. Lixia, C. Muscas, and S. Sulis, "Application of IEEE 1588 to the measurement of synchrophasors in electric power systems," in *Precision Clock Synchronization for Measurement, Control and Communication, 2009. ISPCS 2009. International Symposium on*, oct. 2009, pp. 1 –6.

[3] "IEEE standard for synchrophasor measurements for power systems," *IEEE Std C37.118.1-2011 (Revision of IEEE Std C37.118-2005)*, pp. 1 –61, 28 2011.

[4] "IEEE standard for synchrophasor data transfer for power systems," *IEEE Std C37.118.2-2011 (Revision of IEEE Std C37.118-2005)*, pp. 1 –53, 28 2011.

[5] A. Carta, N. Locci, C. Muscas, and S. Sulis, "A flexible GPS-based system for synchronized phasor measurement in electric distribution networks," *Instrumentation and Measurement, IEEE Transactions on*, vol. 57, no. 11, pp. 2450 –2456, nov. 2008.

[6] A. Carta, N. Locci, and C. Muscas, "GPS-based system for the measurement of synchronized harmonic phasors," *Instrumentation and Measurement, IEEE Transactions on*, vol. 58, no. 3, pp. 586 –593, march 2009.

[7] M. Lixia, A. Benigni, A. Flammini, C. Muscas, F. Ponci, and A. Monti, "A software-only PTP synchronization for power system state estimation with PMUs," in *Instrumentation and Measurement Technology Conference (I2MTC), 2011 IEEE*, may 2011, pp. 1–6.

[8] J. Tang, M. Lixia, J. Liu, C. Muscas, and A. Monti, "Impact of PMU sychronization on wide area state estimation," in *Applied Measurements for Power Systems (AMPS), 2011 IEEE International Workshop on*, sept. 2011, pp. 74 –79.

[9] K. Correll and N. Barendt, "Design considerations for software only implementations of the IEEE 1588 precision time protocol," in *In Conference on IEEE 1588 Standard for a Precision Clock Synchronization Protocol for Networked Measurement and Control Systems*, 2006.

[10] R. Nuqui and A. Phadke, "Phasor measurement unit placement techniques for complete and incomplete observability," *Power Delivery, IEEE Transactions on*, vol. 20, no. 4, pp. 2381 – 2388, oct. 2005.

[11] T. Baldwin, L. Mili, J. Boisen, M.B., and R. Adapa, "Power system observability with minimal phasor measurement placement," *Power Systems, IEEE Transactions on*, vol. 8, no. 2, pp. 707 –715, may 1993.

[12] B. Gou and A. Abur, "An improved measurement placement algorithm for network observability," *Power Systems, IEEE Transactions on*, vol. 16, no. 4, pp. 819 –824, nov 2001.

[13] [Online]. Available: http://www.gps.gov

[14] B. Xu and A. Abur, "Optimal placement of phasor measurement units for state estimation," in *PERSEC*, oct. 2005.

[15] S. Chakrabarti, E. Kyriakides, and D. Eliades, "Placement of synchronized measurements for power system observability," *Power Delivery, IEEE Transactions on*, vol. 24, no. 1, pp. 12 –19, jan. 2009.

[16] F. Aminifar, M. Fotuhi-Firuzabad, M. Shahidehpour, and A. Khodaei, "Probabilistic multistage pmu placement in electric power systems," *Power Delivery, IEEE Transactions on*, vol. 26, no. 2, pp. 841 –849, april 2011.

# Chapter 6

# Impact of the model on synchrophasor measurement accuracy

The uncertainty introduced by a Phasor Measurement Unit can be attributed to four sources: transducers, data acquisition system (conditioning and sampling), synchronization system, and phasor estimation algorithm. The effects of transducers and synchronization system have been analysed in the previous chapters of these thesis, whereas the effects of the data acquisition system (conditioning and sampling) have been deeply studied in the literature. Data acquisition system includes analog signal conditioning devices and Analog-to-Digital Converters (ADCs). The signal conditioning stage performs the tasks of raw signal filtering, signal amplifying or attenuating and its uncertainty is mainly due to system noise, non linearities and gain error. As for ADCs, in commercial PMUs, 14 or 16 bit converters are usually employed. The quantization error is therefore negligible with respect to the other uncertainty sources [1].

On the other hand, the uncertainty due to the digital processing stage has been often considered as a marginal contribution, because in many circumstances the other sources of uncertainty can be prevailing. However, some studies have already pointed out that, in several practical conditions, different theoretical approaches and different algorithms may lead to significant differences in the measurement result [2, 3]. For these reasons, this uncertainty source, which directly involves the model of the measurand, will be analysed more deeply in this last chapter of the thesis.

## 6.1 Phasor Estimation Algorithms

In the literature, several studies on different algorithms under steady state and dynamic conditions have been reported. Every algorithm requires a phasor model and uses specific techniques to match the model parameters. In particular, the algorithms can be divided into two main classes with respect to the measurement model: algorithms relying on a pure sinusoidal signal model (static phasor model) and algorithms based on an intrinsically non-sinusoidal model (dynamic phasor model).

### 6.1.1 Algorithms based on the static phasor model

The static phasor model (2.2) is the underlying model for a wide class of algorithms. The simplest and most widespread algorithm calculates the phasor by a Discrete Fourier Transform (DFT) computation applied to a given observation window (**method A**):

$$\tilde{\mathbf{X}}_{T_r} = \frac{\sqrt{2}}{N} \sum_{n=-\frac{N}{2}}^{j=\frac{N}{2}-1} x\, \Delta t\, e^{-j2\pi \frac{n}{N}} \tag{6.1}$$

where $\tilde{\mathbf{X}}_{T_r}$ is the phasor estimated at the reference time $T_r$, $\Delta t = nT_s - T_r$ is the time shift with respect to $T_r$ and $N$ is the number of samples in a chosen window. The DFT based algorithm works correctly when, in stationary conditions, the observation window perfectly matches an integer number of cycle durations of the periodic signal $x(t)$. Thus, $N$ is usually chosen as a multiple of $N_0 = 1/(f_0 \cdot T_s)$, that is the number of samples in one cycle at nominal frequency. When this condition is not met, in particular under off-nominal frequency conditions, good results can be achieved by both adapting the observation window in order to contain an integer number of cycles at the actual frequency of the system and weighting the samples with a specific window, such as Hamming or Hann (**method $\mathbf{A}_\mathrm{w}$** in the following).

There are algorithms that, while keeping the simple steady-state model, try to compensate the errors of DFT due to dynamic behaviour in the acquired signal. One method (here referred to as **method B**) studied to attenuate the negative effect that arises under off-nominal frequency conditions and to filter the fast transient events, caused by switching operations and faults, has been proposed in [5]. The method is based on a three-point-filter technique and uses three partially overlapping observation windows. Each synchrophasor is obtained by calculating the DFT on a one-cycle observation window centred on the reference time and averaging it with two adjacent DFT-estimated phasors chosen such that their relative phase angles with respect to the central one are $\pm 60°$ at the nominal fundamental frequency.

### 6.1.2 Algorithms based on the dynamic phasor model

Under dynamic conditions, the static model (2.2) might not be able to follow phasor changes that take place in the observation window, thus leading to an incorrect synchrophasor evaluation. In these situations, method based on dynamic model (2.4) can be used.

There are algorithms that are conceived as a post-processing step of DFT calculation aimed at correcting DFT estimation errors due to the mismatch between a dynamic model and the steady-state one. In [6] for instance, the time-changing phasor is described by a first order complex polynomial (always centred in $T_r$) for a 4 parameters algorithm or by a second order one for a 6 parameters algorithm (referred to as **method C** in the following). The expanded model implies that, in the second order modelling, the boxcar one cycle DFT phasor $\tilde{\mathbf{Y}}$ calculated on a window centred on $T_r$ is tied to the zero, first and second order theoretical parameters by the following equation:

$$\tilde{\mathbf{Y}} = \bar{\mathbf{X}}^{(0)} + j\frac{\bar{\mathbf{X}}^{(1)^*}}{2Nf_0\sin(\frac{2\pi}{N})} \tag{6.2}$$

where $\bar{\mathbf{X}}^{(1)^*}$ is the conjugate of the first order phasor derivative $\bar{\mathbf{X}}^{(1)}$. The true phasor $\bar{\mathbf{X}}^{(0)}$ is then estimated from the correction formula:

$$\bar{\mathbf{X}}^{(0)} = \tilde{\mathbf{Y}} - j\frac{\bar{\mathbf{X}}^{(1)^*}}{2Nf_0\sin(\frac{2\pi}{N})} - \frac{\bar{\mathbf{X}}^{(1)^*}}{f_0^2}\left(\frac{N-1}{24N}\right) - \frac{\bar{\mathbf{X}}^{(2)^*}}{f_0^2}\frac{\cos\left(\frac{2\pi}{N}\right)}{2N^2(\sin\frac{2\pi}{N})^2}24N \tag{6.3}$$

where $\bar{\mathbf{X}}^{(1)^*}$ and $\bar{\mathbf{X}}^{(2)^*}$ are the conjugate of the first and second order phasor derivatives $\bar{\mathbf{X}}^{(1)}$ and $\bar{\mathbf{X}}^{(2)}$. Derivatives are computed via finite difference formulations. For instance, $\bar{\mathbf{X}}^{(1)}$ can be calculated by:

$$\frac{\bar{\mathbf{X}}_M^{(1)}}{f_0} \approx \frac{3}{2}\tilde{\mathbf{Y}}_{\mathbf{M}} - 2\tilde{\mathbf{Y}}_{\mathbf{M-1}} + \frac{1}{2}\tilde{\mathbf{Y}}_{\mathbf{M-2}} \tag{6.4}$$

where $M$ is the current window index and the adjacent observation windows ($M-1$ and $M-2$), are also needed (see [6] for details). It is interesting to note that a model of greater order requires more adjacent windows to be estimated and, as a consequence, a greater computational cost. Another technique based on the same concept can be found for instance in [7], where a second order model is used and the finite difference equations are replaced by a least squares approach.

A different approach for signal analysis under oscillations is introduced in [8]. It is based on a linear filter bank, that performs a Least Squares (LS) approximation of an observation window (that can also include a non-integer number of cycles) with

respect to the second order Taylor model. Unlike the algorithms introduced in [6] and [7], such algorithm directly acts on the samples, without any DFT computation. As a consequence, an arbitrary number of samples can be used and the observation window is not required to include an integer number of cycles. A Weighted Least Squares (WLS) can also be used, giving different weights to different samples, as suggested in [9]. The linear non-orthogonal transform, involved in the algorithm, is defined as a Taylor-Fourier transform and is intended to approximate the band-pass signal represented by the dynamic phasor (see (2.4)). The algorithm gives a simultaneous estimation of all the second order model parameters, which are phasor, phasor speed and phasor acceleration (phasor derivatives of zeroth, first and second order, respectively). From these parameters it is straightforward to obtain the amplitude along with its derivatives and the phase along with frequency and Rate of Change of Frequency (ROCOF). The algorithm will be referred as **method D**.

## 6.2 Test setup

The simulated test cases can be divided into two main classes with respect to the dynamics of the reference signal: steady-state and transient conditions. Steady-state includes both the ideal sinusoidal quantities and other important non-sinusoidal conditions that can be found in the practice: additive noise, amplitude and phase modulations, presence of harmonics and interharmonics. In this class, signals that show stable characteristics over time have been included. However, it is important to underline that they can correspond both to static and dynamic phasor behaviour. On the other hand, step signals and linear frequency ramp signals have been chosen as representative of transient conditions of a power network.

All the tests have been designed in the LabVIEW 2010 framework, implementing the reference signal and disturbance generation module, the synchrophasor measurement algorithms under test and the performance evaluation blocks. Method A uses a number of samples corresponding to one cycle at nominal frequency. The other algorithms employ a different number of cycles: method $A_w$ two cycles, according to [3], method B three partially overlapping cycles, method C three cycles, according to [6], and method D four cycles, as suggested in [9].

Tests have been performed by simulations, adopting a 10 kSa/s sampling frequency. A "per sample approach" has been used, that is a phasor computation performed at every sampling period by continuously shifting the observation window by a single sample. The subsequent analysed windows are thus overlapping, except for a sample. Each synchrophasor is referred to the reference time corresponding to the centre of the estimation window. The aim is to precisely follow phasor evolution, to better test estimation algorithms behaviour. In the practice, every PMU will have a

tunable reporting rate ( [10] suggests 10, 25, 50 synchrophasors per second for 50 Hz power systems and 10, 12, 15, 20, 30, 60 synchrophasors per second for 60 Hz power systems), but this is only related to real-time computational issues or bandwidth requirements for data transmission. For the methodological analysis purpose of this work, it is better to have the fastest measurement rate, so that the limit condition is investigated.

### 6.2.1 Steady-state tests

#### Noise

The tests are aimed at emphasizing the rejection property of algorithms with respect to additive white gaussian noise.

#### Harmonics and interharmonics

Harmonics and interharmonics cause signal distortion, that has to be canceled by phasor estimation algorithm in order to retain the fundamental frequency model. As for the harmonics, in order to consider a general situation, rather than introducing one harmonic component at a time, here a signal spectrum composed by the individual harmonics indicated in the power quality standard [11] is used.

Each interharmonic can be considered as a single frequency component that is superimposed to the useful signal. Interharmonics can be extremely difficult to detect and isolate if they are located in the band of interest of the phasor dynamic model (2.4).

#### Modulation

A modulated signal (see equation (2.9)) can be useful to describe power swings. References [5] and [10] suggest to employ sinusoidal functions, at a given frequency and amplitude, to modulate the signal amplitude and phase. An amplitude modulated signal results in three spectral lines. As an example, Fig. 6.1 shows the spectrum of a sinusoidal signal with frequency $\omega$ and amplitude $A_1$ modulated in amplitude by a sinusoidal signal with frequency $\Delta\omega$ and amplitude $A_2$.

It is clear that the modulating frequency determines the position of the two side lines and gives the bandwidth of the signal. According to [5], if the modulating frequency is above 10 Hz, the signal dynamics should be excluded from the dynamic phasor model and should be filtered out by the estimation algorithm. Amplitude and phase modulations can also be simulated separately with a modulating frequency that can vary from a few hertz up to ten hertz.

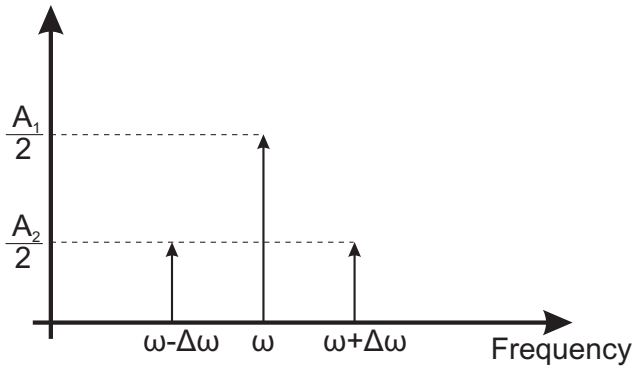


**Figure 6.1:** Spectrum of an amplitude modulated signal.

### 6.2.2 Transient conditions

#### Step tests

The step tests are divided in amplitude and phase steps. Parameters to realize this type of test are suggested for instance in [10, 12]. It is important to notice that the TVE can be a useless index in the sharp transition between two steady states, where it results in very high values in a short time period. As already mentioned in Section 2.2, a suitable index for this type of tests is the response time, to evaluate the promptness of the algorithms.

#### Ramp tests

In the frequency ramp tests the reference signal undergoes a linear change of frequency at a constant rate of change. Parameters for this test can be found in [10, 12]. In [12] for instance, a ROCOF of 1 Hz/s for 10 s is proposed. The ramp evolves between two steady-state conditions. The values of TVE in the proximity of the transitions occurring at the starting and final points of the ramp are almost meaningless and this should be kept into account, by excluding them from the analysis.

## 6.3 Results

### 6.3.1 Noise

Tests have been performed to compare all the considered algorithms when Additive White Gaussian Noise (AWGN) is added to the clean sinusoidal signal, at different levels of Signal to Noise Ratio (SNR). The limit of 1 % of TVE is respected by all the methods, for SNR above 26 dB. With a noise of 40 dB, which is often considered as

a possible lower limit in actual situations, for instance, the TVEs are in the average below 0.1 %, with peaks of about 0.2 % (see also [3]).

### 6.3.2 Off-nominal frequency

Such preliminary tests have been extensively performed by the authors of [2, 3], but an example will be reported here to better understand the relationship between the behaviour at off-nominal frequency and the behaviour in presence of dynamic evolutions.

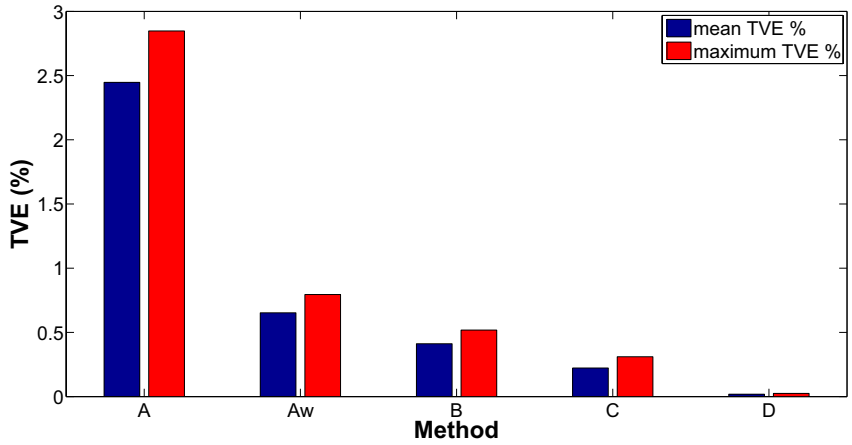


**Figure 6.2:** TVE % results for off-nominal frequency $f = 52.5\,\mathrm{Hz}$.

In Fig. 6.2, the TVE results with working frequency $f = 52.5\,\mathrm{Hz}$ are given. It is shown that algorithms that rely on a dynamic phasor model have better performances even under off-nominal frequency conditions. This fact is due to the pass-band characteristics of such algorithms that are designed to filter disturbances and to let unaffected a signal like that of Fig. 2.2: thus, if a sinusoidal signal oscillates at off-nominal frequency, but it is still inside the band of interest, its features are completely extracted by such algorithms.

Even if the TVE gives synthetic information about behaviour of algorithms, it is not sufficient and can even be misleading, as already pointed out in Section 2.2. As aforementioned, the relationship between the TVE and amplitude or phase error is non linear. An heuristic indicator, derived from (2.12), of the influence of each of the two components on the TVE can be represented by $100 \cdot \Delta a_{\mathrm{rel}}^2/\mathrm{TVE}^2$, that is the percent contribution of the square of relative amplitude error to the square of TVE. Its complementary indicator gives an idea of phase error contribution. Fig. 6.3 reports the average of such quantities, in the same off-nominal simulation of Fig.

6.2, and clearly shows that the TVE can not be considered as a complete index to compare methods performances. In fact, when considering, for instance, method $A_w$ and method C, the maximum TVEs are respectively 0.80 % and 0.31 %. On the contrary the maximum phase errors are, respectively, 0.15 crad and 0.31 crad, showing thus an inversion in the performances of the two methods, if the phase estimation accuracy is considered.

Because of these considerations, in the following both amplitude and phase errors will be presented, whenever possible, to give a better insight into the algorithms behaviour.

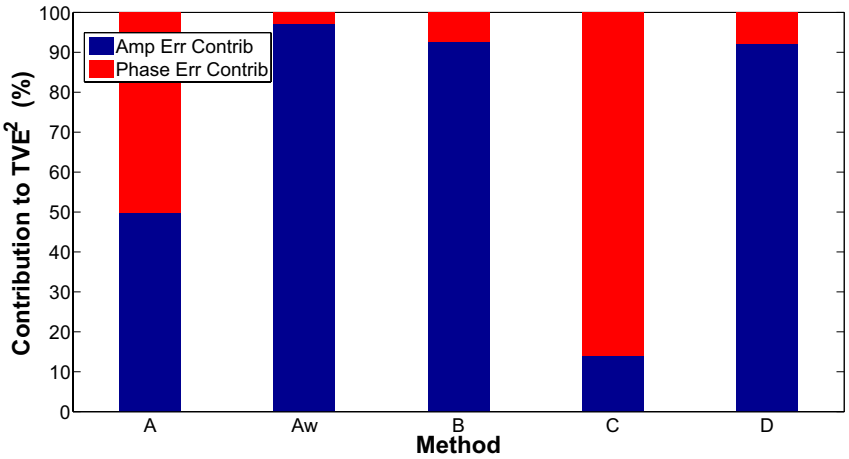


**Figure 6.3:** Influence of amplitude and phase errors on TVE for off-nominal frequency $f = 52.5$ Hz.

### 6.3.3 Harmonics

Tests in presence of harmonics have been performed using different values for the fundamental frequency of the signal (50, 50.05, 50.5, 52.5 and 55 Hz). It should be recalled that the harmonic frequencies are multiples of the actual signal frequency. Forty harmonics were simultaneously added to the signal, with the individual harmonic levels indicated in [13] and a Total Harmonic Distortion (THD) equal to 10 %.

The results show that also in this type of tests, using the TVE as a performance index may lead to some misunderstanding. This is the case, for example, of the test with fundamental frequency equal to 55 Hz (see Table 6.1). In this condition, in fact, the maximum TVE % for methods B and C is similar: 2.52 % and 2.46 %, respectively. However, in the case of algorithm B most of the TVE is caused by an

amplitude error (2.48 %), whereas only a small part of it is caused by the phase error (0.84 crad). Contrariwise, algorithm C shows a phase error (2.27 crad) much larger than the amplitude error (1.61 %) pointing out a completely different behaviour.

**Table 6.1:** Maximum amplitude (%), phase (crad) and TVE (%) results for 55 Hz harmonic test

| **Algorithms** | **55 Hz** | | |
|---|---|---|---|
| | Max Amplitude Error (%) | Max Phase Error (crad) | Max TVE (%) |
| Method A | 6.50 | 4.66 | 6.53 |
| Method $A_w$ | 2.89 | 0.30 | 2.89 |
| Method B | 2.48 | 0.84 | 2.52 |
| Method C | 1.61 | 2.27 | 2.46 |
| Method D | 0.33 | 0.05 | 0.33 |

Fig. 6.4 shows the results of the maximum amplitude error (%) and maximum phase error (crad) for the tests in the presence of harmonics. It should be noticed that the maximum TVE % does not necessarily occur at the same time of the maximum amplitude or phase errors. Thus, it is clear that the different indices provide complementary information.

It can be seen that for the test at 50 Hz all the methods show a good harmonic rejection whereas for the test with fundamental frequency equal to 55 Hz , only method D presents a good harmonic rejection. It is interesting to highlight that, while the performances at off-nominal frequencies strictly depend on the pass-band of the estimators, the harmonic rejection ability is due to the stop band characteristics. Method D, for instance, has a very flat response in the band of interest and thus, as it can be seen in Fig. 6.4, has a behaviour, in presence of harmonics, that does not depend in a significant manner on the fundamental frequency. On the contrary, method A, which perfectly cancels the effects of harmonics at nominal frequency, mainly suffers in the presence of off-nominal conditions.

### 6.3.4 Interharmonics

A single interharmonic line, with a 5 % amplitude with respect to the signal amplitude, has been added to a pure sinusoidal signal at nominal frequency. The interharmonic frequency $f_I$ has been changed during tests, by a 1 Hz step, to sweep a spectrum range from 25 Hz to 95 Hz. Fig. 6.5 shows the results for two specific

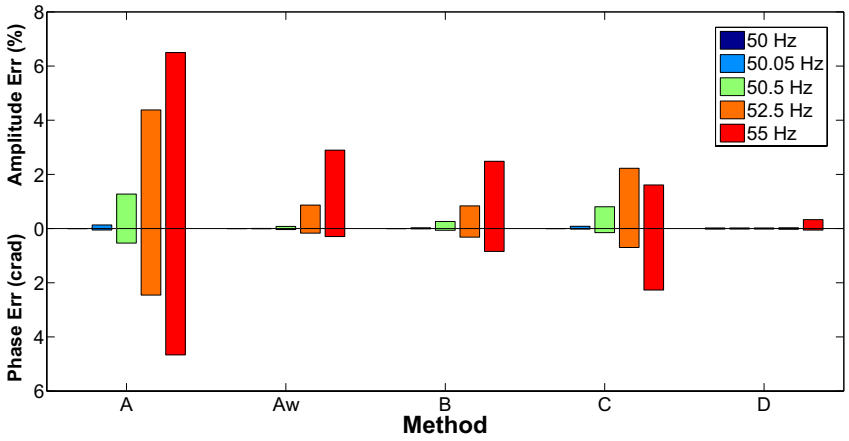


**Figure 6.4:** Maximum amplitude error (%) and maximum phase error (crad) for the tests in the presence of harmonics

interharmonics at frequencies $f_I = 57.5\,\text{Hz}$ and $85\,\text{Hz}$, respectively. The behaviour of the algorithms is related to their filtering capabilities. In fact, when the interharmonic is in the pass-band of the algorithm (designed to include dynamic phenomena of interest), no rejection is obtained and thus the TVE is about 5 %, whereas, for interharmonics at higher frequencies TVE depends on the stop-band attenuation. The results are, qualitatively, the same for amplitude and phase error, because the

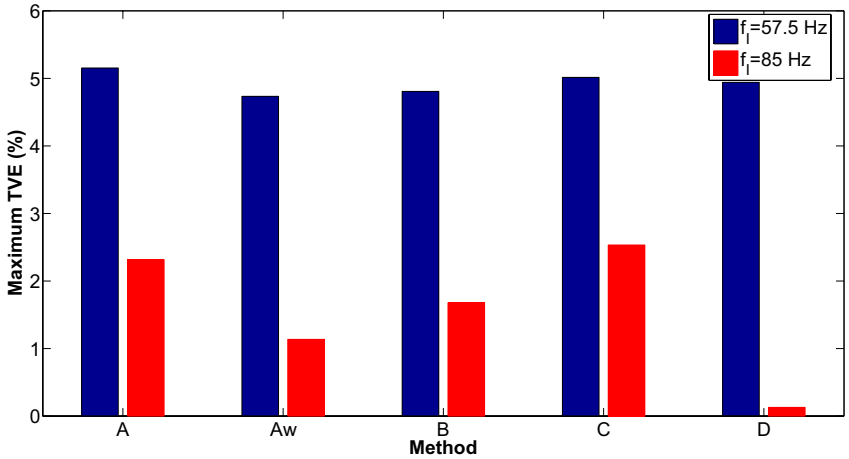


**Figure 6.5:** Maximum TVE % in presence of a single interharmonic at frequency $f_I$.

TVE is alternatively due to the each of the two error components.

### 6.3.5 Modulation

In [5], it is underlined that the dynamic phenomena of interest can be located in a frequency band of 20 Hz around the system frequency. In the following, results for sinusoidal modulation, according to model (2.9), are reported. Table 6.2 shows the maximum percent amplitude error and maximum phase error for two different system frequencies, when an amplitude modulated signal is used ($k_x = 0.1$ and $f_m = 5\,\text{Hz}$).

**Table 6.2:** maximum amplitude error (%) and phase error (crad) for amplitude modulated signal ($k_x = 0.1$ and $f_m = 5\,\text{Hz}$)

| **Algorithms** | **50 Hz** | | **51 Hz** | |
|---|---|---|---|---|
| | Max Amplitude Error (%) | Max Phase Error (crad) | Max Amplitude Error (%) | Max Phase Error (crad) |
| Method A | 0.55 | 0.50 | 1.21 | 1.20 |
| Method $A_w$ | 0.29 | 0.03 | 0.39 | 0.17 |
| Method B | 0.25 | 0.03 | 0.28 | 0.11 |
| Method C | 0.18 | 0.07 | 0.23 | 0.15 |
| Method D | 0.03 | 0.01 | 0.04 | 0.03 |

Algorithms designed on a dynamic model outperform the others under phasor amplitude variations. It can also be highlighted that the behaviour is related to the off-nominal characteristics: in fact, if the estimation method is based on a pass-band model, it gives good results when the system frequency is off-nominal. If the test signal is also modulated in phase, by a sinusoidal modulating function, the band of the signal can be computed by means of a Fourier series that involves Bessel functions of first kind (see [14] for details). For $k_a \ll 1$, the spectrum can be limited to $\pm 2 f_m$ with respect to the fundamental frequency. In Table 6.3, results of tests performed with simultaneous amplitude and phase modulations for two different fundamental frequencies are given.

Similarly to the previous test, method D is able to follow amplitude and phase variations.

### 6.3.6 Step Tests

In order to study the impact of faults and switching operations on the synchrophasor estimation, several tests with amplitude and phase steps have been executed. During the simulations, the signal instantaneously passes from a steady-state condition to

**Table 6.3:** Maximum amplitude error (%) and phase error (crad) for amplitude and phase modulated signal. $k_a = k_x = 0.1$ and $f_m = 5\,\text{Hz}$

| Algorithms | 50 Hz | | 51 Hz | |
|---|---|---|---|---|
| | Max Amplitude Error (%) | Max Phase Error (crad) | Max Amplitude Error (%) | Max Phase Error (crad) |
| Method A | 0.74 | 0.77 | 1.69 | 1.71 |
| Method $A_w$ | 0.29 | 0.27 | 0.44 | 0.38 |
| Method B | 0.27 | 0.24 | 0.30 | 0.28 |
| Method C | 0.22 | 0.22 | 0.28 | 0.31 |
| Method D | 0.04 | 0.04 | 0.06 | 0.06 |

another steady-state condition. To analyse the dynamic behaviour of the studied methods, the TVE response time with $H_T = 1\,\%$ (see equation (2.13)) has been used.

### Amplitude Step

The original signal is a 50 Hz sinusoidal waveform. Two step conditions have been considered during which the amplitude of the observed signal is instantaneously reduced by 20 % and the 50 %, respectively.

### Phase Step

The initial steady state condition is again characterized by a frequency of 50 Hz. Two tests have been performed, where the phase instantaneously passes from 0° to +15° and +45° respectively. Table 6.4 shows the results of these tests.

It should be highlighted that the $\Delta t_R$ may be misleading because it is strictly dependent on the chosen threshold $H_T$. As an example, Fig. 6.6 shows the TVE trends of the five methods for the $-20\,\%$ magnitude step test. Threshold $H_T = 1\,\%$ and $H_T = 3\,\%$ have been indicated in Fig. 6.6 with two dashed horizontal lines. It is possible to see that, if 3 % is considered as threshold, according to definition (2.13), all the methods presents similar TVE response time. These may be interpretable as a similar behaviour of both the algorithms designed on a static and dynamic model. However, if 1 % is chosen as threshold, algorithms C and D show a completely different behaviour characterized by a $\Delta t_R$ much bigger than methods A and B. $\Delta t_R$ values for $H_T = 1\,\%$ and $H_T = 3\,\%$ have been reported in Table 6.5.

**Table 6.4:** TVE response time results for amplitude and phase step tests

| Algorithms | $\Delta t_R$(ms) | | | |
|---|---|---|---|---|
| | Amplitude step | | Phase step | |
| | −20 % | −50 % | +15° | +45° |
| Method A | 19 | 20 | 17 | 19 |
| Method $A_w$ | 27 | 31 | 25 | 28 |
| Method B | 24 | 26 | 21 | 23 |
| Method C | 44 | 54 | 47 | 49 |
| Method D | 38 | 66 | 53 | 66 |

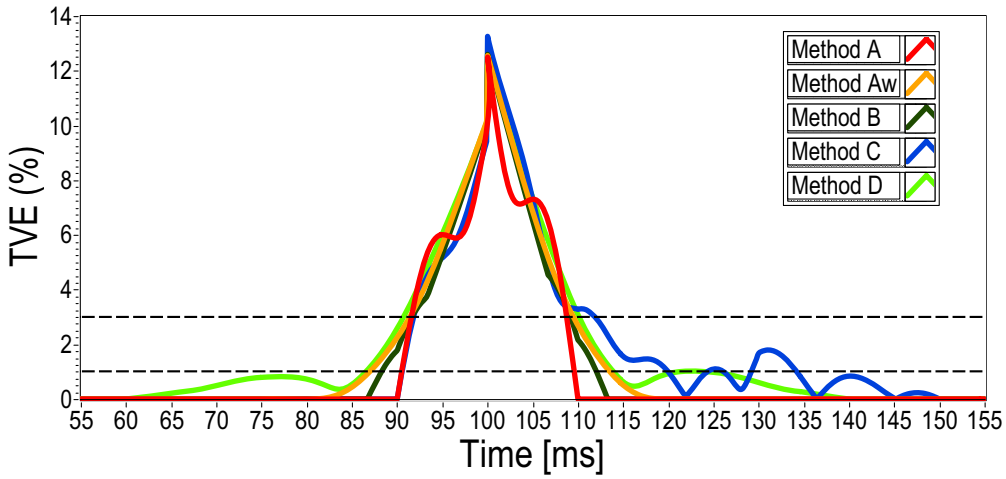


**Figure 6.6:** TVE trends for the −20 % magnitude step test

### 6.3.7 Ramp Tests

Several frequency ramp tests have been executed choosing different ROCOF varying from ±0.01 Hz/s to ±1 Hz/s.

Table 6.6 shows the results of the maximum amplitude error (%) and maximum phase error (crad) of the ramp test with a ROCOF of 1 Hz/s. Also in this case, methods based on a dynamic model perform better then methods based on a static model. This is due to their off-nominal frequency behaviour and tracking capabilities.

**Table 6.5:** $\Delta t_R$ values for $H_T = 1\,\%$ and $H_T = 3\,\%$ in the $-20\,\%$ amplitude step test.

| **Algorithms** | $\mathbf{\Delta t_R (ms)}$ | |
|---|---|---|
| | $H_T = 1\,\%$ | $H_T = 3\,\%$ |
| Method A | 19 | 17 |
| Method $A_w$ | 27 | 18 |
| Method B | 24 | 18 |
| Method C | 44 | 20 |
| Method D | 38 | 20 |

**Table 6.6:** Maximum amplitude and phase for ramp test (ROCOF=1 Hz/s)

| **Algorithms** | **1 Hz/s** | |
|---|---|---|
| | Max Amplitude Error (%) | Max Phase Error (crad) |
| Method A | 6.71 | 3.05 |
| Method $A_w$ | 2.85 | 0.23 |
| Method B | 2.22 | 0.38 |
| Method C | 0.98 | 1.43 |
| Method D | 0.32 | 0.23 |

# Bibliography


[1] (2007, Feb.) Model 1133A phasor measurement specifications. [Online]. Available: http://www.arbiter.com/files/product-attachments/1133_phasor_measurement_specifications.pdf

[2] P. Castello, M. Lixia, and C. Muscas, "Measurement of synchrophasors under dynamic conditions," in *Applied Measurements For Power Systems (AMPS), 2010 IEEE International Workshop on*, Sep. 2010, pp. 1–6.

[3] P. Castello, C. Muscas, and P. A. Pegoraro, "Performance comparison of algorithms for synchrophasors measurements under dynamic conditions," in *Applied Measurements For Power Systems (AMPS), 2011 IEEE International Workshop on*, Sep. 2011, pp. 25–30.

[4] *IEEE Standard for Synchrophasors for Power Systems*, IEEE Std C37.118-2005 (Revision of IEEE Std 1344-1995), 2006.

[5] A. G. Phadke and J. S. Thorp, *Synchronized Phasor Measurements and Their Applications*. Springer Science, 2008.

[6] W. Premerlani, B. Kasztenny, and M. Adamiak, "Development and implementation of a synchrophasor estimator capable of measurements under dynamic conditions," vol. 23, no. 1, pp. 109–123, Jan. 2008.

[7] R. K. Mai, Z. Y. He, L. Fu, B. Kirby, and Z. Q. Bo, "A dynamic synchrophasor estimation algorithm for online application," vol. 25, no. 2, pp. 570–578, Apr. 2010.

[8] J. A. de la O Serna, "Dynamic phasor estimates for power system oscillations," vol. 56, no. 5, pp. 1648–1657, Oct. 2007.

[9] M. A. Platas-Garza and J. A. de la O Serna, "Dynamic phasor and frequency estimates through maximally flat differentiators," vol. 59, no. 7, pp. 1803–1811, Jul. 2010.

[10] *IEEE Standard for Synchrophasor Measurements for Power Systems*, IEEE Std C37.118.1-2011 (Revision of IEEE Std C37.118-2005), Dec. 2011.

[11] *Voltage characteristics of electricity supplied by public distribution networks*, Std. EN 50160 CENELEC, Bruxelles, Belgium, 2004.

[12] "PMU system testing and calibration guide," North American SynchronPhasor Initiative (NASPI), Performance and Standards Task Team (PSTT), Nov. 2007.

[13] *Voltage characteristics of electricity supplied by public distribution systems*, European standard EN 50160 Std., 1999.

[14] A. B. Carlson, P. B. Crilly, and J. C. Rutledge, *Communication systems: an introduction to signal and noise in electrical communication*. MacGraw-Hill, 2002.

# Conclusions

The deep changes of power systems, due to technical and economical reasons, are leading to several system management and protection issues. Recent blackouts occurred all-over the world are a clear evidence of the situation of modern transmission network, which often operate close to their limits.

These changes in the configuration of power systems lead to the need to develop measurement systems distributed on a large scale to address monitoring and control problems. Phasor Measurement Units are becoming a key element, and are the basis for the implementation of Wide Area Monitoring Systems. Besides the current applications in WAMSs applied to transmission systems, the accurate measurement of synchrophasors is expected to become a fundamental task also for the monitoring and management of the electric distribution grids of the future (smart grids).

In this thesis, different sources that may affect PMU performances have been studied. In particular, the aspect of the synchronization of PMUs has been analysed. Besides the traditional synchronization solution based on GPS technology, this work explores the possibility of distributing an accurate time reference by means of Precision Time Protocol, defined in the standard IEEE 1588. To test this solution, two experimental systems for the measurement of synchrophasors have been implemented: the first one is synchronized by means of PTP with hardware-assisted time-stamp mechanism whereas the second one is synchronized by means of PTP with software-only time-stamp mechanism. Several tests have been performed to verify the performances of the two proposed synchronization solutions.

The results have given clear indications on the possible use of PTP-based systems (with hardware-assisted or software-only time-stamping) for the synchronization of the PMUs.

In fact, tests performed on the system based on hardware-assisted time-stamping showed that the synchronization obtained by a GPS-PTP solution is comparable to that obtained using a GPS receiver on each device, and that the contribution to the synchrophasor measurement uncertainty due to the utilization of transformers may be more significant than the uncertainty contribution due to PTP synchronization. On the other hand, tests performed on the system based on software-only time-

stamp showed that this solution would also be suitable for the synchronization of PMUs under particular conditions (substations with hardware-synchronized infrastructure) and that the uncertainty of synchronization may have minimal impact on applications such as the State Estimation.

Furthermore, the contribution of the phasor estimation models to the PMU performances has also been analysed. Many test cases are necessary to describe a phasor estimation algorithm in a meaningful manner. A rich test suite, designed to simulate algorithms behaviour under different realistic conditions, both steady-state and transient, has been illustrated. Test results show that algorithms performances cannot be fully described by means of Total Vector Error, because a different behaviour in terms of amplitude and phase error arises for each method when stressed by specific tests. Results also point out that algorithms specifically designed for dynamic phasor estimation are needed when relevant oscillations or frequency changes are present in the reference signal. In particular, methods based on an intrinsically dynamic model tend to outperform those based on a static model and also those based on post processing correction formulas.

# List of Figures

# List of Tables